

Advanced Control of Domestic Grid Connected Photovoltaic Systems with Battery Storage

Aziz Ahmad

A thesis submitted to

Auckland University of Technology

in fulfilment of the requirements for the degree of

Doctor of Philosophy (PhD)

2017

School of Engineering, Computer and Mathematical Sciences

ABSTRACT

With the increasing use of solar thermal energy systems and small-scale photovoltaic (PV) energy generation, there is a need to develop intelligent controllers to manage efficiently the energy generated by these systems. Ideally, these intelligent controllers will be able to predict the availability and magnitude of the solar resource and energy demand to plan in advance for periods when the solar resource is low or when energy demand is high.

This work demonstrates that it is possible to deliver a viable energy management strategy for a small-scale photovoltaic-battery-grid (PBG) system that is capable of coordinating the energy flows among the different energy sources. In doing so, the problems of modelling and control of the energy distribution for the PBG system using model predictive control (MPC) were addressed.

In devising this strategy, this work developed a nonlinear autoregressive recurrent neural network with exogenous inputs (NARX) and demonstrated that such a network was able to forecast both the energy demand for a typical New Zealand house, and the solar irradiation levels across a number of different locations (within New Zealand). Following on from this it was shown that using artificial neural network (ANN) based solar radiation and energy demand forecasts as measured disturbances allowed the MPC to plan for periods of low sunshine or high-energy demand.

The performance of the overall ANN informed model predictive control system was verified using simulation results and compared with the open-loop optimal control approach. The results showed that, for a typical Auckland weekly household load of 355 kWh, the MPC approach imported approximately 110 kWh less energy from the

grid than the optimal control approach. Furthermore, for the one-week period examined, the MPC approach managed to export over 15 kWh more energy to the grid than a controller based on the optimal control approach using the same PV production and energy demand data with the same objective function and constraints.

ACKNOWLEDGEMENTS

I gratefully acknowledge Callaghan Innovation and Ian Sumner from Energy Conscious Design Ltd for the financial support of the scholarship that made this project a reality.

First and foremost, I would like to thank my two supervisors. Dr. Timothy N. Anderson and Prof. Tek J. Lie for opening my eyes to MPC and process control and for guiding me to write valuable scientific papers. Dr. Akshya Swain, for his insight in control theory and great skills within predictive control and Matlab. I'm looking very much forward to future collaboration. Dr. Jonathan Curie, for always keeping his door open and having a good control-theory-angle-of-attack on my problems.

I would also like to thank Wayne Holmes at Unitec Institute of Technology for his patience and continuous support.

Also, to my loving parents, who raised me with a love of science and supported me in all my pursuits.

To School of Engineering, Auckland University of Technology for the tuition fee scholarship. Finally, I would like to thank my wife F. Aziz for her constant support and encouragement.

LIST OF PUBLICATIONS

The following papers have been published over the course of this research. Though covered by this thesis, they form an additional body of work the reader may wish to refer to.

Journal papers:

Ahmad, A, Anderson, T.N. and Lie T.T., 2015, “Hourly Global Solar Irradiation Forecasting for New Zealand”, *Solar Energy*, vol. 122, pp. 1398–1408

Conference papers:

Ahmad, A. Anderson, T.N. Swain, A.K. and Lie, T.T., 2017, “Maximizing Photovoltaic Array Energy Usage Within a House Using Model Predictive Control”, *Proceedings of the Asian Conference on Energy, Power and Transportation Electrification (ACEPT 2017), Singapore*

Ahmad, A. Anderson, T.N. Swain, A.K. Lie, T.T. Currie, J. and Holmes, W., 2016, “Residential Household Electrical Appliance Management using Model Predictive Control of a Grid Connected Photovoltaic-Battery System”, *Proceedings of the 2016 Asia-Pacific Solar Research Conference, Canberra, Australia*

Ahmad, A, Anderson, T.N. and Lie T.T., 2015, “A Platform for Analysing Advanced Photovoltaic Energy Controllers”, *Proceedings of the 2015 Asia-Pacific Solar Research Conference, Brisbane, Australia*

Mutaz, T. and Ahmad, A., 2015, "Solar Radiation Prediction Using Radial Basis Function Models", *Eighth International Conference on Developments in eSystems Engineering, DeSE 2015, Dubai, UAE*

Ahmad, A., Anderson, T.N., Lie, T.T. and Alradadi, H., 2015, “Excel Based Tool for Global Solar Radiation Forecasting using Artificial Neural Network Models”, *Meteorological Society of New Zealand Annual Conference*, Raglan, New Zealand

Ahmad, A. and Anderson, T.N., 2014, “Hourly Electrical Power Consumption Prediction for New Zealand Residential Houses Using Artificial Neural Network Models”, *Proceedings of the 2014 Asia-Pacific Solar Research Conference*, Sydney, Australia

Ahmad, A and Anderson, T.N., 2014, “Global Solar Radiation Prediction using Artificial Neural Network Models for New Zealand”, *Proceedings of the 52nd Annual Australian Solar Council Scientific Conference*, Melbourne, Australia

TABLE OF CONTENTS

ABSTRACT.....	I
ACKNOWLEDGEMENTS.....	III
LIST OF PUBLICATIONS.....	IV
TABLE OF CONTENTS.....	VI
LIST OF FIGURES.....	9
LIST OF TABLES.....	11
LIST OF SYMBOLS AND NOMENCLATURE.....	12
DECLARATION.....	15
CHAPTER 1. INTRODUCTION.....	16
1.1. Introduction.....	16
1.2. Photovoltaic and battery based energy systems.....	16
1.3. Control of renewable electric power systems.....	18
1.4. Control of residential electrical energy systems.....	18
1.5. Thesis objective.....	23
CHAPTER 2. HOURLY GLOBAL SOLAR IRRADIATION PREDICTION FOR A PREDICTIVE CONTROLLER.....	24
2.1. Introduction.....	24
2.2. Methodology.....	28
2.2.1. Input variables selection for all prediction methods... ..	28
2.2.2. Nonlinear autoregressive with exogenous input (NARX).....	30
2.2.3. Number of hidden neurons and delays.....	33
2.2.4. NARX results.....	35
2.2.5. Other forecasting techniques.....	39
2.2.6. Multilayer perceptron (MLP).....	39
2.2.7. Auto regressive moving average (ARMA).....	42
2.2.8. Persistence forecasting approach.....	45
2.3. Results.....	46
2.3.1. Comparison of methods.....	46
2.3.2. Irradiation prediction for New Zealand cities.....	48
2.4. Summary.....	49
CHAPTER 3. HOURLY ENERGY CONSUMPTION PREDICTION FOR A PREDICTIVE CONTROLLER.....	51
3.1. Introduction.....	51

3.2.	Methodology	53
3.2.1	Persistence model.....	53
3.2.2	Nonlinear autoregressive with exogenous input (NARX).....	54
3.3.	Electricity consumption prediction for a residential house.....	60
3.4.	Summary	61
CHAPTER 4.	ADVANCED CONTROL DEVELOPMENT.....	63
4.1.	Overview	63
4.2.	Predictive control for domestic energy systems.....	63
4.3.	Structure of the photovoltaic-battery-grid system.....	69
4.4.	Outline of the MPC approach and implementation.....	72
4.4.1	MIMO state-space model of the proposed system.....	74
4.4.2	Objective function for the MPC.....	77
4.4.3	MPC algorithm and optimization.....	78
4.4.4	Constraints for the MIMO linear system	79
4.4.5	Battery parameters estimation.....	83
4.5.	Summary	86
CHAPTER 5.	RESULTS AND DISCUSSION	87
5.1.	Simulation results of the proposed MPC	87
5.2.	Optimal control method	97
5.2.1.	Results of the optimal control	99
CHAPTER 6.	CONCLUSION AND FUTURE WORK	103
6.1.	Conclusion.....	103
REFERENCES	106
APPENDIX A: MODEL PREDICTIVE CONTROL WITH CONSTRAINTS		
	114	
A.1.	MIMO State-space models.....	114
A.2	Prediction of state and output variables	117
A.3	Optimization.....	121
A.4	Constraints for the MIMO state-space model	122
A.5	Constraints as part of the optimal solution.....	124
A.6	Numeric solution of MPC using quadratic programming.....	126
A.7	Quadratic programming for equality and inequality constraints	127
A.8	Hildreth's quadratic programming procedure.....	127
A.9	Summary	130

APPENDIX B: HOURLY LOAD ENERGY DEMAND AND PV ARRAY PRODUCTION DATA.....	131
B.1 Hourly load energy demand data	131
B.2 Hourly PV array production data	133

LIST OF FIGURES

Figure 1. Map of New Zealand with major cities.....	27
Figure 2. NARX block diagram	31
Figure 3. Regression analysis of the network outputs with respect to targets for training, validation and test sets.....	36
Figure 4. Measured and predicted irradiation values for Auckland using NARX ANN	38
Figure 5. Measured and predicted solar irradiation values using NARX ANN.....	38
Figure 6. Multi-layered perceptron (MLP) network	40
Figure 7. Detail of the perceptron process	40
Figure 8. Measured and predicted solar irradiation values using an MLP ANN	42
Figure 9. Measured and predicted solar irradiation values using ARMA.....	44
Figure 10. Measured and predicted solar irradiation values using a benchmark persistence approach	45
Figure 11. Day ahead solar irradiation forecast and actual data for Auckland on 1 January 2014	47
Figure 12. Predicted irradiation for New Zealand cities	49
Figure 13. Measured and predicted load values using the benchmark persistence model with RMSE = 0.486 kWh.....	54
Figure 14. Mean Square Error (MSE) performance of the network	59
Figure 15. Measured and predicted electricity consumption values for the first 6 models	60
Figure 16. Measured and predicted values for a residential house in Auckland with RMSE = 0.252 kWh using the NARX approach	61
Figure 17. Basic principal of the MPC for buildings	68
Figure 18. Overall structure of the photovoltaic-battery-grid energy system	70
Figure 19. Configuration of the photovoltaic-battery-grid energy system.....	71
Figure 20. Flow chart of the MPC approach	73
Figure 21. PV array production and total energy demand of the house	88
Figure 22. Switching behaviour of the MPC (On=1, Off=0)	89
Figure 23. MPC performance in the presence of disturbance (PV energy prediction) (On=1, Off=0)	90
Figure 24. MPC performance in the presence of disturbance (Energy demand prediction) (On=1, Off=0)	91
Figure 25. 24-hours energy demand, PV production and energy flow to and from the grid	92

Figure 26. Energy flow from the PV array to battery and battery to satisfy load	93
Figure 27. State-of-charge of the battery bank (Capacity=30 kWh).....	93
Figure 28. PV energy flow priorities according to demand	94
Figure 29. Controller output signal 1 vs reference signal 1	96
Figure 30. Controller output signal 2 vs reference signal 2	96
Figure 31. 24-hours analysis of grid imports/exports for the MPC and open-loop optimal control	100
Figure 32. One-week analysis of grid imports/exports for MPC and open-loop optimal control	101

LIST OF TABLES

Table 1. Regression values for input weather variables vs global solar irradiance....	29
Table 2. Test cases based on different combinations of input variables	30
Table 3. RMSE, R and computing time values for different numbers of neurons and delays using Case 2 weather data.....	35
Table 4. RMSE and Regression values for all 12 NARX networks.....	37
Table 5. Orders and coefficients of the realized ARMA system.....	44
Table 6. RMSE and nRMSE values for all forecasting approaches.....	46
Table 7. Models based on different combinations of input variables	55
Table 8. RMSE and Regression values for different number of neurons and delays.	57
Table 9. RMSE and Regression values for all 12 ANN models	59
Table 10. Constraints for the MIMO system.....	80
Table 11. Battery constraints.....	82
Table 12. Discharging constraint.....	83
Table 13. Values of the system parameters	87
Table 14. Values of the control parameters.....	88
Table 15. Energy variables replacement for the open-loop optimal control approach	98
Table 16. Photovoltaic-battery-grid system Parameters.....	99
Table 17. One-week comparison of the MPC and optimal control approaches.....	101
Table 18. Load energy demand ($E_d(k)$) profiles in kWh for a residential house.....	131
Table 19. PV Array production ($E_{PV}(k)$, kWh)	133

LIST OF SYMBOLS AND NOMENCLATURE

A	State matrix of state-space model
B	Input-to-state matrix of state-space model
C	State-to-output matrix of state-space model
D	Direct feed-through matrix of state-space model
(A, B, C, D)	State-space realization
ΔU	Parameter vector for the control sequence
$\Delta u(k_i + m)$	Future incremental control at sample m
$\Delta u^{min}, \Delta u^{max}$	Minimum and maximum limits for Δu
F, Φ	Pair of matrices used in the prediction equation $Y = Fx(k_i) + \Phi\Delta U$
$I_{q \times q}$	Identity matrix with appropriate dimensions
J	Performance index for optimization
K_{lqr}	Feedback control gain using LQR
K_{mpc}	Feedback control gain using MPC
K_x	State feedback control gain vector related to $\Delta x_m(\cdot)$ or $\dot{x}_m(\cdot)$
K_y	State feedback control gain related to y
$l_i(\cdot)$	The i th discrete or continuous-time Laguerre function
λ	Lagrange multiplier
$\lambda_i(A)$	The i th eigenvalue of matrix A
m	Number of inputs, also the m th future sample in discrete time
M, γ	Pair of matrix, vector for inequality constraints ($Mx \leq \gamma$)
N	Number of terms used in Laguerre function expansion, both continuous and discrete time
N_c	Control horizon
N_p	Prediction horizon
o_m	Zero vector with appropriate dimension
o_k	Zero row vector ($k = 1, 2, \dots$) with appropriate dimension
$o_{q \times q}$	$q \times q$ zero matrix
$o_{q \times m}$	$q \times m$ zero matrix
q	Number of outputs
$r(\cdot)$	Set-point signal
$u(\cdot)$	Control signal
$x(\cdot)$	State variables
$x(k_i + m k_i)$	Predicted state variable vector at time τ given current state $x(k_i)$
$\hat{x}(\cdot)$	Estimated state variable vector
$y(\cdot)$	output signal
Y	Predicted output data vector
$S_{oc}(k)$	The current state of charge of the battery bank
$E_{PV1}(k)$	Control variable representing energy flow from the PV array to the load at the k_{th} hour (kW)

$E_{PV2}(k)$	Control variable representing energy flow from the PV array to the hot water cylinder at the k_{th} hour (kW)
$E_{PV3}(k)$	Control variable representing energy flow from the PV array to the grid at the k_{th} hour (kW)
$E_{PVb}(k)$	Control variable representing energy flow from the PV array to the battery bank at the k_{th} hour (kW)
$E_{PV}(k)$	The hourly energy output from a PV array at the k_{th} hour (kWh/m^2)
$E_b(k)$	Control variable representing energy flow from the battery bank to the load at the k_{th} hour (kW)
$E_g(k)$	Control variable representing energy flow from the grid to the load at the k_{th} hour (kW)
$E_d(k)$	Control variable representing the load at the k_{th} hour (kW)
GHG	Green House Gas
PV	Photovoltaic
BOS	Balance of System
MPC	Model Predictive Control
EMS	Energy Management System
FIT	Feed-in Tariffs
BIPVT	Building Integrated Photovoltaic Thermal
PDB	Photovoltaic-Diesel-Battery
ESTTP	European Solar Thermal Technology Platform
AR	Autoregressive
MA	Moving Average
ARMA	Autoregressive Moving Average
ARIMA	Autoregressive-Integrated Moving Average
ANN	Artificial Neural Network
ANFIS	Adaptive Neuro-Fuzzy Inference System
GCHP	Ground Coupled Heat Pump
LM	Levenberg Marquardt
RMSE	Root Mean Square Error
nRMSE	Normalized Root Mean Square Error
RH	Relative Humidity
SZA	Solar Zenith Angle
NIWA	National Institute of Water and Atmosphere
R	Regression (Pearson correlation coefficient)
NARX	Nonlinear Autoregressive Recurrent Neural Network
MLP	Multilayer Perceptron
MSE	Mean Square Error
SRP	Solar Radiation Prediction
EDP	Energy Demand Prediction
SOC	State of Charge
DOD	Depth of Discharge
PE	Persistently Exciting
MIMO	Multi Input Multi Output
FIR	Finite Impulse Response
DMC	Dynamic Matrix Control
GPC	Generalized Predictive Control

QP
LP

Quadratic Programming
Linear Programming

DECLARATION

I hereby declare that except where specific reference is made to the work of others, the contents of this dissertation are original and have not been submitted in whole or in part for consideration for any other degree or qualification in this, or any other university. This dissertation is my own work and contains nothing, which is the outcome of work done in collaboration with others, except as specified in the text and acknowledgments.



.....

(Aziz Ahmad)

December 2017

Chapter 1. INTRODUCTION

1.1. Introduction

The growing concerns of global warming, diminishing world supplies of the non-renewable fuels, as well as economic aspects, are driving factors in the current efforts to save energy (Tiwari & Dubey, 2010). The United Nations Environment Programme indicates that buildings use about 40% of global energy, 25% of global water, 40% of global resources, and they emit approximately 1/3 of greenhouse gas (GHG) emissions. Therefore, addressing energy use in buildings offers great potential for achieving significant GHG emission reductions in different countries. Furthermore, energy consumption in buildings can be reduced by using advanced technologies and management (Thi et al., 2015) as well as advanced control concepts in building management systems (Laustsen, 2008).

Energy derived from the sun, the wind, the Earth's heat, water and the sea has the potential to meet the world's energy needs (Hallett & Wright, 2011). Unfortunately, these sustainable resources are often intermittent, thus needing storage and intelligent control strategies to utilize these resources to their full potential (Hove & Tazvinga, 2012), this is particularly the case for solar energy.

1.2. Photovoltaic and battery based energy systems

In recent years, the installed photovoltaic (PV) capacity in the world has rapidly increased. In 2013, PV capacity of more than 37 GW was installed worldwide, adding up to a cumulative capacity of approximately 137 GW (Wang, 2012).

Electricity generation by PV systems is often portrayed as the quintessential “green” energy option for the future and an attractive energy return on investment (Fthenakis & Alsema, 2004). PV installations can be identified as grid-connected centralised (large power plants), grid-connected distributed (smaller rooftop and façade systems), off-grid non-domestic (power plants and industrial installations in remote areas), or off-grid domestic (mainly stand-alone rooftop systems for houses in remote areas). The main discriminating aspect among these four types of installations is the requirement for battery storage as well as the difference due to the balance of system (BOS) components, size and location. PV systems with battery storage usually work well to provide continuous and stable energy and to overcome the intermittent nature of solar energy i.e., the PV-battery hybrid system (Fthenakis et al., 2008).

That said; many domestic systems installed in recent times have been grid-connected PV systems without battery storage. In this respect, the grid acts as a “battery” to backup these systems and so they do not require complex energy dispatch strategies, but rather can rely on simple load management strategies. Prioritizing the use of a PV system is the only rule when the PV energy is less than the energy requirement of the load. In contrast, battery storage brings a number of challenges to energy dispatch and load management strategies, as more complicated scenarios must be considered; such as charging the battery during the daytime, discharging during the night or when there is high demand. As a result, advanced controllers are needed for hybrid PV-battery systems, such that the utilisation of the PV array can be enhanced and the grid regulation can be improved in terms of safety and efficiency (Zhu et al., 2015).

For grid-connected hybrid PV-battery systems, the changing electricity price, the timing of energy transactions, the mismatch between solar energy generation and energy

demand are the main challenges and have been discussed by both Arun & Banerjee, (2009) and Giraud & Salameh, (2001). Hence energy management for hybrid systems with battery storage is an issue that has attracted significant interest from researchers (Palma et al., 2013; Levron et al., 2013).

1.3. Control of renewable electric power systems

The control of large-scale solar energy systems has received some attention, with most researchers having considered energy management and demand response for large-scale integration of renewable energy at the utility side (Moura & de-Almeida, 2010; Huang, et al., 2012). In this respect, numerous utility companies are investigating and implementing “smart” grids (SG) with a view to making the existing power generation system advanced, reliable, self-healing and economical. To achieve this requires the use of sensors, communication and controllers to enhance the overall operation of electric power systems (Nalbalwar et al., 2012). In saying this most optimal scheduling methods cannot handle complicated cases when hybrid systems experience external disturbances, with only a few closed-loop control methods having been designed (Palma et al., 2013) and (Zervas et al., 2008). Furthermore, the uncertainties associated with forecasting of renewable energy availability and energy demand have been studied for utility scale integration of renewable energy (Makarov et al., 2011), but the impact of these on small-scale renewable energy systems has not been fully evaluated.

1.4. Control of residential electrical energy systems

In addition to the attention that has been paid to larger renewable electrical energy systems a number of studies have attempted apply similar strategies to residential scale electricity use. Patel and Khosla, (2015) reviewed a number of research studies on energy

management controllers for smart homes where the aims were to address reducing energy consumption, peak to average ratio and energy wastage. They identified various control and pricing schemes, such as real time pricing (RTP), critical peak pricing (CPP), time of use (TOU) and day ahead pricing (DAP). In one particular study, Liu et al., (2014), used peak to average ratio (PAR), daily energy demand, electricity cost and the hourly energy demand of shiftable electrical appliances of the consumers as the constraints in a control system. The objective function was to minimize the energy cost of the consumers through the determination of the optimal power usage and operation time of the appliances. This was achieved by shifting the high energy consuming loads to off peak hours, which helped minimize the energy consumption in the peak hours.

In a later study Rahim et al., (2016), presented a demand side management (DSM) model for a residential energy management system in order to avoid peak formation while decreasing electricity demand and preserving user comfort levels within specified limits. In their work, three heuristic algorithms were used to evaluate the objective function. They suggested that the genetic algorithm based controller was better in term of electricity cost reduction, PAR minimization and maximization of user satisfaction than binary particle swarm optimization (BPSO). However, the computational time of the algorithm was higher. In a similar vein, Arafa et al., (2014), reduced the computational time for load scheduling in homes by introducing an evolutionary algorithm, that improved the performance (convergence rate and accuracy) of differential evolution (DE). On this basis there appears to be scope for advanced control strategies in renewable electric power systems.

In this vein, Erol-Kantarci and Mouftah, (2010), studied a linear programming (LP) based model to minimize the electricity cost in a residential dwelling. In their study, a day

was divided into time slots of equal lengths with different pricing rates, similar to a TOU scheme. In their LP model the home appliances were scheduled in appropriate time slots to reduce the electricity bill such that the consumer could enter the schedule detail in the LP model which would then deliver the most efficient and optimal scheduling output.

On a more simplistic level rule-based strategies have also developed for energy management of hybrid systems, (Wang & Nehrir, 2008; Jain & Agarwal, 2008; Teleke et al., 2010) which can obtain promising but not optimal solutions to ensure practical constraints are satisfied. In Kanchev et al., (2011), a deterministic planning method was proposed in order to perform day-ahead energy flow scheduling for conventional and renewable energy systems. Similarly, Tazvinga et al., (2013) studied an optimal control approach to improve the performance of EMS for scheduling of energy flow for a hybrid energy system with a view to minimizing the cost of electricity and maximizing PV energy usage.

In their work to achieve maximum efficiency from photovoltaic systems using small-scale batteries and flexible thermal loads, Vrettos et al., (2013), proposed four rule-based control algorithms and calculated the building energy flows and PV self-consumption ratios (the consumption of most of the PV energy within the building premises) on an annual basis. Results showed that installing batteries for local PV utilization was an attractive investment due to decreasing trends in battery cost and feed-in tariffs (FIT). In a more general sense, Wang & Nehrir, (2008) discussed the effectiveness of a rule-based energy management strategy for a hybrid wind/PV/fuel-cell stand-alone application. In their work, real weather and load profile data were utilized such that the proposed controller managed the energy flow among different energy sources and storage units under realistic conditions.

Residential energy management systems were also studied in Mohsenian-Rad & Leon-Garcia, (2010) where an optimal and automatic residential energy consumption-scheduling framework was proposed. The aim of this work was to achieve a desired trade-off between minimizing the electricity cost and minimizing the waiting time for the operation of each appliance in the households. In Juan et al., (2012), an optimal load management strategy for residential households was examined that utilized the communication infrastructure of the future smart grid. The proposed controller utilized predictions of electricity prices, energy demand and renewable energy production in determining the optimal relationship between hourly electricity prices and the use of different household appliances and electric vehicles in a typical smart house. Results showed that the proposed model allowed users to reduce their electricity bill between 8% and 22% for a typical summer day analysed and adapt the electricity bill to their actual economic situation.

In a subsequent, and similar, study by Chen et al., (2013), an appliance scheduling scheme for residential building energy management was proposed. This system utilized a time-varying retail pricing structure that was enabled by two-way communication infrastructure. In realising this, finite-horizon scheduling optimization problems were formulated to exploit the operational flexibilities of the thermal and non-thermal appliances, and incorporated both forecasts and newly updated information. Their simulation results showed that customers can have notable energy cost savings on their electricity bills with the time-varying pricing.

One of the challenges of a residential energy controller is the variation in daily energy requirement between summer and winter period. Qi et al., (2011) examined this problem for a stand-alone PV-battery energy system. The operational efficiency of the

proposed system over a 24 h period was evaluated and they concluded that optimal solutions could be found to reduce the corresponding fuel costs. This resulted in fuel savings of 73-77% in winter and 80.5-82% in summer.

Despite simple rule and schedule based controllers achieving good outcomes, predictive control strategies for hybrid renewable energy systems have been shown to be more efficient when compared to conventional, non-predictive strategies for energy efficient home automation (Bourgeois & Macdonald, 2006; Cho & Zaheer, 2003; Henze et al., 2005). Wu et al., (2015) proposed a demand side management system for PV-battery hybrid systems using a model predictive control (MPC) approach. In this system the battery would be charged by the grid during off-peak times and discharged during peak times to minimize grid imports when electricity prices were higher. The proposed MPC achieved improved control performance in terms of accuracy and robustness. Furthermore, it was shown that greater cost savings could be achieved by using closed-loop control.

This finding is analogous to proposed developments in the field of solar thermal energy systems (where the thermal storage system is equivalent to an electrical battery). In particular, the European Solar Thermal Technology Platform's (ESTTP) recent industry report on "Solar Heating and Cooling for a Sustainable Energy Future in Europe" stresses that one central control system is vital to maximize the overall efficiency of solar energy systems. It also discusses that to achieve renewable energy targets by 2030 "Advanced control concepts for components and overall systems, including self-learning control, fuzzy logic and adaptive control techniques should be adopted" (Stryi-Hipp et al., 2012). In addition, it noted the need for:

- Development of advanced control equipment that is easy to use and standardized
- Self-adapting and self-optimizing strategies
- Control systems responsive to weather forecasts
- Integration of new automated methods, such as “fuzzy logic” controllers and control algorithms based on optimization theory

In this respect, it raises questions as to why a similar line of enquiry has not yet been raised with respect to photovoltaic energy systems, and grid connected photovoltaic-battery power systems in particular.

1.5. Thesis objective

The literature has shown that very few attempts have been made towards the development of an advanced controller for grid connected photovoltaic-battery power systems. Furthermore, relatively few attempts have been found in the literature where solar radiation prediction and energy consumption prediction are used in control strategies to plan in advance for periods of low sunshine or periods when energy demand is more than usual. These factors, combined with the industry-identified needs, suggest that there is significant demand for controllers that incorporate solar radiation and load energy prediction to improve efficiency, and maximise self-consumption of electricity. Therefore, this work aims to explore this and answer the question:

Can a controller that incorporates energy generation and consumption forecasts be developed to manage the electricity produced by domestic grid connected photovoltaic-battery power systems?

Chapter 2. HOURLY GLOBAL SOLAR IRRADIATION PREDICTION FOR A PREDICTIVE CONTROLLER

2.1. Introduction

In the preceding chapter it was noted that with the growing use of solar energy systems by domestic users, there is an increasing need to develop intelligent controllers that allow these users to efficiently manage the energy generated by these systems. Ideally, these intelligent controllers will be able to forecast the availability and magnitude of the solar resource, more accurately than a persistence approach, to plan for periods when the solar irradiance magnitude is small or unavailable. In addition, the method used to provide this forecast needs to be adaptable to a range of timescales and locations.

In many cases limited coverage of irradiation measuring networks prompts the development of techniques for estimating and forecasting the global irradiation using climatological parameters (Maitha et al., 2011). Several techniques have been developed in order to estimate solar irradiance data at different scales including empirical (Loutzenhier et al., 2007), analytical (Ulgen & Hepbasli, 2009) and numerical techniques, as well as neural network approaches (Moustrisa et al., 2008). Additionally, a significant number of studies have used physics-based approaches as shown by Gueymard, (2005, 2008), & Perez at al., (2007) and also statistical forecasting of solar irradiation (Goh & Tan, 1977).

Approaches based on statistical processes such as autoregressive (AR), moving-average (MA), autoregressive moving-average (ARMA), autoregressive-integrated moving-average (ARIMA) and Markov chain have also been widely used. However, these approaches require some statistical transformations to the data before they are

applied. Due to these transformations, it is not possible to ensure that the results are accurate and represent a precise correlation with the measured solar irradiance values (Al-Alawi & Al-Hinai, 1998) and so it is necessary to develop alternative approaches (Mellit et al., 2010).

In this regard, artificial neural network (ANN) techniques for predicting irradiation have been shown to have greater accuracy than other techniques such as linear, nonlinear and fuzzy approaches (Yadav & Chandel, 2014) and so have been used in a number of solar energy applications. Kalogirou, (2001) has reviewed the use of ANN in renewable energy systems applications while Mellit & Kalogirou, (2008) and Mellit et al., (2009) reviewed ANN's in photovoltaic applications and for sizing of photovoltaic systems respectively. Similarly authors such as Esen et al., (2008) have examined adaptive neuro-fuzzy inference systems (ANFIS) and ANN models of ground-coupled heat pump (GCHP) systems.

Based on the predictive capabilities of ANN systems, a number of studies have begun to examine the ability of these systems to forecast future values of solar irradiation. Mellit & Alessandro, (2010) presented a review of artificial intelligence techniques for solar radiation forecasting and concluded that ANN models can be generalized to be used in different locations around the world.

In an early study in this area Sfetsos and Coonick, (2000) introduced an approach for a one-step ahead prediction of mean hourly solar radiation received by a horizontal surface through ANN and ANFIS models. It was shown that the performance of the models was enhanced when a wind direction term was included in the input list. They also found that the best prediction resulted from the use of a multivariate Levenberg Marquardt (LM) case that exhibited a 74% improvement in the Root Mean Square Error

(RMSE) when compared with a benchmark persistence approach. The results indicated that the ANN models predict the solar radiation time series more effectively than procedures based on the clearness index.

Paoli et al., (2010) also used an ANN prediction approach based on Multi-Layer Perceptron to determine global irradiation at daily horizon (d+1). Their proposed model was compared with AR, ARMA, k-Nearest Neighbors (k-NN) and Markov Chains approaches. Without pre-processing AR and ANN models showed a daily normalised Root Mean Square Error (nRMSE) of approximately 21% compared to Markov chain, Bayes and k-NN methods where nRMSE was in the order of 25–26%. However, annual pre-processing ANN methods based on clearness index and clear sky index reduce forecasting errors of about 5–6% (nRMSE~20%) compared to classical predictors as Markov chains.

More recently, Voyant et al., (2014) developed an ANN based MLP model that was applied to two years of pre-treated time series data in order to forecast global solar irradiation 24-hours ahead. The results of the MLP were compared with those of ARMA and the benchmark persistence approaches and showed that the prediction error could be reduced by using the proposed approach.

Similarly, Rich et al., (2013) developed statistical models, ANN models, satellite imaging based models, numerical based models and hybrid methods for solar irradiance forecasting. In their work, they found that regressive methods such as AR, MA, ARMA and ARIMA take advantage of the correlated nature of the irradiance observations and tend to work well in both data-poor and data-rich environments. However, it was concluded that ANN modelling offers improved nonlinear approximation performance

and provides an alternative approach to physical modelling for irradiance data when enough historical data is available and are not typically temporally limited.

Now, it is noted in the literature that physics-based, statistical and ANN based feed-forward network techniques have demonstrated their ability to predict future values of solar irradiation, however, recurrent neural network based methods have received little attention. Therefore, this study aims to investigate several techniques for forecasting solar irradiation that could be implemented into future solar control systems, and particularly, the ability of nonlinear autoregressive recurrent neural networks to forecast global solar irradiation 24 hours in advance for a number of major New Zealand cities, as shown in Figure 1.

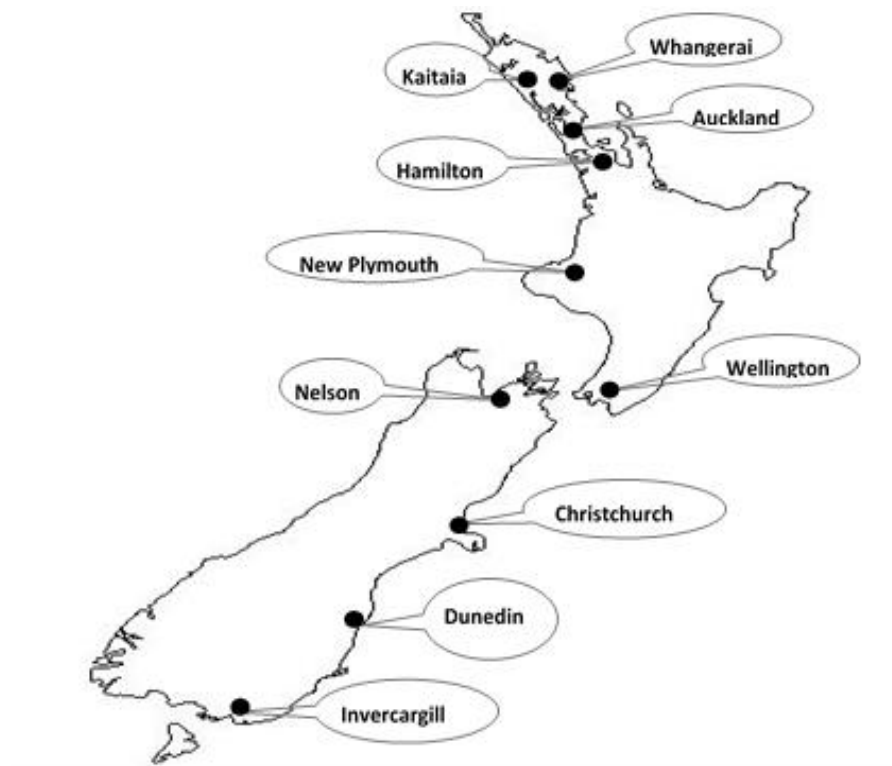


Figure 1. Map of New Zealand with major cities

2.2. Methodology

For this work several forecasting techniques were utilised: NARX, MLP, ARMA and a benchmark persistence forecast. However, given the lack of attention it has received in the literature, the NARX ANN architecture is the main typology described in this paper.

For each approach mentioned in this study, three years of historic hourly data for: global solar irradiation, Temperature (T_{max}, T_{min}), Barometric Pressure (P), Relative Humidity (RH), Solar Zenith Angle (SZA), Azimuth Angle (A_z), Rain amount (R_a), Wind speed (W_s) and Wind direction (W_d) were taken from the National Institute of Water and Atmosphere's (NIWA) CliFlo database (2014) to test each method. Hourly global solar irradiation 24 hours in advance being the target output variable.

For the ANN approaches, that is NARX and MLP, the input weather data was presented as unprocessed data, to study the effect of real input variables on the predicted values of the target variable. In doing this 70% of the historic data was presented to the network during training, allowing the network to be adjusted according to its error. Subsequently 15% of the data was used to measure network generalization, and to halt training when generalization stops improving. Finally, the remaining 15% of the data was used to test the network thus providing an independent measure of the network performance during and after training. For the ARMA and the benchmark persistence approach, the same data was utilised in developing the forecast, however, a more detailed account of these methods is provided in the latter discussion for each of these.

2.2.1. Input variables selection for all prediction methods

The prediction accuracy of the proposed methods is dependent on the combination of weather predictor variables and training algorithm (Yadav & Chandel, 2014). This is

particularly pertinent, as one of the key tasks in time series prediction is the selection of the input variables and the choice of variables depends on data availability, its quality and their correlation. To provide a sound analytical basis for the choice of variables, a statistical analysis was carried out to check the correlation of each input variable with global solar irradiance. The Pearson correlation coefficient (R) is a measure of the linear correlation between two variables, giving a value between +1 and -1 inclusive, where 1 is total positive correlation, 0 is no correlation, and -1 is total negative correlation. MATLAB neural network toolbox was used to perform the regression analysis. Regression takes cell array or matrix targets (T) and output (Y), each with total matrix rows of N , and return the linear regression for each of the N rows. Here a feedforward network was trained and regression performed on its targets and outputs. The R values for each input variable with respect to global solar irradiance is shown in Table 1.

Table 1. Regression values for input weather variables vs global solar irradiance

Input variables	R
Max Temperature (T_{\max})	0.462
Min Temperature (T_{\min})	0.404
Relative Humidity (RH)	0.505
Rain Amount (R_a)	0.055
Solar Zenith Angle (SZA)	0.066
Azimuth (A_z)	0.183
Pressure (P)	0.020
Wind Speed (W_s)	0.002
Wind Direction (W_d)	0.005

From Table 1 it can be seen that RH, T_{\max} and T_{\min} have a reasonable degree of correlation with solar irradiance, while W_s and W_d have almost no correlation. To group the input weather variables, Moody et al., (1995), two-step sensitivity analysis technique was utilized. Once the most significant variables were determined (based on the regression values), twelve significant combinations of the nine weather predictor variables as shown in Table 2 were tested in order to investigate their effect on the accuracy of the global solar irradiation forecast for Auckland.

Table 2. Test cases based on different combinations of input variables

Case	Input Parameters	Case	Input Parameters
1	$T_{\max}, T_{\min}, P, RH, SZA, A_z, R_a, W_s, W_d$	7	P, RH, SZA, A_z, R_a
2	$T_{\max}, T_{\min}, P, RH, SZA, A_z, R_a$	8	T_{\max}, T_{\min}, SZA
3	$T_{\max}, T_{\min}, P, RH, SZA, A_z$	9	$T_{\max}, T_{\min}, P, SZA, A_z$
4	$P, RH, SZA, A_z, R_a, W_s, W_d$	10	RH, SZA, A_z, R_a
5	$T_{\max}, T_{\min}, P, RH, SZA$	11	T_{\max}, T_{\min}, P
6	$T_{\max}, T_{\min}, SZA, A_z$	12	$T_{\max}, T_{\min}, W_s, W_d$

2.2.2. Nonlinear autoregressive with exogenous input (NARX)

Having determined the input variables, a NARX recurrent neural network was developed to forecast future values of global solar irradiation in Auckland, based on the previous values of global solar irradiation and the nine weather predictor variables described. The approach can be expressed mathematically by predicting future values of the solar irradiation time series $y(k)$ from past values of that time series and past values of the weather predictor variables time series $x(k)$. This NARX approach is based on the linear ARX approach that is commonly used in time-series modelling and can be

represented by Equation (1), where the next value of the dependent output signal (global solar irradiation) $y(k)$ is regressed on previous values of the output signal and previous values of an independent input signal (historic weather data).

$$y(k) = f\left(y(k-24), y(k-25), \dots, y(k-n_y), x(k-24), x(k-25), \dots, x(k-n_x)\right) \quad (1)$$

The NARX approach is implemented using a feed-forward neural network to approximate the function f . A diagram of the resulting network is shown in Figure 2, where the $y(k)$ output series is predicted from past values of $y(k)$ and another input series $x(k)$.

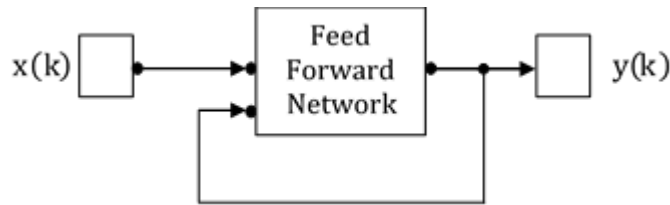


Figure 2. NARX block diagram

There are different connection styles and learning algorithms in neural networks, the most common being the back propagation algorithm. The back propagation algorithm consists of two phases: a training phase and recall phase (Fatih et al., 2008). Before the training phase starts, the weights of the network are randomly initialized. Then the output of the network is calculated and compared to the desired value. At each step during training, error of the network is calculated by means of gradient methods and used to adjust the weights of the output layer (Haykin, 1998). In the case of more than one network layer the error is propagated backward to adjust the weights of the previous layers. Once the weights are determined, after several training steps and correlation between different combinations of input variables with targets are finalized, the recall

phase may run. In doing this the network output computations are performed using finalized iterations of input data and weights from the training phase.

The training phase is important as it determines the success of the resulting network. In back propagation, there are two methods of updating the weights. In the first method, weights are updated for each of the input patterns using an iteration method. In the second method, used in this study, the mean value of input and output patterns of the training sets is calculated (Yousefizadeh & Zilouchian, 2001). As soon as the weight update values are obtained, the new weights and biases can be calculated using Equation (2).

$$W_{ij,n} = U_n + \alpha W_{ij,n} - 1 \quad (2)$$

where $W_{ij,n}$ is a vector of current weights and biases, α is the momentum factor rate which determines how the past weights will reflect to the current value, and U_n is the update function which can be chosen according to the problem and data type.

According to Fatih et al., (2008) and Yousefizadeh & Zilouchian, (2001) the most commonly used equation solving algorithm is the LM algorithm. It can be considered as an alternative to the conjugate methods for second derivative optimization. In LM, the update function, U_n can be calculated using Equation (3).

$$U_n = -[J^T \times J + \mu I]^{-1} \times J^T \times e \quad (3)$$

where J is the Jacobian matrix that contains the first derivatives of the network errors with respect to the weights and biases, and e is a vector of network errors. The parameter μ is a scalar number and I is the identity matrix. Depending on when the μ parameter is large, the update function U_n becomes identical to the basic back propagation (with a small step size). During processing the μ value decreases after each successful

step and should be increased only when a tentative step increases the error term or performance function. Consequently, the performance function is guaranteed to reduce or to become bounded at each iteration (Martin & Mohammad, 1994).

In order to determine the performance of developed ANNs quantitatively, and verify whether there was any underlying trend in performance of the ANNs, the regression (R) and root mean squared error (RMSE) values were analysed. The root mean squared error (Equation 4) provides information on the short term performance and is a measure of the variation of predicated values around the measured data, where the lower the RMSE, the more accurate is the estimation.

$$RMSE = \sqrt{\frac{1}{N} \sum_{i=1}^N (I_p - I_i)^2} \quad (4)$$

where I_p is the predicted solar irradiance in MJ/m^2 , I_i is the measured solar irradiance in MJ/m^2 , and N denotes the number of observations.

2.2.3. Number of hidden neurons and delays

Now in developing a NARX ANN there is an important trade-off to be made between the size and the predictive capability of the network. If the number of neurons or number of delays is increased, the network has the tendency to over-fit the data and allows the network to solve more complicated problems but on the other hand requires more computation. Therefore, the effect of changing the number of neurons in the hidden layer, increasing and decreasing the number of delays was also investigated. During experiments, both the number of neurons in the hidden layer and the number of delays in the tapped delay lines were increased until the network performed well in terms of the

root mean square error and the regression values. Using tapped delay lines in the network is essential as it stores previous values of $x(k)$ and $y(k)$ sequences. The number of hidden neurons, network delays and time steps for training, validation and test were varied to determine which network exhibited the best performance.

In this respect, an initial network was developed with the minimum number of neurons and this the number was increased until the network performed well in terms of the root mean square error and regression values. During this phase, each proposed configuration was trained multiple times to stabilize the weight initialization process and deliver the best accuracy in the shortest processing time. As such, networks with up to 250 neurons were examined as part of this sensitivity analysis, however, it was found that a network of 90 neurons was more than adequate, as beyond this the computing time of the network increased significantly without significant increase in the accuracy, similarly delays between 1 and 5 were also tested.

Computing time was observed and it was noted that time increased with increasing numbers of neurons or delays. However, after several trials, it was decided that the most suitable network, considering accuracy and computing time, had 90 hidden neurons and 2 delays in the tapped delay lines. The reason computing time was closely monitored, was because if the approach was to be implemented on a standalone hardware platform, such as a solar controller, processing power and memory would be limited compared to desktop resources. Using the weather data for Auckland from Case 2 as an example, Table 3 shows the RMSE and R values for various numbers of neurons in the hidden layer.

Table 3. RMSE, R and computing time values for different numbers of neurons and delays using Case 2 weather data

Number of Neurons	Number of Delays	RMSE (MJ/m ²)	R	Computing Time (min: sec)
5	2	0.287	0.950	00:20
10	2	0.277	0.951	00:24
20	2	0.274	0.952	00:22
30	2	0.266	0.955	00:48
40	2	0.257	0.957	00:53
50	2	0.263	0.956	00:50
50	3	0.249	0.964	01:02
90	2	0.243	0.963	01:20
90	3	0.232	0.966	02:20
90	5	0.221	0.969	04:42
150	2	0.251	0.963	02:02
200	2	0.251	0.963	04:33
250	2	0.247	0.964	05:10

2.2.4. NARX results

To validate the approach used, the root mean squared error (RMSE) performance function was examined during the training phase. Network training could be stopped early by the validation vectors if the network performance on the validation vectors failed to improve or remained the same, as indicated by an increase in the root mean square error of the validation samples. Test vectors were used as a further check that the network was generalizing well, but did not have any effect on training. The best validation performance for the Auckland weather data shown in Case 2 was 0.2699 MJ/m² at epoch 9 (a measure

of the number of times all of the training vectors are used once to update the weights) with seven input variables.

Further, the network outputs with respect to the target for training, validation, and test sets are shown in Figure 3. The dashed line in each axis represents the perfect result, that is: outputs = targets. The solid line represents linear best fit between the outputs and targets. For this problem, the fit is reasonably good for all data sets, with the overall regression values as high as 0.963.

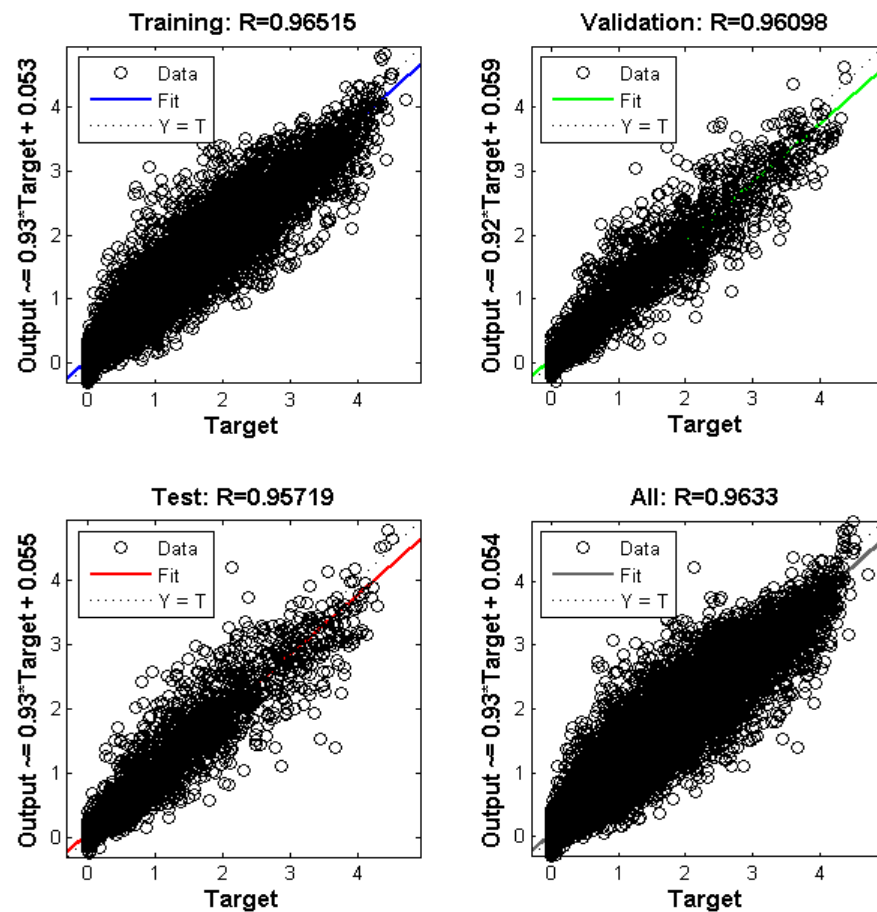


Figure 3. Regression analysis of the network outputs with respect to targets for training, validation and test sets

For the twelve cases described in Table 2, the NARX network architecture with LM training algorithm was trained, validated and tested. Values of RMSE and regression were closely monitored to find the best approach; Table 4 shows the RMSE and R values for 90 neurons in the hidden layer.

Table 4. RMSE and Regression values for all 12 NARX networks

Case	RMSE (MJ/m ²)	R	Case	RMSE (MJ/m ²)	R
1	0.259	0.956	7	0.270	0.953
2	0.243	0.963	8	0.270	0.953
3	0.257	0.957	9	0.259	0.956
4	0.266	0.953	10	0.274	0.952
5	0.268	0.953	11	0.280	0.949
6	0.261	0.956	12	0.277	0.950

Figure 4 illustrates this point further, by showing the forecast for an arbitrarily selected single day, that for the first three cases there is correlation between the measured and NARX forecast values for global solar irradiation in Auckland. However, in Table 4, it can be seen that Case 2 has the lowest RMSE among all 12 configurations, with a 0.243 MJ/m² RMSE and a 0.963 regression value. As shown in Table 2, all twelve cases have different combinations of weather variables. The combination of weather variables in Case 2 produces lower RMSE values as compared to other combinations. Further, RMSE values for all the prediction methods were compared with a benchmark persistence approach and RMSE values lower than the persistence approach was considered as acceptable in this study.

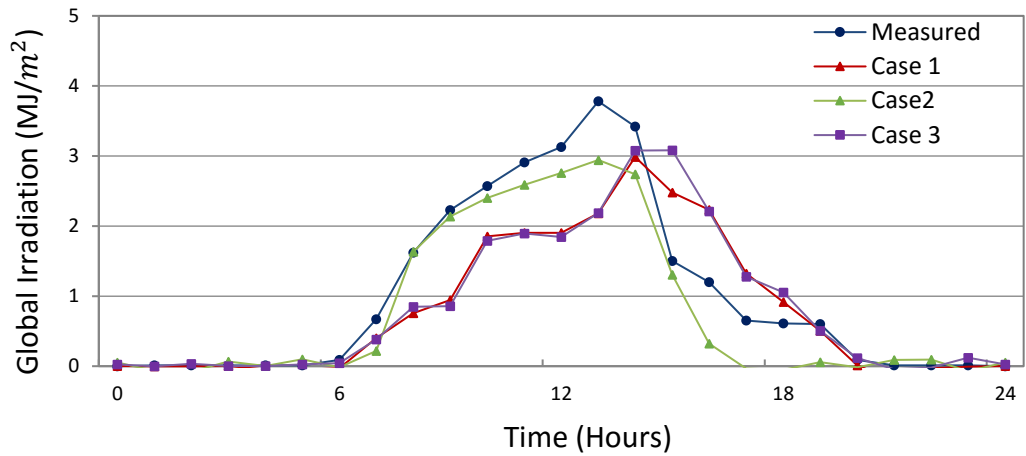


Figure 4. Measured and predicted irradiation values for Auckland using NARX ANN

Exploring the predictive capability of the NARX architecture further, Figure 5 shows a randomly selected one week forecast of global solar irradiation in Auckland using the weather data from Case 2, presented earlier. It can be seen that over this single week, that the NARX forecasts the global solar irradiation.

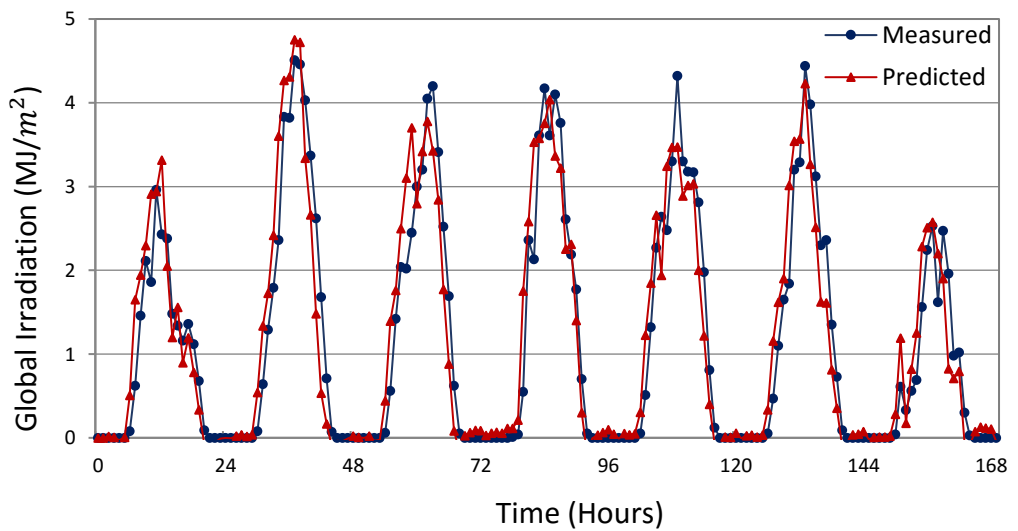


Figure 5. Measured and predicted solar irradiation values using NARX ANN

2.2.5. Other forecasting techniques

Having developed an appropriate NARX ANN forecasting system for Auckland, it was decided to benchmark this approach against three other common forecasting approaches: A Multilayer Perceptron ANN (MLP), an Auto Regressive Moving Average (ARMA) prediction and a benchmark persistence forecast to provide a comparative assessment of their forecasting abilities in Auckland.

2.2.6. Multilayer perceptron (MLP)

MLP is a feed forward ANN approach that maps a set of input data onto a set of appropriate output data. An MLP is made of several layers: one input layer, one or several intermediate layers and one output layer as shown in Figure 6. Neurons in input layer only act as buffers for distributing the input signals x_i ($i = 1, 2, \dots, n$) to neurons in the hidden layer. As shown in Figure 7, each neuron j in the hidden layer sums up its input signals x_i after weighting them with the strengths of the respective connections w_{ji} from the input layer and computes its output y_i as a function f of the sum given by Equation (5).

$$y_i = f\left(\sum_{i=1}^n w_{ji}x_i\right) \quad (5)$$

f can be a simple threshold function or a sigmoidal, hyperbolic tangent or radial basis function.

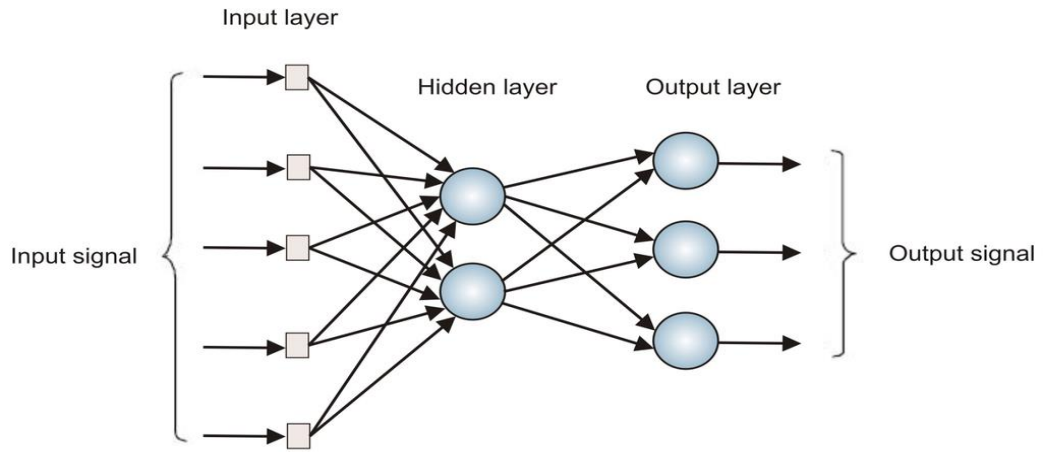


Figure 6. Multi-layered perceptron (MLP) network

In most cases, a single neuron is of no interest however, interconnected single neurons build a network of neurons that can solve complex problems such as classification, pattern recognition and time series prediction. The output of neurons in the output layer is computed similarly and the backpropagation and gradient descent are the most commonly adopted MLP training algorithm. The MLP gives the change Δw_{ji} the weight of a connection between neurons i and j as given by Equation (6).

$$\Delta w_{ji} = \eta \delta_j x_i \quad (6)$$

where η is a parameter called the learning rate and δ_j is a factor depending on whether neuron j is an input neuron or a hidden neuron.

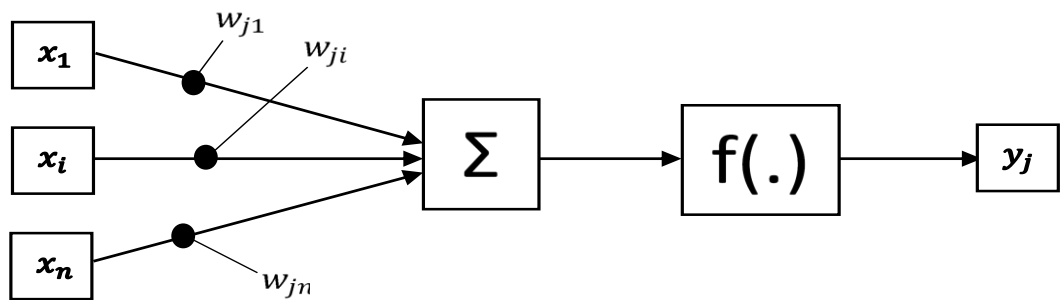


Figure 7. Detail of the perceptron process

For output neurons, Equation (7) applies, where net_j is the total weighted sum of input signals to neurons j and $y_j^{(t)}$ is the target output for neuron j .

$$\delta_j = \left(\frac{\partial f}{\partial net_j} \right) (y_j^{(t)} - y_j) \quad (7)$$

And for hidden neurons as there are no target outputs Equation (8) applies, where the difference between the target and actual output of a hidden neurons j is replaced by the weighted sum of the δ_q terms already obtained for neurons q connected to the output of j .

$$\delta_j = \left(\frac{\partial f}{\partial net_j} \right) (\sum_q w_{jq} \delta_q) \quad (8)$$

The process begins with the output layer, the δ term is computed for neurons in all layers and weight updates determined for all connections, iteratively. The weight updating process can happen after the presentation of each training pattern (pattern-based training) or after the presentation of the whole set of training patterns (batch training). Training the epoch is completed when all training patterns have been presented once to the MLP.

A commonly adopted method to speed up the training is to add a ‘‘momentum’’ term to Equation (9), which effectively lets the previous weight change influence the new weight change

$$\Delta w_{ij}(I + 1) = \eta \delta_j x_i + \mu \Delta w_{ij}(I) \quad (9)$$

where $\Delta w_{ij}(I + 1)$ and $\Delta w_{ij}(I)$ are weight changes in epochs $(I + 1)$ and (I) , respectively, and μ is the “momentum” coefficient (Jayawardena & Fernando, 1998). Using the weather data from Case 2, presented earlier, Figure 8 shows a randomly selected one week forecast of global solar radiation in Auckland using the ANN based MLP architecture. RMSE for the ANN based MLP approach was found to be $0.484 \text{ MJ}/\text{m}^2$ and it can be seen that, in general, the MLP network is able to provide a reasonable forecast of the future irradiation values when compared with the benchmark persistence approach.

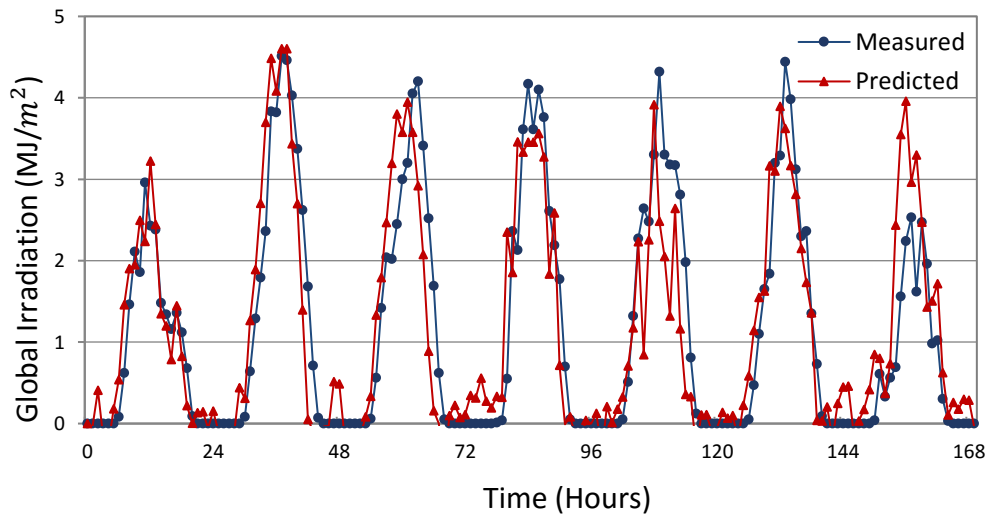


Figure 8. Measured and predicted solar irradiation values using an MLP ANN

2.2.7. Auto regressive moving average (ARMA)

ARMA is a type of the time-series analysis that can be used in situations that deal with a large amount of observed data from the past. The ARMA system is developed using Equation (10) and consists of two parts, the auto-regressive (AR) part and the moving average (MA) part.

$$S(k) = \sum_{i=1}^p \alpha_i S(k-i) + \sum_{j=1}^q \beta_j e(k-j) \quad (10)$$

where $S(k)$ is the forecasted solar irradiance at time instant k . In the AR part, p is the order of the AR process, and α_i is the AR coefficient. In the MA part, q is the order of the MA error term, β_j is the MA coefficient and $e(k)$ is the white noise that produces random uncorrelated variables with zero mean and constant variance (Rajagopalan & Santoso, 2009). Typically, this method requires large amount of historical data to obtain the ARMA, that is, to find the orders p , q and the coefficients α_i and β_j . In addition, due to the geographical differences, each location requires its own unique coefficients. Based on the given historical data, the construction of the ARMA for each location consists of two phases, identifying the orders p , q and determining the coefficients α_i and β_j .

The mathematical methods of finding the orders and coefficients of the ARMA architecture are introduced in Torres et al., (2005). The order identification is proposed by Daniel & Chen (1991), and coefficients determination is calculated by applying the Yule-Walker relations for i and the Newton-Raphson algorithms for j .

The ARMA approach was implemented using the MATLAB System Identification Toolbox using the same three years of historical data used for ANN based NARX and MLP approaches. Orders and coefficients for the ARMA model were calculated, as shown in Table 5.

Table 5. Orders and coefficients of the realized ARMA system

p	q	α_i	β_j
2	3	$\alpha_1 = -1.662$ $\alpha_2 = 0.7856$	$\beta_1 = -0.3223$ $\beta_2 = 0.6074$ $\beta_3 = 0.0591$

Utilising these parameters the global solar irradiance in Auckland was forecasted using Equation (11) giving the results for a single week (as used in the MLP forecast) as shown in Figure 9, with a RMSE of $0.315 \text{ MJ}/\text{m}^2$. From this it can be seen that on the first and seventh day the ARMA forecast values vary considerably from the actual data, while on days 2-6 the forecasted values resemble the actual data. From this it can be suggested that the ARMA approach performs well on a sunny days and its accuracy decreases with increasing clouds cover.

$$S(k+h) = \sum_{i=1}^p \alpha_i S(k-i) + \sum_{j=1}^q \beta_j e(k-j) \quad (11)$$

where $S(k+h)$ is the forecasted solar irradiance at time $k+h$.

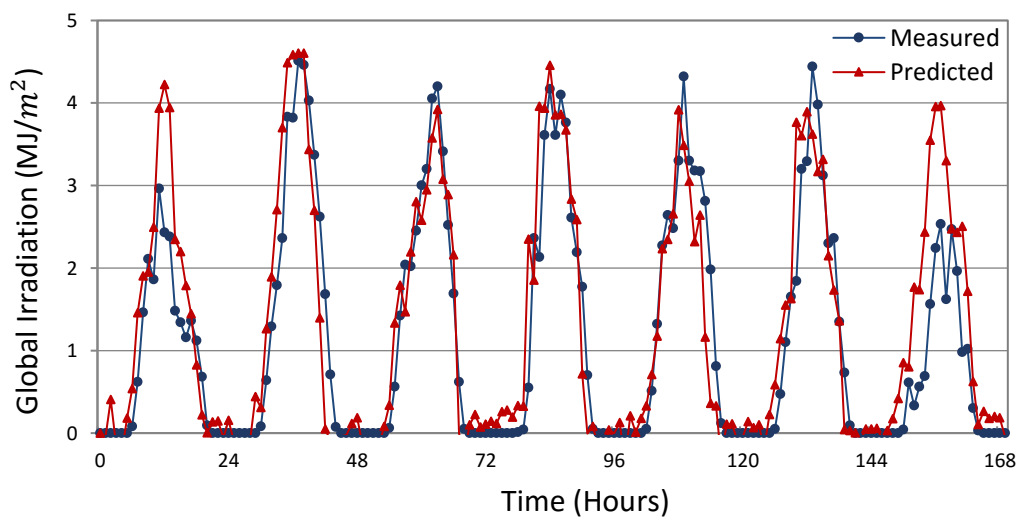


Figure 9. Measured and predicted solar irradiation values using ARMA

2.2.8. Persistence forecasting approach

As a benchmark study, a persistence forecast was developed using Equation (12) to provide the day-ahead forecast ($h = 24$ hours).

$$S(k + h) = S(k) \quad (12)$$

where $S(k + h)$ is the forecast solar irradiance at time $k + h$.

Figure 10 shows a one week forecast of global solar irradiance in Auckland using a persistence approach and the same data used for the MLP and ARMA systems. The average RMSE for the benchmark persistence forecast was found to be $0.514 \text{ MJ}/\text{m}^2$, which was the highest of all the prediction methods discussed. It can be seen in Figure 10 that the persistence model performs well on days 3, 4, 5 and 6 whereas the forecasted values for days 1, 2, and 7 vary considerably from the actual data.

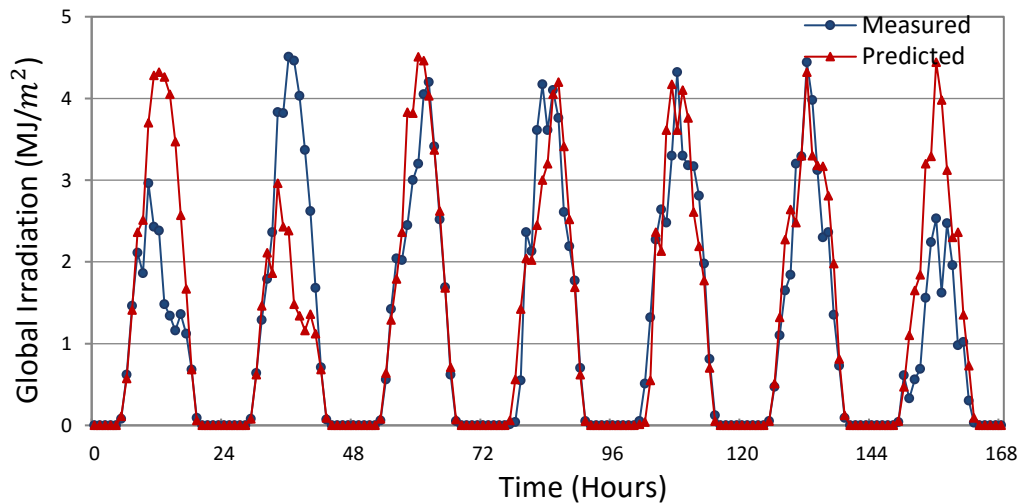


Figure 10. Measured and predicted solar irradiation values using a benchmark persistence approach

2.3. Results

2.3.1. Comparison of methods

In the previous section a discussion of each method was presented and some broad findings were presented, where the same three years of measured data used for the ARMA, MLP and NARX approaches were utilized, with global solar irradiation as the objective function. For each forecast approach the root mean square errors were closely monitored to quantify the performance of the approach and assess their accuracy. Now, Table 6 shows the RMSE and nRMSE values using Equation (4) and (13) respectively for all four approaches, where the same number of hourly data (26363 samples) points for the input variables and the target variable (Global Solar Irradiance) were used to forecast the day ahead solar irradiance in MJ/m^2 for a single year.

$$nRMSE = \sqrt{\frac{1}{N} \sum_{i=1}^N \frac{(I_i - I_p)^2}{I_{i,max}} - I_{i,min}} \quad (13)$$

where I_p is the predicted solar irradiance in MJ/m^2 , I_i is the measured solar irradiance in MJ/m^2 , and N denotes the number of observations.

Table 6. RMSE and nRMSE values for all forecasting approaches

Approach	RMSE (MJ/m^2)	nRMSE (MJ/m^2)
MLP	0.484	0.0968
NARX	0.243	0.0495
ARMA	0.315	0.0656
Persistence	0.514	0.0901

From Table 6 it can be seen that the ARMA approach performs well in terms of the weekly RMSE value. Similarly, it was previously demonstrated that the MLP approach performed well for certain days but the RMSE value increases as the number of data sets increases due to the feed-forward architecture of the approach, this is borne out by its poor RMSE. In contrast the NARX approach appears to perform well in terms of short term and long term forecasting, and has the lowest weekly RMSE of the forecasting approaches tested.

To illustrate this point further, Figure 11 shows an example of the day ahead solar irradiation forecast and measured data curves for all four methods for 1 January 2014 in Auckland. From this it can be seen that the NARX forecast closely follows the actual measurements, whereas the benchmark persistence forecast shows a significant under-prediction.

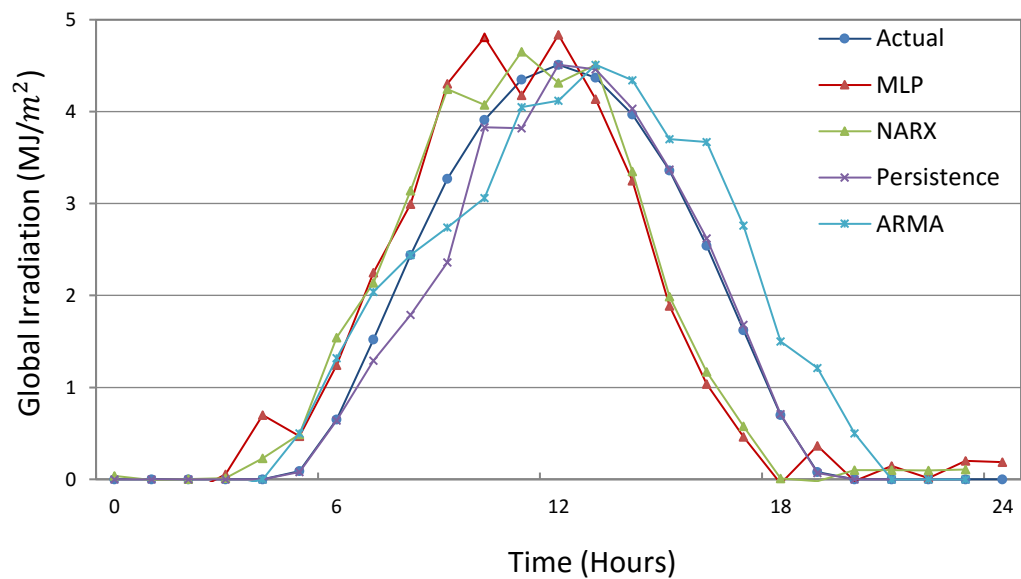
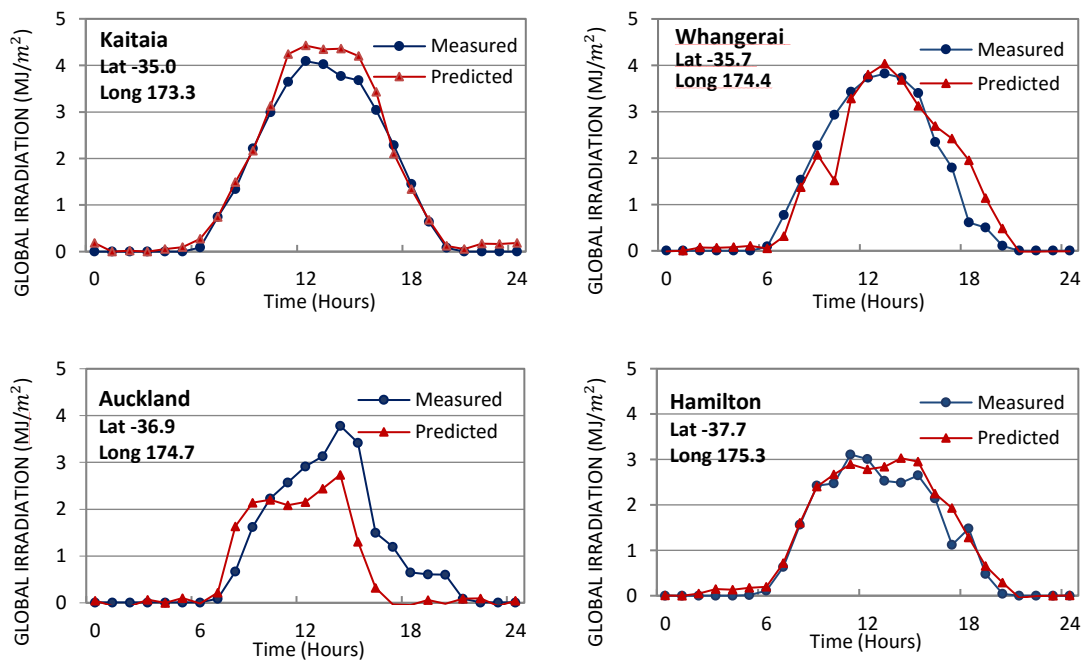


Figure 11. Day ahead solar irradiation forecast and actual data for Auckland on 1 January 2014

2.3.2. Irradiation prediction for New Zealand cities

Having determined the most suitable method for forecasting solar irradiation for Auckland, the NARX based Case 2 (as given in Table 2 and trained with data from each location) was used to predict global solar irradiation in ten cities across New Zealand. Figure 12 shows the forecast and measured results for a common single arbitrary day from a one-week prediction horizon. Though there is a degree of variation for some locations, as a result of choosing a common single day rather than the best day. More work is needed to investigate, why global solar radiation prediction and actual values differ towards the lower South Island of New Zealand. It can be seen that using real data to train the ANN gives predicted values of global irradiation similar to those measured for the majority of the locations. In this regard, it suggests that recurrent NARX with the LM training algorithm offers a suitable predictive tool for global irradiation in New Zealand. Moreover, it shows that training neural networks with real data can deliver satisfactory prediction of the output variable, in this case the solar irradiation.



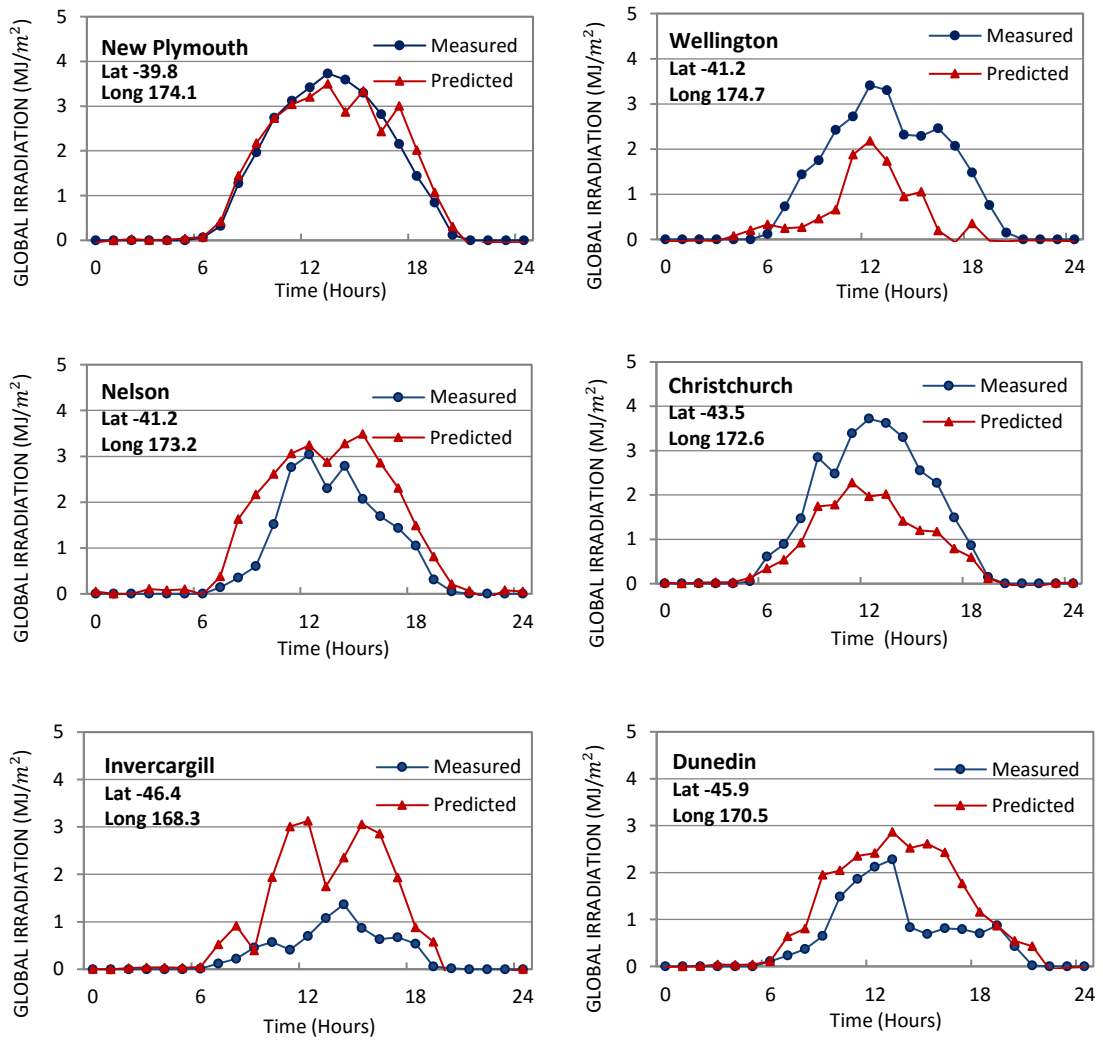


Figure 12. Predicted irradiation for New Zealand cities

2.4. Summary

The need for improved solar controllers necessitates the ability of such devices to have an understanding of the future magnitude of the solar resource. This work has examined possible ways in which this can be achieved, with particular reference to a NARX ANN forecasting method. In testing the methods input and target data were used unprocessed to study the real effects of input variables on outputs. Based on an analysis of the root mean squared error, regression and time series response, a NARX approach was proposed as a means to forecast global solar irradiation values at a later time.

Subsequently, the NARX architecture was used to successfully forecast global solar irradiation in ten major cities across New Zealand. These results have demonstrated the generalization capability of this approach and its ability to produce forecasts for global irradiation that can be translated to a number of diverse locations. On this basis it is conceivable that such a NARX ANN forecasting approach could be embedded into model predictive controllers to better manage the energy generated by solar energy systems.

Chapter 3. HOURLY ENERGY CONSUMPTION PREDICTION FOR A PREDICTIVE CONTROLLER

3.1. Introduction

Previously it was noted that one element of a predictive controller could be a solar forecasting system. Similarly, prediction of energy consumption would allow the capability of such controllers to be further enhanced. One reason for this is that predicting electricity consumption 24 hours in advance would help optimize energy distribution between loads, particularly in buildings, and the local grid. Energy consumption prediction is essential for generators, wholesalers and retailers of electric energy, who buy and sell, switch loads, plan maintenance and unit commitment and much more. However, with increasing costs being passed to consumers, there is also a need for consumers to be able to predict their requirements with a view to better utilizing on-site generators such as photovoltaic panels and grid-tied storage systems, thus delivering intelligent buildings.

In Flax, (1991) an intelligent building was defined as the one which maximizes the efficiency of the service and minimizing the use of grid energy. The author lists intelligent building components, with the energy management system (EMS) ranked most highly. Such a system controls and monitors energy consumption of the building. However, for effective operation of an EMS, an accurate prediction of energy consumption is needed. Such a system would ideally be able to plan and take actions to avoid power shortages, as well as shift loads to off peak time when electricity prices are lower.

In this regard, short-term load prediction has attracted significant attention from scientists and engineers. Various mathematical techniques have been widely used for load energy consumption prediction including regressive analysis, wavelet analysis, fuzzy system modelling, neural network modelling and evolutionary algorithms (Xia et al., 2010). There are also a large variety of models presented in the literature, both simple and hybrid, created by combining two or more approaches (Maia & Goncalves, 2009; Niu et al., 2009). These models are attractive because some physical interpretation may be attached to their components, allowing engineers and system operators to understand their behaviour. However, they are basically linear devices, and the load series they try to explain are known to be distinctly nonlinear functions of the exogenous variables.

In recent years, much research has been carried out on the application of ANN techniques to the load energy demand forecasting problem. As such, expert systems have been tried out (Ho et al., 1990; Rahman & Hazim, 1993), and compared with traditional methods (Moghram & Rahman, 1989). The advantage of using ANN as compared to the other models is the ability to extract the implicit non-linear relationships among the variables by means of “learning” with training data. Many interesting ANN applications have been reported in power system areas, due to their computational speed, their ability to handle complex non-linear functions, robustness and great efficiency, even in cases where full information for the studied problem is absent. Also it appears that the use of ANN for load forecasting has been well accepted in practice, and is used by many utilities (Khotanzad et al., 1998). On this basis, it appears that ANN may be able to play a part in forecasting loads in a domestic situation with this to be incorporated into an advanced controller for a domestic energy system.

3.2. Methodology

Given the capabilities of ANN as a forecasting tool it was decided to try and predict the electricity consumption in a typical NZ residential house with four occupants (2 adults & 2 children), 24 hours into the future. Having shown the generalisability of ANN's to radiation forecasting it is likely that a similar model could be used for forecasting electricity usage at a range of locations and with a varying number of household occupants.

3.2.1 Persistence model

As a benchmark study, the persistence model was developed using Equation (14) to predict the h hour-ahead forecasting ($h = 1, 2, 3, \dots$ hours).

$$S(k + h) = S(k) \quad (14)$$

where $S(k + h)$ is the forecasted electricity consumption at time $k + h$.

The same three years measured data for eight weather variables used for the ANN models were utilized for the persistence model, with electricity consumption prediction as the objective function. RMSE, as defined in Equation (14), was calculated to validate the prediction method and compare the model performance. Figure 15 shows a comparison of the benchmark persistence model prediction with the measured data.

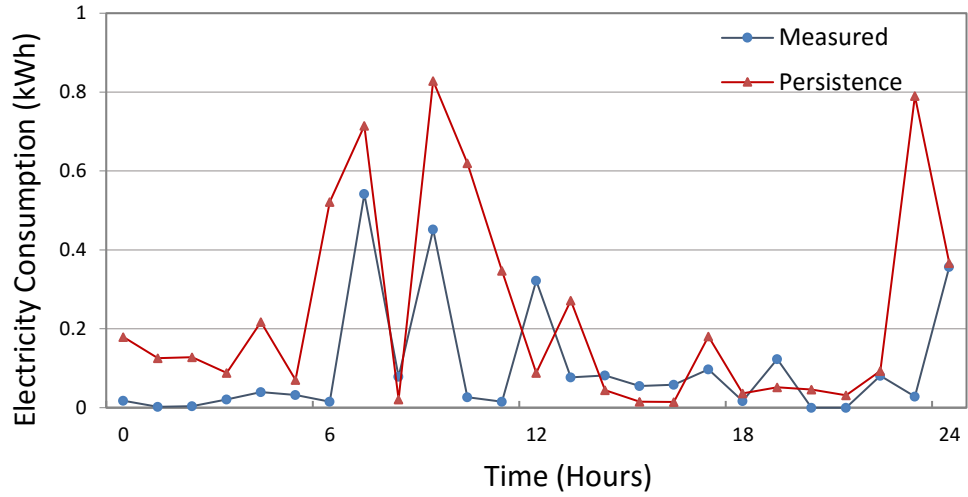


Figure 13. Measured and predicted load values using the benchmark persistence model with RMSE = 0.486 kWh

3.2.2 Nonlinear autoregressive with exogenous input (NARX)

Nonlinear autoregressive recurrent neural network with exogenous input (NARX) based predictive models were developed to forecast future values of electricity consumption, based on the previous values of electricity consumption and eight input variables (Temperature (T_{air}), Barometric Pressure (P), Relative Humidity (RH), Rain amount (R_a), Wind speed (W_s), Wind direction (W_d), Hour of the Day (HD) and Day of the Week (DW)). The predictive model can be expressed mathematically by predicting future values of the electricity consumption time series $y(k)$ from past values of that time series and past values of input variables time series $x(k)$ as expressed in Equation (1).

Three years of hourly data for eight input variables along with three-years hourly electricity consumption data from a residential house in Auckland were used as inputs to the ANN. Input weather data were downloaded from the National Institute of Water and Atmospheres CliFlo database, (2014) to train the ANN with electricity consumption as the target variable.

The data was presented in an unprocessed format, to study the effect of real input variables on target to predict the output. Input and target data were used to train, validate and finally, test the network ability to predict 24 hours in advance electricity consumption for a residential house with four occupants.

As there were 256 possible combinations of eight weather predictor variables, testing the network with all combinations was taking a long time. Therefore, Moody et al., (1995), two-step sensitivity analysis technique was utilized to determine the most significant training variables. Once the most significant variables were determined, the network was trained with every selected variable, until the training error was minimized and the influence of each variable was removed by replacing it with its mean value or zero. To simplify the process, the twelve most significant combinations of the eight weather predictor variables were tested in order to investigate their effect on the electricity consumption prediction accuracy, as shown in Table 7.

Table 7. Models based on different combinations of input variables

Model	Input variables	Model	Input variables
1	T _{air} , RH, P, W _s , W _d , R _a , HD, DW	7	T _{air} , RH, W _s , W _d , R _a , HD, DW
2	T _{air} , RH, P, W _s , W _d , R _a , HD	8	T _{air} , P, W _s , W _d , R _a , HD, DW
3	T _{air} , RH, P, W _s , W _d , R _a , DW	9	RH, P, W _s , W _d , R _a , HD, DW
4	T _{air} , RH, P, W _s , W _d , HD, DW	10	T _{air} , RH, HD, DW
5	T _{air} , RH, P, W _s , R _a , HD, DW	11	T _{air} , RH, P, R _a
6	T _{air} , RH, P, W _d , R _a , HD, DW	12	T _{air} , RH, P, HD, DW

In order to determine the performance of developed ANN models quantitatively, and verify whether there was any underlying trend in performance of ANN models, the

regression (R) (Pearsons correlation coefficient) and root mean squared error (RMSE) values were analysed. The root mean squared error (Equation 15) provides information on the short term performance and is a measure of the variation of predicated values around the measured data, where the lower the RMSE, the more accurate the estimation.

$$RMSE = \sqrt{\frac{1}{N} \sum_{i=1}^N (I_p - I_i)^2} \quad (15)$$

Where $I_{p,i}$ is the predicted electricity consumption in kWh, I_i is the measured electricity consumption in kWh, and N denotes the number of observations.

If the number of neurons or number of delays is increased, the network has a tendency to over-fit the data and also allows the network to solve more complicated problems, but on the other hand requires more computation. During experiments both the number of neurons in hidden layer and the number of delays in the tapped delay lines were varied until the network performed well in terms of the mean square error values. Therefore, the effect of changing the number of neurons in the hidden layer, increasing and decreasing the number of delays was also investigated. Using tapped delay lines in the network is essential as it stores previous values of $x(k)$ and $y(k)$ sequences. The number of hidden neurons, network delays and time steps for training, validation and test were varied to determine which network exhibited the best performance. The number of neurons was changed between 10 and 250 and delays between 2 and 5 were tested in order to come up with the most suitable ANN prediction model. Table 8 shows the RMSE and Regression values for various numbers of delays and number of neurons in the hidden layer.

Table 8. RMSE and Regression values for different number of neurons and delays

Neurons	Delays	RMSE (kWh)	R	Processing Time (mm:ss)
10	2	0.255	0.524	00:04
20	2	0.259	0.509	00:06
30	2	0.261	0.528	00:12
40	2	0.263	0.476	00:13
50	2	0.254	0.514	00:18
60	2	0.264	0.472	00:23
60	3	0.259	0.529	00:42
60	4	0.260	0.489	01:05
60	5	0.261	0.508	01:32
70	5	0.252	0.517	01:55
70	2	0.267	0.513	00:26
90	3	0.270	0.479	01:04
90	2	0.269	0.496	00:38
100	2	0.260	0.515	00:50
120	2	0.262	0.486	00:59
150	2	0.279	0.484	01:49
150	4	0.275	0.455	08:58
200	2	0.272	0.469	03:31
250	2	0.275	0.458	04:36

Processing time was also observed and it was noted that time increased exponentially with increasing numbers of neurons or delays. After several trials, it was decided that the most suitable network, considering accuracy and processing time, had 50 hidden neurons and 2 delays in the tapped delay lines. Processing time was closely monitored because if the model were to be implemented on a hardware platform, processing power and memory would be limited compared to desktop resources.

Network training can be stopped early by the validation vectors if the network performance on the validation vectors fails to improve or remains the same, as indicated by an increase in the mean square error of the validation samples. Test vectors are used as a further check that the network is generalizing well, but do not have any effect on training. The best validation performance for Model 4 is 0.0622 at epoch 4 with seven input variables as shown in Figure 13. It is shown that training, validation and testing errors decreased and merges with the dotted line on epoch 4 thus demonstrating the best validation performance.

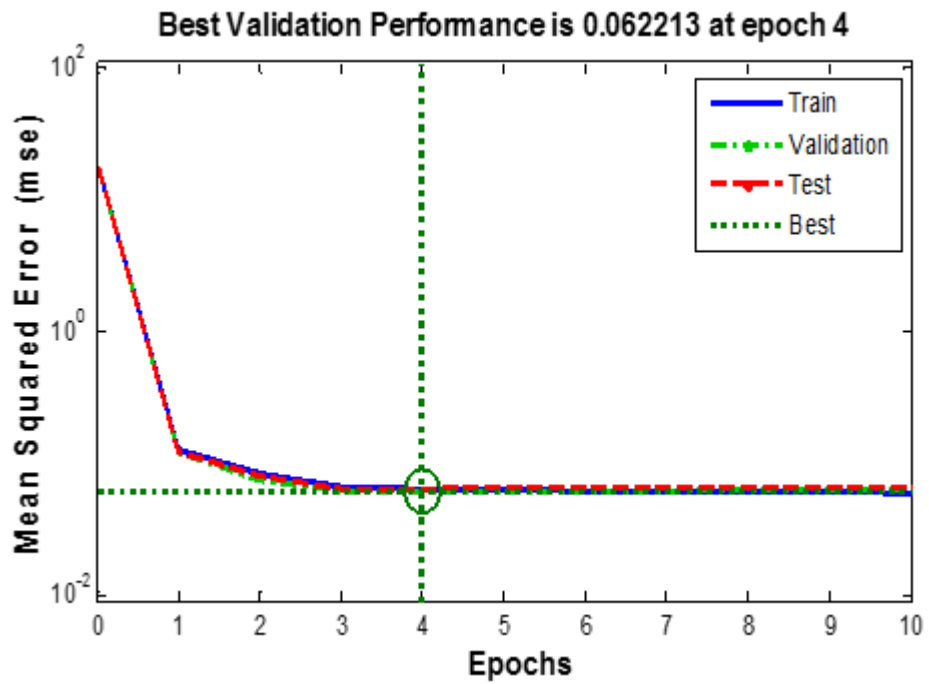


Figure 14. Mean Square Error (MSE) performance of the network

For the twelve models described in Table 7, the NARX network architecture with LM training algorithm was trained, validated and tested. Values of RMSE and regression were closely monitored to find the best model; Table 9 shows the RMSE and regression values for 50 neurons in the hidden layer with 2 delays in the tapped layers.

Table 9. RMSE and Regression values for all 12 ANN models

Model	RMSE	Regression (R)	Model	RMSE	Regression (R)
1	0.253	0.514	7	0.264	0.514
2	0.282	0.504	8	0.265	0.487
3	0.263	0.470	9	0.261	0.516
4	0.252	0.527	10	0.259	0.514
5	0.258	0.508	11	0.265	0.491
6	0.261	0.519	12	0.259	0.518

Figure 14 illustrates this point further, by showing for a single day, that for the first six models there is close correlation between the measured and ANN predicted values for electricity consumption in Auckland, when compared with the benchmark persistence approach values. However, in Table 9, it can be seen that Model 4 has the lowest RMSE of 0.252 and highest R value of 0.527 among all 12 models. RMSE and regression values in Table 9 are average of one week prediction horizon and does not directly correspond to the plots in Figure 14.

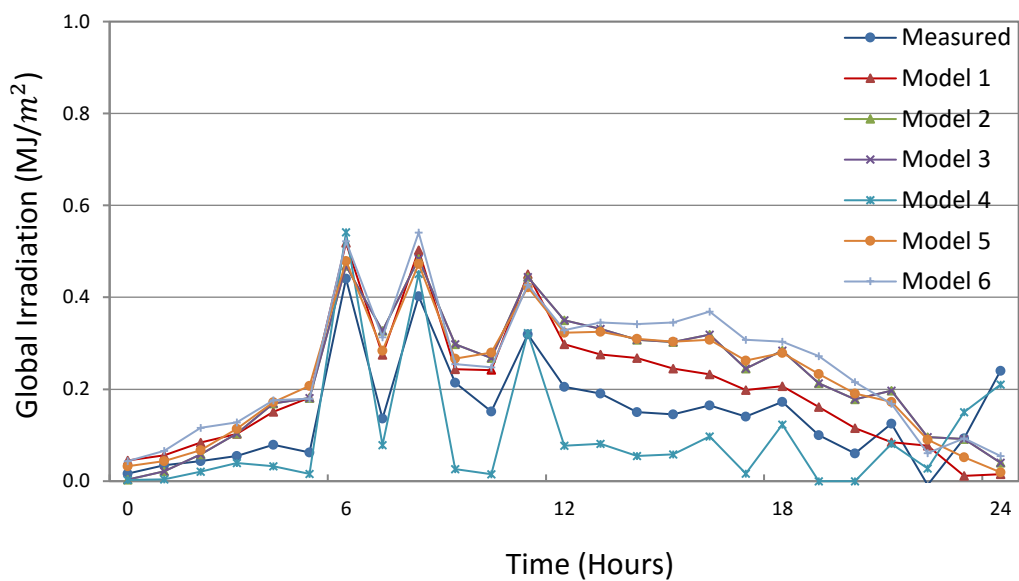


Figure 15. Measured and predicted electricity consumption values for the first 6 models

3.3. Electricity consumption prediction for a residential house

Having determined the most suitable configuration of ANN, Model 4 was used to predict electricity consumption of a house with four occupants (2 adults & 2 children) in Auckland, New Zealand, as shown in Figure 16. In Figure 16, it can be seen that predicting electricity consumption using the proposed NARX approach produces similar consumption pattern to those measured by the electricity meter. In this regard, it suggests

that the ANN with the LM training algorithm offers a suitable predictive tool for electricity consumption. Moreover, it shows that training neural networks with real data can deliver satisfactory prediction of the output variable. Predicting electricity in residential houses is a complex problem and other factors for example users behaviour should be incorporated in the model to improve prediction accuracy.

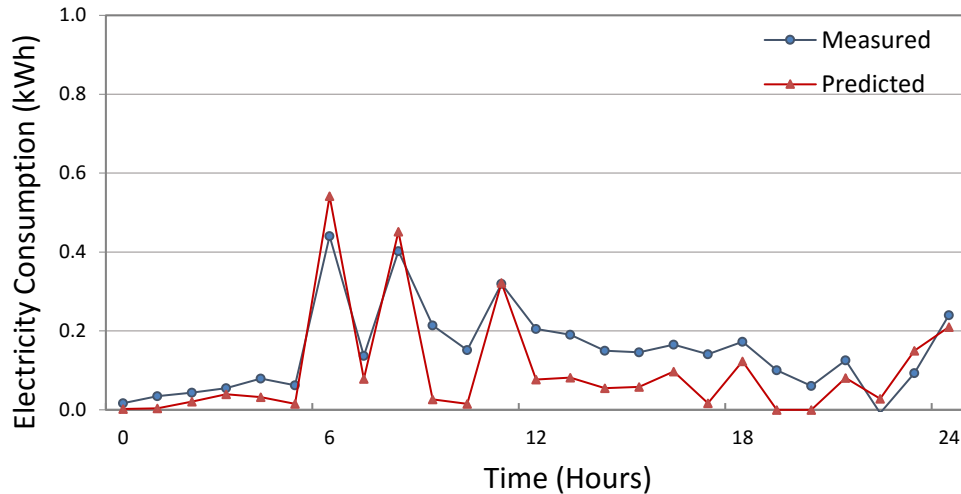


Figure 16. Measured and predicted values for a residential house in Auckland with RMSE = 0.252 kWh using the NARX approach

3.4. Summary

A predictive model based on a recurrent neural network, was developed in this chapter to forecast hourly electricity consumption using three years of historical electricity consumption and weather data. Twelve different combinations of eight weather variables were used to train, validate and test twelve ANN models. Real-time input and target data were used without normalizing to study the effects of input variables on outputs. Subsequently, one model, with the lowest RMSE value, highest regression value and lowest processing time was used to predict electricity consumption for a house with four occupants in Auckland, New Zealand. Predicted values were compared with measured data from the house’s electricity meter and showed similar consumption

patterns. The proposed NARX approach was compared with a benchmark persistence approach and found that the root mean square error with the NARX approach was 0.252 kWh and 0.486 kWh with the persistence approach.

Based on the RMSE and regression analysis, the proposed ANN model illustrated the ability to predict 24 hours ahead electricity consumption patterns for the house. Hence this model has the potential to be implemented in a predictive controller with a view to providing it with knowledge of upcoming energy demand.

Chapter 4. ADVANCED CONTROL DEVELOPMENT

4.1. Overview

In the preceding chapters the use of forecasting methods was examined with a view to providing a controller with knowledge of future energy demand and availability. That said, there is a need for these controllers to manage the interaction of photovoltaic and storage systems with wider electricity distribution networks. The integration of photovoltaic energy systems into the grid has attracted interest due to their many benefits, such as: high reliability, low maintenance, decreasing prices of PV panels and the regulatory incentives established in many countries. However, the disadvantage of these PV energy systems is that solar energy is subject to daily and seasonal variations (Belfkira et. al., 2011). To overcome the intermittent nature of PV based systems, battery storage can be used to store excess solar energy, and to supply energy when the solar energy is not sufficient to satisfy demand.

Sometimes the daily energy demand might be so high that it cannot be satisfied by the PV energy and battery storage together. In this situation, the imbalance must be met by some other means, such as a diesel generator or utility grid (Shaahid & Elhadidy, 2008) and it is this fact that necessitates the development of advanced controllers to manage this situation.

4.2. Predictive control for domestic energy systems

As mentioned previously, a number of control strategies have been applied to energy management in buildings, most commonly rule or scheduled based systems. An attempt to advance this situation was made by Wahab et al., (2011) who used TRNSYS

and Matlab/Simulink for predictive control of a building integrated photovoltaic thermal (BIPVT) energy system. They suggested that further research was needed to design and develop advance predictive control strategies to improve the performance of the overall system.

That said, one particular control strategy that has shown significant promise, but little application to grid connected photovoltaic systems, is model predictive control (MPC). MPC is a method for constrained optimal control, which originated in the late seventies and early eighties in the process industries (oil refineries, chemical plants, etc.) (Richalet, et al., 1976; Maciejowski, 2002; Richalet, et al., 1978; Kwon, 1983). MPC is a class of control methods with the model of the process explicitly expressed in order to obtain a control signal by minimizing an objective function subject to some constraints. In the case of domestic energy system control, one would aim at optimizing the energy delivered (or cost of the energy) subject to comfort and the power system constraints.

The basic idea of MPC is to predict future behaviour using a system model, given measurements or estimates of the current state of the system and a hypothetical future input trajectory. During each sampling interval, a finite horizon optimal control problem is formulated and solved. The result is a trajectory of inputs and states into the future, respecting the dynamics and constraints of the domestic energy system while optimizing an objective function. In terms of domestic energy system control, this means that at the current control step, energy demand and PV energy production measurements are obtained for the next hour. Predictions of any other disturbances (e.g. internal gains), time-dependencies of the control costs (e.g. dynamic electricity prices), solar radiation, electricity demand or of the constraints (e.g. thermal comfort range) can be readily included in the optimization (Cigler, 2013).

The first step of the control plan is applied to the building, then the process moves one step forward and the procedure is repeated at the next time instant. This receding horizon approach is what introduces feedback into the system, since the new optimal control problem solved at the beginning of the next time interval will be a function of the new state at that point in time and hence of any disturbances that have acted on the domestic energy system.

Some attempts have been made to test MPC for small scale distributed power generation systems, including the work of Qi, et al., (2011), which proposed a supervisory control, focused on the optimal management and operation of small-scale hybrid wind-solar energy system. Two local controllers were used to drive the two subsystems to the power references and MPC capability to reduce the peak values of inrush or surge currents was discussed. In Sossan et al., (2013), a model predictive control strategy was utilized to maximize PV self-consumption in a household context exploiting the flexible demand of an electric water heater. The controller used a water heater model and forecast of the hot water consumption in order to predict the future temperature of the water, and managed its state (on and off) according to the forecasted PV energy production. Simulations showed the ability of MPC to move the consumption of the heater to a time when there was energy production from the PV system.

Zhu et al., (2015), developed a switched MPC approach for energy dispatching of a PV-diesel-battery (PDB) hybrid system. Simulation results and comparison with the open-loop optimal control approach showed that the performance of the proposed switched MPC algorithm was satisfactory in dispatching energy usages for the PDB energy system. Diesel energy consumption for the proposed MPC was 63.9 kWh, while 81.4 kWh for the open loop optimal control approach. Similarly, a photovoltaic-diesel-

battery hybrid energy system was proposed in Tazvinga et al., (2013) to supply daily energy requirements in a rural Zimbabwean public clinic. In this case a diesel generator was used to cover the imbalance when PV energy and battery storage could not satisfy energy demand. In this work the diesel generator has not been included, because energy produced by diesel generators is typically costlier than grid energy.

The reasons for MPC in domestic energy systems being rarely used until now are primarily due to the complicated derivation of a correct model for the building that can be used in the MPC controller and the fact that energy cost played a minor role in the past. Using the energy savings potential of buildings, by applying MPC, has become more realistic recently, due to several developments. Computational power of devices has significantly increased during the last decade and the possibility to shift computations to external servers or clouds; the use of simulation tools in building planning are becoming standard and can help to obtain models for the MPC; the accuracy of weather predictions is increasing and hence its usefulness for building climate control. Energy cost is rising, and finally, there is a need to formulate control strategies, which can handle time-varying electricity prices. According to Oldewurtel et al., (2012), MPC has the ability to improve energy efficiency of the building and handle time-varying electricity prices.

Domestic energy systems are subject to intermittent disturbances, i.e. the weather, the energy consumption of building's appliances and the number of occupants, who set demands for temperature, illuminance and air quality. Also, the building dynamics are typically slow which gives rise to a constrained control problem and the goal is to use weather as well as energy demand predictions in order to be able to make appropriate use of the thermal storage capacity of a building, electrical appliances and energy dispatch strategies. Model Predictive Control (MPC) is an ideal framework to tackle this problem

(Oldewurtel et al., 2010). Given that MPC has been widely used in closed-loop control for adaptively changing control variables according to external disturbances (Duran et al., 2011; Barrero et al., 2011; Thomsen et al., 2011). It was decided to examine its application in this work because of its capability to explicitly handle constraints and to adjust the energy flows when disturbances occur.

Figure 17 summarizes the basic principle of MPC for a domestic energy system where time-varying parameters (i.e. the electricity price, the comfort criteria, energy demand prediction, solar radiation prediction and occupancy) are inputs to the MPC. One can see that the modelling and design effort consist of specifying a dynamic model of the domestic energy system, as well as constraints of the control problem and a cost function that encapsulates the desired behaviour. At each sampling interval, these components are combined and converted into an optimization problem depending on the MPC framework chosen.

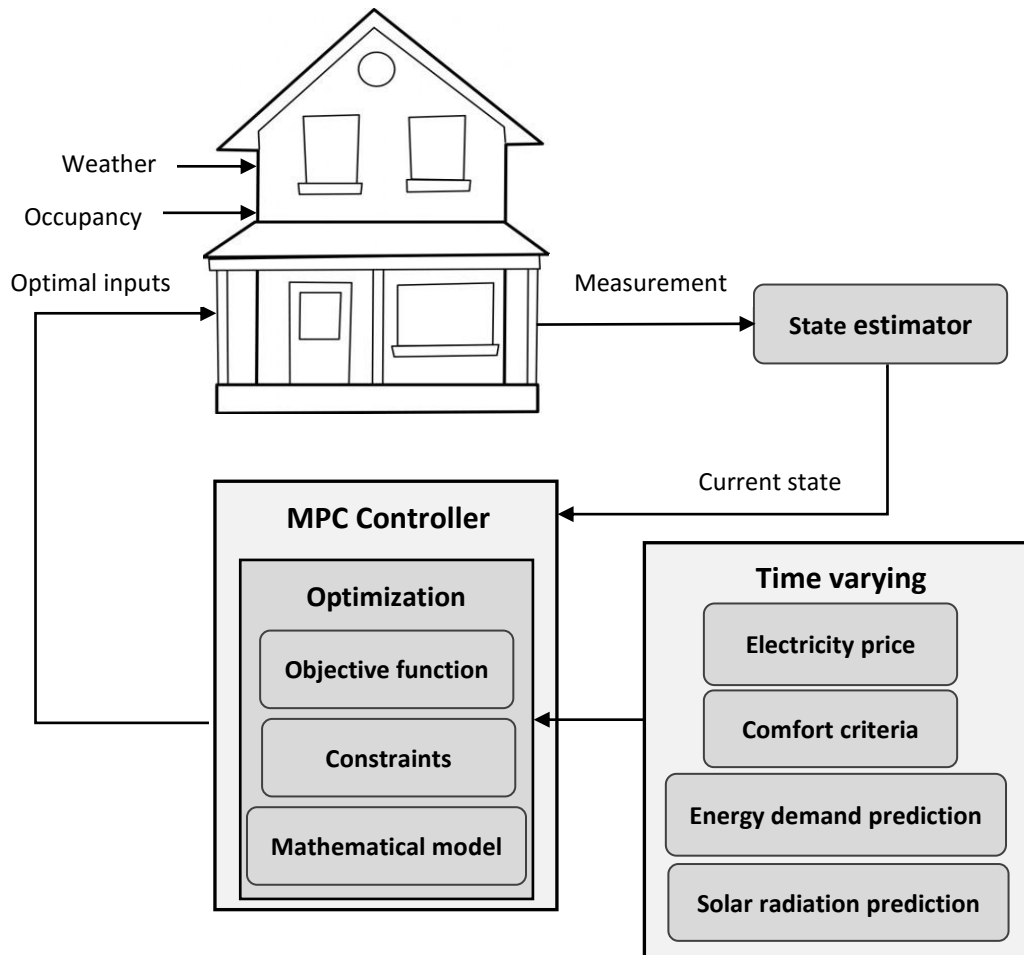


Figure 17. Basic principal of the MPC for buildings

In this work, a photovoltaic-battery-grid system is proposed; where, PV energy and battery storage can be used to cover the energy demand of a residential house. In situations where both the PV array and the battery bank cannot satisfy energy demand; non-critical loads in the house would be deactivated. If the energy demand is still greater than the combined energy available from the PV and battery bank the deficit would be imported from the local grid.

4.3. Structure of the photovoltaic-battery-grid system

In order to achieve the outcome described previously, a model predictive control setup was developed with a view to ensuring PV energy usage within the house is maximized, by storing excess PV energy in the hot water cylinder, rather than exporting available excess energy to the grid. Additionally, grid imports are to be minimized by reducing energy demand in situations where the PV energy and battery storage cannot satisfy demand. In doing this, solar radiation and energy demand predictions are utilized by the MPC to plan in advance for periods of low sunshine or periods of high energy demand.

The overall structure of the proposed PBG system is shown in Figure 18, where future values of global solar radiation and electricity consumption predictions were calculated as discussed in Chapter 2 and 3 respectively. These predictions are made available to the MPC to activate or deactivate non-critical loads and so adjust current energy demand of the house according to the availability or unavailability of the PV energy. Model predictive control uses the energy consumption of the house and the PV array production as reference signals with the objective of the controller being to:

- minimize the difference between the PV array production and the electricity consumption
- to maximize the usage of PV energy within the house
- extend battery life by reducing excessive charge-discharge cycles

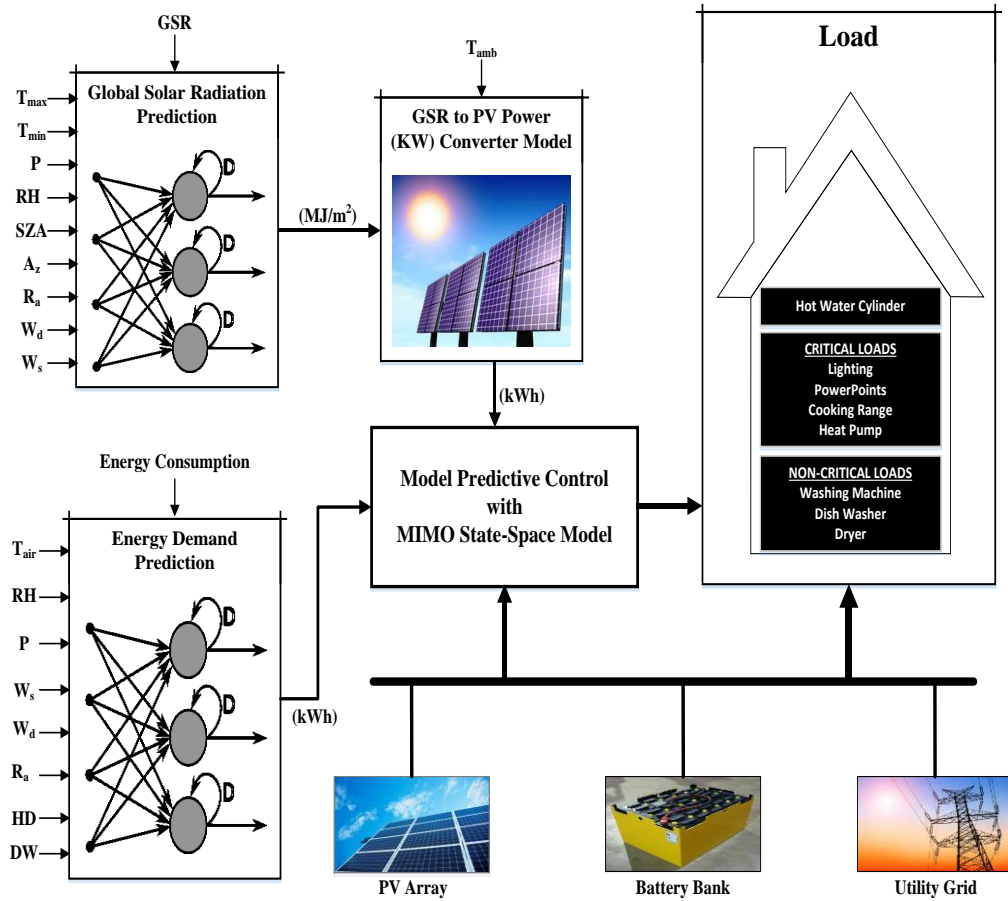


Figure 18. Overall structure of the photovoltaic-battery-grid energy system

At a holistic level the energy dispatching procedures are shown in Figure 19, where the energy from the PV array, battery bank and grid are used to satisfy the load. The arrows in Figure 19 show direction of energy flow in the system. The output energy of the PV array is used to satisfy energy demand of the house and charge the battery bank. At any given time, 80% of the PV energy (E_{PV1}) is used to satisfy the energy demand of the house and 20% of PV energy (E_{PVb}) to charge the battery bank. When the battery bank is fully charged and excess PV energy is available, the temperature in the hot water cylinder is increased using E_{PV2} . Further, if the PV array is still producing more energy than required at any given time, it is exported to the grid as a last priority (represented by E_{PV3}). If energy demand of the house is larger than the PV array production, the energy

requirements should be met by the battery bank using E_b or the grid energy E_g in the case where the battery bank is fully depleted.

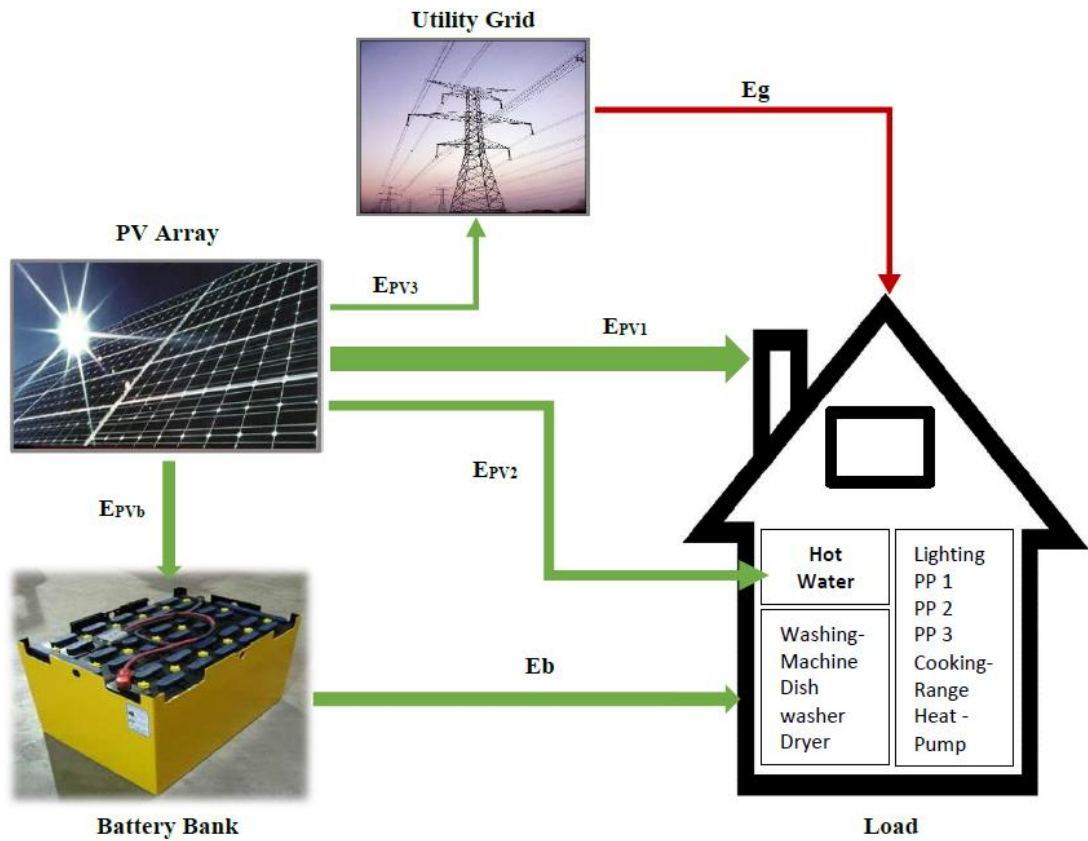


Figure 19. Configuration of the photovoltaic-battery-grid energy system

Hence, several priorities are specified in the MPC design for the PV array energy. E_{PV1} is the PV energy to satisfy energy demand of the house with first priority, E_{PV2} is the PV energy to increase hot water cylinder temperature to its maximum threshold with second priority and E_{PV3} is the PV energy flowing to the grid with third priority. E_{PVb} is the PV energy to charge the battery bank, E_b is battery bank energy to satisfy energy demand of the house when energy from the PV array is not sufficient and E_g is the energy flowing from the grid whenever, energy from both the PV array and the battery bank is not sufficient to satisfy energy demand of the house.

4.4. Outline of the MPC approach and implementation

Following on from this broad description of the system, Figure 20 shows the process flow for the MPC design. In this the model states $x(k)$ are initialized and updated to initial values. Concurrently one-step ahead prediction states for global solar radiation and electricity consumption are initialized and process variables are calculated at the current time step.

The MPC gains are calculated and model states are updated within the specified constraint limits. The PV array production $E_{PV}(k)$ at any instant is compared with the energy demand $E_d(k)$. The hour-ahead solar radiation prediction $SRP(k)$ and energy demand prediction $EDP(k)$ are checked to decide if non-critical loads of the house should be ON or OFF. If the PV production is less than demand, non-critical loads are turned OFF to reduce the total energy demand of the house. Further, if PV production is still less than the limited demand $E_d(k)_{Lim}$, then the battery energy (E_b) is used to satisfy the limited demand. Lastly, if PV production is still less than the limited demand of the house, the required energy is imported from the grid (E_g). Otherwise, if PV production is more than the energy demand and no negative disturbance exists, PV energy charges the battery (E_{PVb}). When the battery is fully charged and excess PV energy is still available; the hot water cylinder temperature is increased to its maximum level. At this stage if excess PV energy is available, it is exported to the grid.

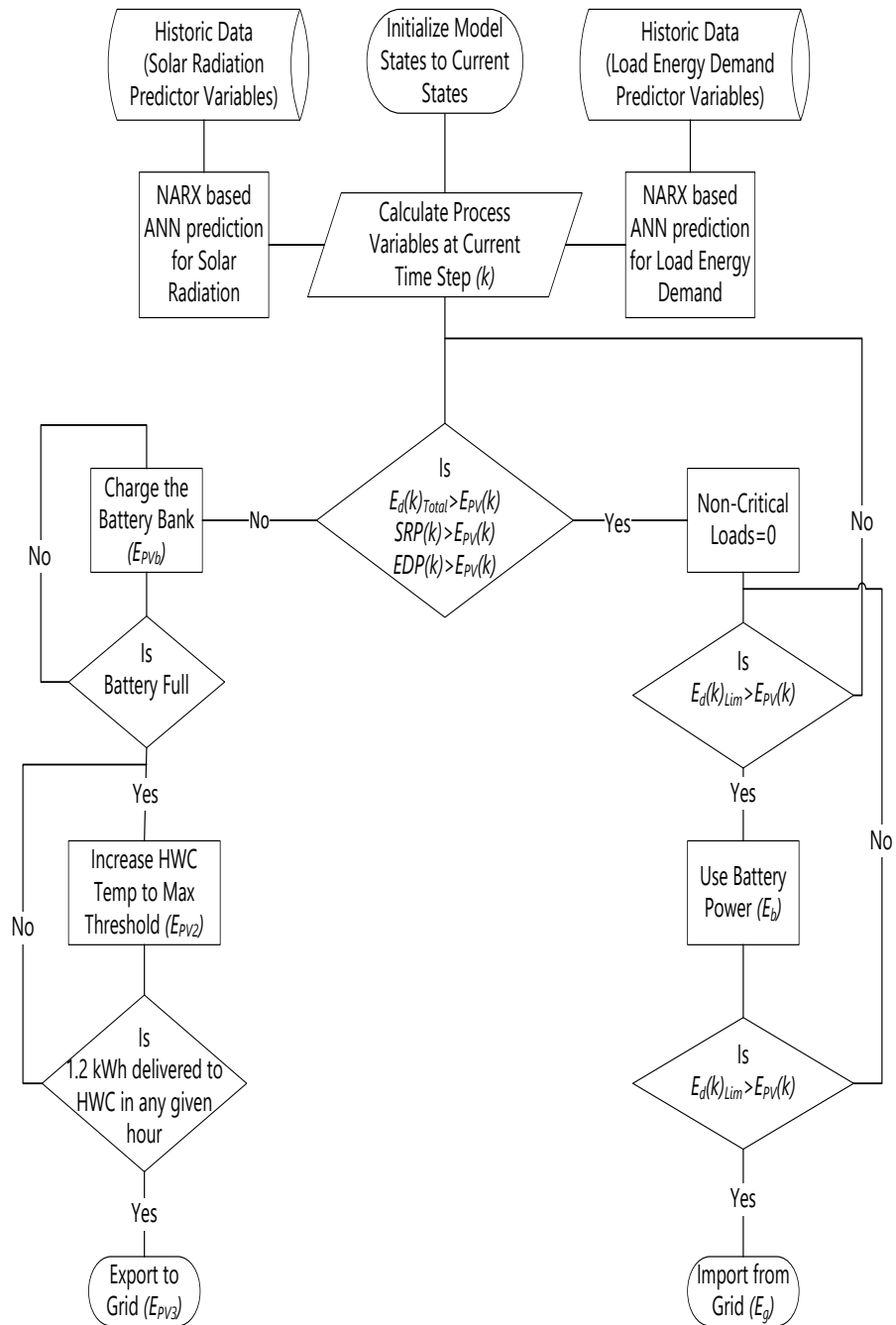


Figure 20. Flow chart of the MPC approach

More specifically, the PV array is generating E_{PV1} , E_{PV2} , E_{PV3} and E_{PVb} as shown in Figure 19. These are used to satisfy the energy demand of the house, increase the hot water cylinder temperature to its maximum threshold, export excess PV energy to the grid and charge the battery bank respectively. E_b is the energy which flow from the battery to the load and E_g is the grid energy to satisfy energy requirement of the load.

The mathematical model of the proposed system is similar to that used by Zhu et al., (2015), for a photovoltaic-diesel-battery (PDB) hybrid energy system that was used to supply daily energy requirement for an off-grid medical clinic. However, in the proposed MIMO state-space model the use of a diesel generator is replaced with a model of the grid.

4.4.1 MIMO state-space model of the proposed system

Model predictive control systems are designed based on a mathematical model of the plant. In this work a MIMO state-space model has been used for the MPC design. By using a state-space model, the current information required for predicting ahead is represented by the state variable at the current time. In order to explain the design procedures of the MPC, MIMO state-space model transformation is presented first followed by objective function, MPC algorithm, optimization and constraints.

The proposed photovoltaic-battery-grid model has five inputs (Equation (16)) and three outputs (Equations (17), (20) & (23)). The number of outputs are less than the number of inputs, therefore, each of the measured output can be controlled independently with zero steady-state errors. The plant model inputs are defined as

$$u(k) \triangleq [E_{PV1}(k), E_{PV2}(k), E_{PV3}(k), E_{PVb}(k), E_b(k)]^T \quad (16)$$

and the outputs of the model are defined as

$$y_1(k) = w_1 (E_d(k) - E_g(k)) \quad (17)$$

where $E_d(k)$ is the energy demand of the house, E_g is the grid energy to satisfy energy requirement of the load and w_1 is a positive weight coefficient.

$$E_d(k) = E_{PV1}(k) + E_{PV2}(k) + E_b(k) + E_g(k)$$

$$E_d(k) - E_g(k) = E_{PV1}(k) + E_{PV2}(k) + E_b(k)$$

Therefore $y_1(k) = w_1(E_{PV1}(k) + E_{PV2}(k) + E_b(k))$

And the first controller reference is given by

$$y_{ref,1}(k) = w_1 E_d(k) \quad (18)$$

which gives

$$\sum (y_{ref,1}(k) - y_1(k))^2 = \sum w_1^2 E_g(k)^2 \quad (19)$$

It can be seen that minimizing $\sum (y_{ref,1}(k) - y_1(k))^2$ is equivalent to minimizing $\sum w_1^2 E_g(k)^2$, which is used to minimize the grid imports. Similarly, the second output of the model is given by

$$y_2(k) = w_2(E_{PV1}(k) + E_{PV2}(k) + E_{PV3}(k) + E_{PVb}(k)) \quad (20)$$

where w_2 is a positive weight coefficient. From Figure 19, it can be seen that the PV array energy is equal to

$$E_{PV}(k) = E_{PV1}(k) + E_{PV2}(k) + E_{PV3}(k) + E_{PVb}(k)$$

thus

$$\begin{aligned} y_2(k) &= w_2 E_{PV}(k) \text{ or} \\ w_2 E_{PV}(k) - y_2(k) &= 0 \end{aligned} \quad (21)$$

which shows that PV array usage can be maximized by minimizing $\sum(w_2 E_{PV}(k) - y_2(k))^2$

$$y_{ref,2}(k) = w_2 E_{PV}(k) \quad (22)$$

Similarly, output 3 is given by

$$y_3(k) = w_3(E_{PVb}(k) + E_b(k)) \quad (23)$$

and

$$y_{ref,3}(k) = w_3(0) \quad (24)$$

Next, the augmented system states are given by

$$x(k) = [S_{oc}(k), y_1(k-1), y_2(k-1), y_3(k-1)]^T \quad (25)$$

and the augmented system output is given by

$$y(k) = [y_1(k-1), y_2(k-1), y_3(k-1)]^T \quad (26)$$

Such that a linear state-space model can be determined as

$$\begin{cases} x(k+1) = Ax(k) + B\Delta u(k) \\ y(k) = Cx(k) + D\omega(k) \end{cases} \quad (27)$$

where A, B, C and D are the linear state-space system matrices. $\omega(k)$ is the measured output disturbance which represents the ANN based solar radiation and electricity consumption predictions. As such it affects two of the controller outputs $y_1(k)$ and $y_2(k)$.

where

$$A = \begin{bmatrix} 1 & 0 & 0 & 0 \\ 0 & 0 & 0 & 0 \\ 0 & 0 & 0 & 0 \\ 0 & 0 & 0 & 0 \end{bmatrix}$$

$$B = \begin{bmatrix} 0 & 0 & 0 & \eta_c & -\eta_d \\ w_1 & w_1 & w_1 & 0 & w_1 \\ w_3 & w_3 & w_3 & w_3 & 0 \\ 0 & 0 & 0 & w_2 & w_2 \end{bmatrix}$$

$$C = \begin{bmatrix} 0 & 1 & 0 & 0 \\ 0 & 0 & 1 & 0 \\ 0 & 0 & 0 & 1 \end{bmatrix}$$

$$D = \begin{bmatrix} 1 & 0 \\ 0 & 1 \\ 0 & 0 \end{bmatrix}$$

The linear state-space system in Equation (27) is the plant controlled using the MPC approach.

4.4.2 Objective function for the MPC

MPC is developed for the closed-loop control, in which the objective of the controller is to manage the scheduling of E_{PV1} , E_{PV2} , E_{PV3} , $E_{PVb}(k)$, E_b and E_g for the PBG system. In doing so, it must efficiently optimize charging and discharging coefficients (η_c and η_d), ensure electricity imports from the grid are minimized and the PV energy usage in the house is maximized. Excessive usage of the battery is avoided to extend battery life and usage of non-critical loads in the house is deferred to periods when excess PV energy is available. For the MPC to reduce grid energy imports it plans in advance for periods of low sunshine, or periods of high energy demand, by utilizing solar radiation and electricity consumption predictions. As such, the overall objective function is given by

$$J(k) = \sum_k^{k+N_p} \left\{ \begin{aligned} & [w_1 E_d(k) - w_1 E_{PV1}(k) - w_1 E_{PV2}(k) - w_1 E_{PV3}(k) - w_1 E_b(k)]^2 + \\ & [E_{PV}(k) - w_2 E_{PV1}(k) - w_2 E_{PV2}(k) - w_2 E_{PV3}(k) - w_2 E_{PVb}(k)]^2 + \\ & [w_3 E_{PVb}(k) + w_3 E_b(k)]^2 \end{aligned} \right\} \quad (28)$$

where N_p represent the number of hours in the prediction horizon for the MPC design.

4.4.3 MPC algorithm and optimization

In the proposed MPC approach, an optimal control problem over the prediction horizon is repeatedly solved ($k = 0, \dots, N - N_p$). With the linear state-space Equation (27), the objective function (28) and the constraints (Table 10, Table 11 & Table 12), a MIMO MPC is developed for the PBG system in Figure 19. The optimization variable is the energy flow sequence at each sampling period. At the k th sample, an optimal solution $[U(k), U(k+1), \dots, U(k+N_p-1)]^T$ can be obtained after solving the optimal problem. Only the first part of the solution, i.e. $U(k)$, is used in the current period. At each instant, k is set to $k+1$ and system states, inputs and outputs are updated. Also, the estimated parameters $\hat{\eta}_c$ and $\hat{\eta}_d$ are updated using the proposed updating law (Equation (38)). The objective function J is expressed as

$$\begin{aligned} \min J(k) &= \min \frac{1}{2} U(k)^T H U(k) + U(k)^T F \\ \text{s. t.} & \text{ constraints in Table 10, Table 11 and Table 12} \end{aligned} \quad (29)$$

where H and F are MPC gains calculated based on the objective function (Equation (28)). MPC gains are calculated according to classical MPC design (Wang, 2009). The output vector can be expressed with respect to input vector as

$$Y(k) = Fx(k) + \Phi U(k)$$

where F and Φ are MPC gains matrices and calculated as follows

$$F(k) = [(CA)^T, (CA^2)^T, \dots, (CA^{N_p(k)})^T]^T$$

and

$$\Phi(k) = \begin{bmatrix} \Phi_{11} & 0 & \dots & 0 \\ \Phi_{21} & \Phi_{22} & \dots & 0 \\ \vdots & \vdots & \ddots & \vdots \\ \Phi_{N_p,1} & \Phi_{N_p,2} & \dots & \Phi_{N_p,N_c} \end{bmatrix}$$

Where $\Phi_{i,j} = CA^{i-j}\hat{B}$ and \hat{B} is in the form of B with η_c and η_d replaced by $\hat{\eta}_c$ and $\hat{\eta}_d$. The objective function is given by

$$\min J(k) = \min (Y(k) - R(k))^T (Y(k) - R(k))$$

$$\min J(k) = \min [2(Fx(k) - R(k))^T \Phi U(k) + U(k)^T \Phi^T \Phi U(k)]$$

$$\min J(k) = \min (U(k)^T H U(k) + 2W U(k))$$

where $H(k) = \Phi(k)^T \Phi(k)$, and $W(k) = (Fx(k) - R(k))^T \Phi$.

4.4.4 Constraints for the MIMO linear system

The constraint variables are parametrized using the same parameter vector ΔU as the one used in the predictive control design. Therefore, the constraints are expressed in a set of linear equations based on the parameter vector ΔU . Constraints are categorized as shown in Table 10.

Table 10. Constraints for the MIMO system

<i>Constraints</i>	<i>M</i>	<i>γ</i>
$E_{PV1}(k) > 0$	-1 0 0 0 0	0
$E_{PV2}(k) > 0$	0 -1 0 0 0	0
$E_{PV3}(k) > 0$	0 0 -1 0 0	0
$E_{PVb}(k) > 0$	0 0 0 -1 0	0
$E_b(k) > 0$	0 0 0 0 -1	0
$E_{PV1}(k) + E_{PV2}(k) + E_b(k) < E_d(k)$	1 1 0 0 1	$E_d(k)$
$E_{PV1}(k) + E_{PV2}(k) + E_{PV3}(k) + E_{PVb}(k) < E_{PV}(k)$	1 1 1 1 0	$E_{PV}(k)$
$E_{PV1}(k) < E_{PV1}^{max}$	1 0 0 0 0	E_{PV1}^{max}
$E_{PV2}(k) < E_{PV2}^{max}$	0 1 0 0 0	E_{PV2}^{max}
$E_{PV3}(k) < E_{PV3}^{max}$	0 0 1 0 0	E_{PV3}^{max}
$E_{PVb}(k) < E_{PVb}^{max}$	0 0 0 1 0	E_{PVb}^{max}
$E_b(k) < E_b^{max}$	0 0 0 0 1	E_b^{max}
$E_{PV1}(k) + E_{PV2}(k) + E_b(k) > E_g^{max} - E_d(k)$	-1 -1 0 0 -1	$E_g^{max} - E_d(k)$

In Table 10, E_{PV1}^{max} , E_{PV2}^{max} , E_{PV3}^{max} and E_{PVb}^{max} are the maximum amount of energy that can be transmitted to the load, hot water cylinder, utility grid and battery bank respectively from the PV array during any 1 hour period. E_b^{max} is the maximum amount of energy that can flow from the battery to the load in situation where PV array energy is not sufficient to satisfy demand. The utility grid energy (E_g) is used to cover the imbalance when the PV array energy and the battery bank energy are not sufficient to cover the energy demand of the house. In this work, positive values of E_g represent grid

imports and negative values of E_g represent grid exports. $E_g(k)$ is subject to the following constraint

$$-E_g^{max} \leq E_g(k) \leq E_g^{max}$$

where E_g^{max} is the maximum amount of energy that can be imported from the grid and $-E_g^{max}$ is the maximum amount of energy that can be exported to the grid during 1 hour. Energy demand of the house at any given hour should satisfy the following condition

$$E_{PV1}(k) + E_{PV2}(k) + E_b(k) + E_g(k) \geq E_d(k)$$

where $E_d(k)$ represent the energy demand of the house at any given hour.

Constraints for the state-of-charge of the battery should be in the form similar to the predictive control vector $U(k)$. Predicted values of x_m for the SOC can be calculated by

$$S_{oc}(k+i|k) = S_{oc}(k) + b_m \sum_{j=k}^{j \leq k+i-1} u(j) \quad (30)$$

where $S_{oc}(k+i|k)$ is the predicted value of S_{oc} from sampling time k . It follows from Equation (30) that

$$X_m(k) \triangleq [S_{oc}(k)[1, 1, \dots, 1]^T + B_m U(k)]^T$$

where

$$X_m(k) \triangleq [S_{oc}(k), S_{oc}(k+1|k), \dots, S_{oc}(k+N_c-1|k)]^T$$

$$B_m(b_m) = \begin{bmatrix} b_m & 0 & \dots & 0 \\ b_m & b_m & \ddots & \vdots \\ \vdots & \vdots & \ddots & 0 \\ b_m & b_m & \dots & b_m \end{bmatrix}$$

As b_m is uncertain, its estimated value $\hat{b}_m = [0, 0, 0, \hat{\eta}_c, \hat{\eta}_d]$ is used in calculating B_m .

Further the state of charge of the battery is restricted between its minimum and maximum values, such that

$$B_c^{min} \leq S_{oc}(k) \leq B_c^{max}$$

Which can be written in a compact form as follow and as shown in Table 11

$$M_2 U(k) \leq \gamma_2 \quad (31)$$

Table 11. Battery constraints

M_2	γ_2
$-B_m$	$(S_{oc}(k) - B_c^{min})[1, 1, \dots, 1]^T$
B_m	$(B_c^{max} - S_{oc}(k))[1, 1, \dots, 1]^T$

$$B_m(\hat{b}_m) = \begin{bmatrix} \hat{b}_m & 0 & \dots & 0 \\ \hat{b}_m & \hat{b}_m & \ddots & \vdots \\ \vdots & \vdots & \ddots & 0 \\ \hat{b}_m & \hat{b}_m & \dots & \hat{b}_m \end{bmatrix}$$

Which shows that battery constraints are expressed with respect to the predictive control vector $U(k)$ and $S_{oc}(k)$ can be obtained in real-time.

To avoid charging and discharging the battery simultaneously, $E_{PVb} = 0$ can be set for charging and $E_b = 0$ can be set for discharging. The procedure mentioned applies for charging, whereas for discharging row 4 in Table 10 is replaced by

Table 12. Discharging constraint

<i>Constraints</i>	<i>M</i>	<i>γ</i>
$E_{PVb}(k) < 0$	0 0 0 1 0	0

4.4.5 Battery parameters estimation

In a domestic setting, PV installations are located close to the loads so require the storage of energy at appropriate times to minimize the imbalance between generation and consumption. The charging and discharging model of the battery for the MPC computation is given by Equation (32)

$$S_{oc}(k + 1) = S_{oc}(k) + \eta_c E_{PVb}(k) - \eta_d E_b(k) \quad (32)$$

where $S_{oc}(k)$ is the state-of-charge (SOC) at sampling time k and $S_{oc}(k + 1)$ is the SOC at the next hour. E_{PVb} and E_b are charging and discharging energies respectively. η_c and η_d are charging and discharging efficiencies respectively. η_c and η_d are uncertain constant parameters, which are estimated online in the MPC design. Discrete model of the SOC in Equation (32) is based on the continuous model proposed in Vahidi et al. (2006), where, variation of the SOC is proportional to the charging and discharging currents. According to Equation (32), the current SOC ($S_{oc}(k)$) can be expressed by the initial SOC ($S_{oc}(0)$) and can be expressed as

$$S_{oc}(k) = S_{oc}(0) + \eta_c \sum_{k=0}^{k+N_c-1} E_{PVb}(k) - \eta_d \sum_{k=0}^{k+N_c-1} E_b(k) \quad (33)$$

The SOC of the battery is subject to several constraints, such as the maximum allowable charge limit and the minimum allowable discharge limit, referred to as the depth of discharge (DOD). The lower and upper bounds of SOC are subject to the following constraint

$$B_c^{min} \leq S_{oc}(k) \leq B_c^{max}$$

where B_c^{min} and B_c^{max} are the minimum and maximum allowable SOC of the battery bank respectively.

The battery bank is charged during the day time when PV energy is available and discharged during night time. Simultaneous charging and discharging are avoided using Equation (34) in the MPC design.

$$E_{PVb}(k)E_b(k) = 0 \quad (34)$$

When PV array production exceeds total energy demand of the house, the battery bank is set in charging mode and when total energy demand of the house exceeds PV production, the battery bank is set in discharging mode.

SOC of the battery bank can be expressed by

$$S_{oc}(k) = S_{oc}(k-1) + b_m u(k-1) \quad (35)$$

where $b_m \triangleq [0, 0, 0, \eta_c, -\eta_d]$, therefore

$$S_{oc}(k) = S_{oc}(k-1) + b_p u_b(k-1) \quad (36)$$

where $b_p \triangleq [\eta_c, -\eta_d]$ and $u_b \triangleq [E_{PVb}(k), E_b(k)]^T$

The estimated battery dynamic system is given by

$$\hat{S}_{oc}(k) = S_{oc}(k-1) + \hat{b}_p(k-1)u_b(k-1) \quad (37)$$

Where $\hat{S}_{oc}(k)$ is the estimated SOC and $\hat{b}_p \triangleq [\eta_c, -\eta_d]$ is estimated battery charge and discharge parameters.

Online identification is designed using the cost function J .

$$J = \frac{1}{2}(\tilde{S}_{oc}(k))^2$$

$$J = \frac{1}{2}(S_{oc}(k) - S_{oc}(k-1) - \hat{b}_p(k-1)u_b(k-1))^2$$

where $\tilde{S}_{oc}(k) \triangleq S_{oc}(k) - \hat{S}_{oc}(k)$. The gradient with respect to \hat{b}_p can be calculated by

$$\nabla J = -(\Delta S_{oc}(k) - \hat{b}_p(k-1)u_b(k-1))u_b(k-1)$$

where $\Delta S_{oc}(k) \triangleq S_{oc}(k) - S_{oc}(k-1)$. Next the updating law for \hat{b}_p can be calculated by

$$\hat{b}_p(k) = \hat{b}_p(k-1) - \nabla J$$

Similarly the updating law for \hat{b}_m can be calculated by

$$\hat{b}_m(k) = [0, 0, 0, \hat{\eta}_c(k), -\hat{\eta}_d(k)] = [0, 0, 0, \hat{b}_p(k)] \quad (38)$$

The proposed updating law in Equation (38) facilitate the convergence of estimated parameters to their actual values if the control u_b is persistently exciting (PE) as discussed in Ioannou, (2012).

PE of $u_b(k)$ can be explained as

$$u_b(k)u_b(k)^T = \begin{bmatrix} E_{PVb}(k)^2 & E_{PVb}(k)E_b(k) \\ E_{PVb}(k)E_b(k) & E_b(k)^2 \end{bmatrix}$$

where $E_{PVb}(k)E_b(k) = 0$ as in Equation (34), which shows that simultaneous charging and discharging are not allowed.

4.5. Summary

In this chapter the MPC strategy was developed for the energy dispatching of a PBG energy system using solar radiation and electricity consumption predictions as a measured disturbance. A detailed structure of the PBG system was presented along with the step-by-step process flow, as well as the process model, objective function and optimization techniques. Various switched states of the battery were described by switched constraints, so that the PBG system could be expressed by a unified linear MIMO state-space model, and the difficulty of constructing a complicated switched predictive state-space model was avoided.

Chapter 5. RESULTS AND DISCUSSION

5.1. Simulation results of the proposed MPC

In order to examine the behaviour of the proposed MPC a simulation of a photovoltaic-battery-grid system was undertaken using a week's measurements of the PV array production ($E_{PV}(k)$) and the energy demand ($E_d(k)$) taken from a real house (Appendix B). Values of the system parameters and control parameters are listed in Table 13 and Table 14, respectively. Initial values of $E_{PV1}(k)$, $E_{PV2}(k)$, $E_{PV3}(k)$, $E_{PVb}(k)$, $E_b(k)$ and $E_g(k)$ are set to zeros. Initial values of S_{oc} are set to $x_m(1) = 0.5B_c^{max} \cdot E_{PV2}^{max}$ is the maximum energy that could be used to increase hot water temperature within any given hour. MATLAB[®] code was used for simulation and implementation of the proposed MPC framework.

Table 13. Values of the system parameters

Notations	Values	Notations	Values
E_{PV1}^{max}	7 kWh	E_{PVb}^{max}	7 kWh
E_{PV2}^{max}	1.2 kWh	E_b^{max}	7 kWh
E_{PV3}^{max}	7 kWh	$E_g(k)$	+/- 7 kW
B_c^{max}	60 kWh	B_c^{min}	15 kWh
η_c	0.8	η_d	1.0

It should be noted that, although MPC is applied, the energy dispatching of the PBG system is fundamentally an optimization problem rather than a control design problem,

therefore, stability of the closed-loop system is not assured by the proposed MPC approach. However, states of the closed-loop system are guaranteed bounded, since the optimization in the MPC is processed with constraints on E_{PV1} , E_{PV2} , E_{PV3} , E_{PVb} , E_b , E_g and S_{oc} .

Table 14. Values of the control parameters

Notations	Values	Notations	Values
w_1	1.0	w_3	0.2
w_2	0.8		

The total energy demand in Figure 21 represents the sum of the critical loads (hot water cylinder, lighting, fridge/freezer, power sockets and cooking range) and non-critical loads (dish washer, washing machine & dryer).

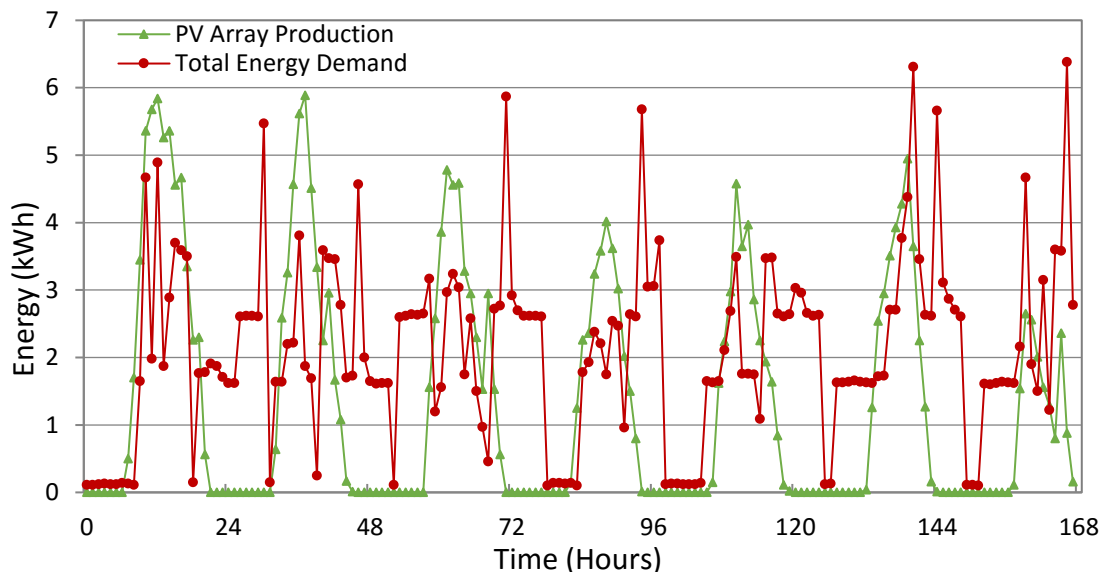


Figure 21. PV array production and total energy demand of the house

On this basis the behaviour of the MPC was analysed in the presence of two measured disturbances (solar radiation & electricity demand forecasts). In doing this the global solar radiation and electricity demand forecasts were used to test if the controller was able to respond if one or both the forecasts were unfavourable. If the energy demand forecast was more than current demand and PV array production could not satisfy the forecasted demand, then the controller would aim to reduce total demand of the house by switching off non-critical loads to avoid grid imports and utilize PV energy or battery energy. Figure 22 shows the MPC behaviour for this particular week, as such, whenever the PV array production is less than the demand, usage of the non-critical loads is deferred until periods when excess PV energy is available. By doing so, grid imports would be reduced and PV energy utilized within the house. As such, it can be seen that non-critical loads in the house would be used mainly during the day, when energy is available from the PV array.

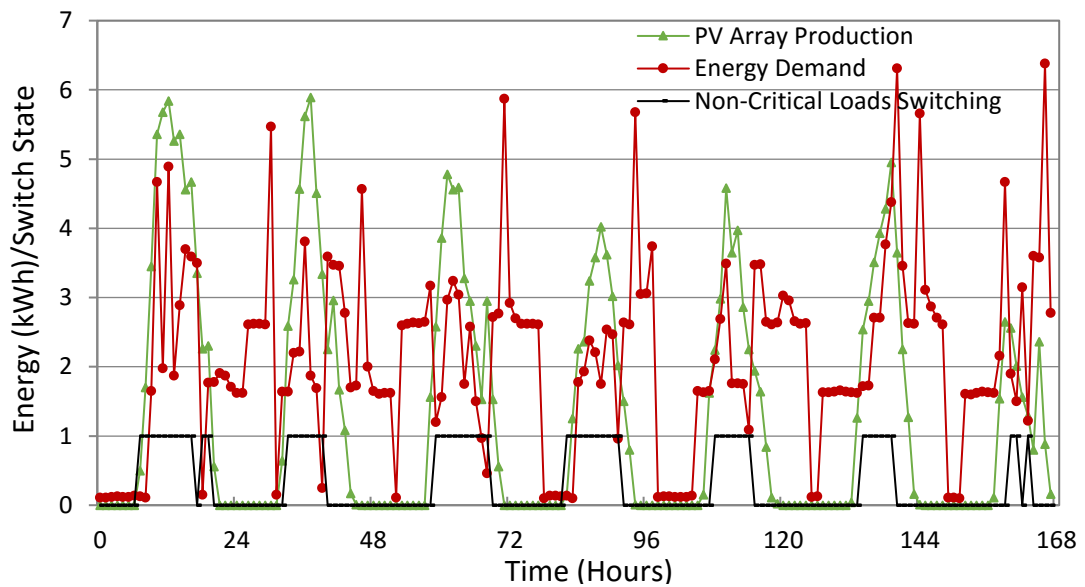


Figure 22. Switching behaviour of the MPC (On=1, Off=0)

Figure 23 shows switching behaviour of the MPC, where, if the predicted PV energy is significantly less than the current PV production, or predicted load demand is more than the current load demand, non-critical loads remain off (even during the day) to reduce total load of the house. To avoid switching due to small weather variations, a weighting factor was added to reduce switching sensitivity. For example, if predicted PV energy at any hour is 1.5 times more than the current PV energy or predicted energy demand is 1.5 times more than the current load demand, non-critical loads would be turned off.

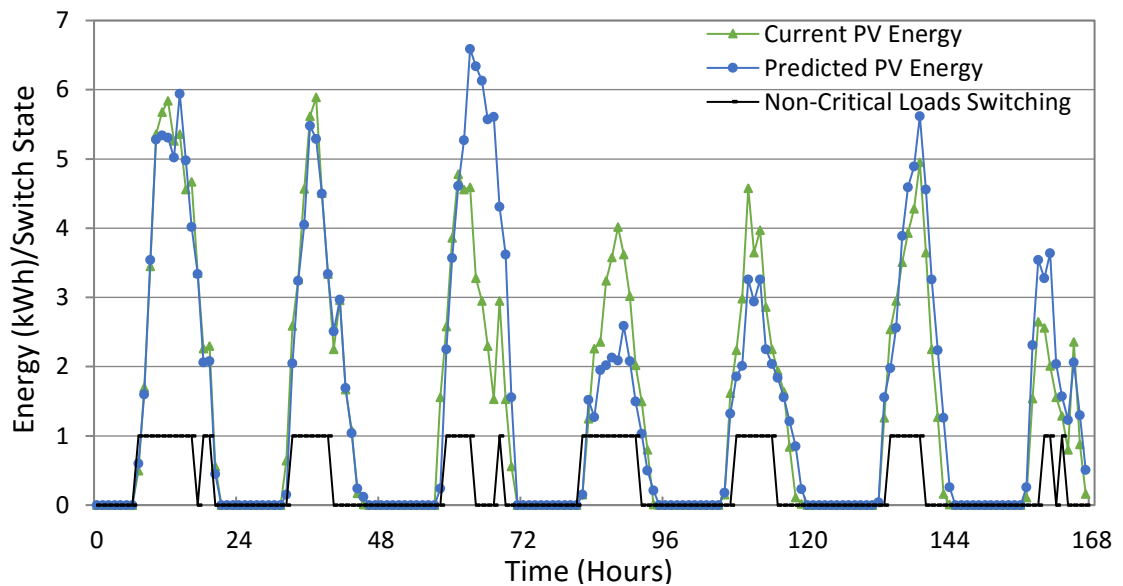


Figure 23. MPC performance in the presence of disturbance (PV energy prediction) (On=1, Off=0)

Further, MPC performance is analysed by using energy demand prediction as a disturbance. It can be seen in Figure 24 that, whenever the energy demand prediction is more than the current demand and PV production is less than the current demand, non-critical loads would be turned off. This shows the capability of the MPC to adjust the energy demand of the house according to the predicted PV production and predicted energy demand for the house.

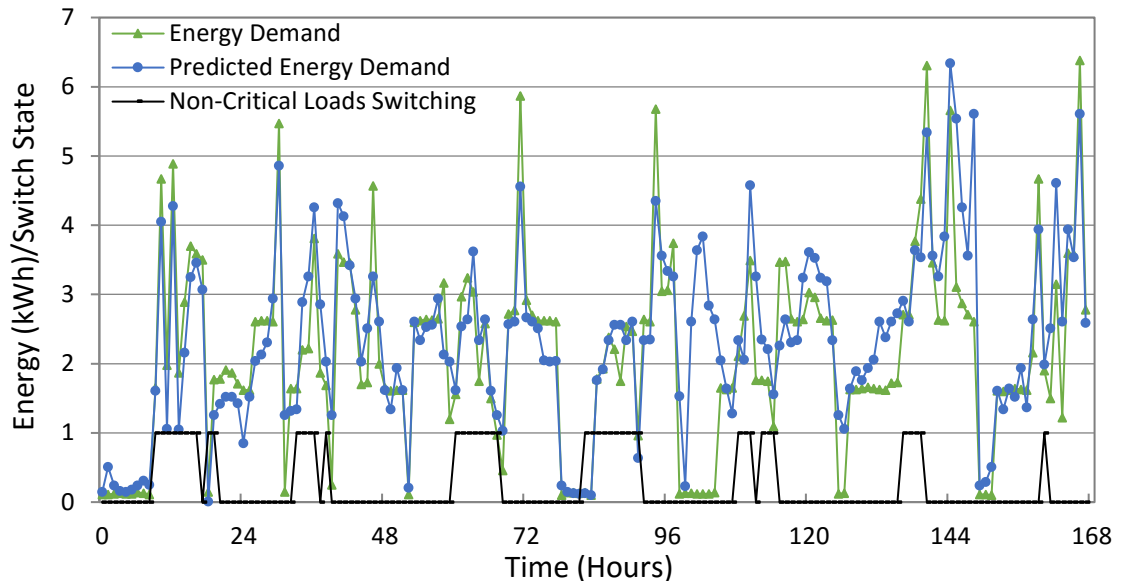


Figure 24. MPC performance in the presence of disturbance (Energy demand prediction) (On=1, Off=0)

To further analyse the performance of the proposed MPC, Figure 25 shows energy demand and PV production. When PV energy is sufficient to satisfy demand and excess energy is available, the battery would be charged. Negative values in Figure 25 show that energy would be exported to the grid when energy demand is satisfied and the hot water temperature has been increased to the specified level. Positive values represent energy imports from the grid when PV and battery energy combined are not sufficient to satisfy demand.

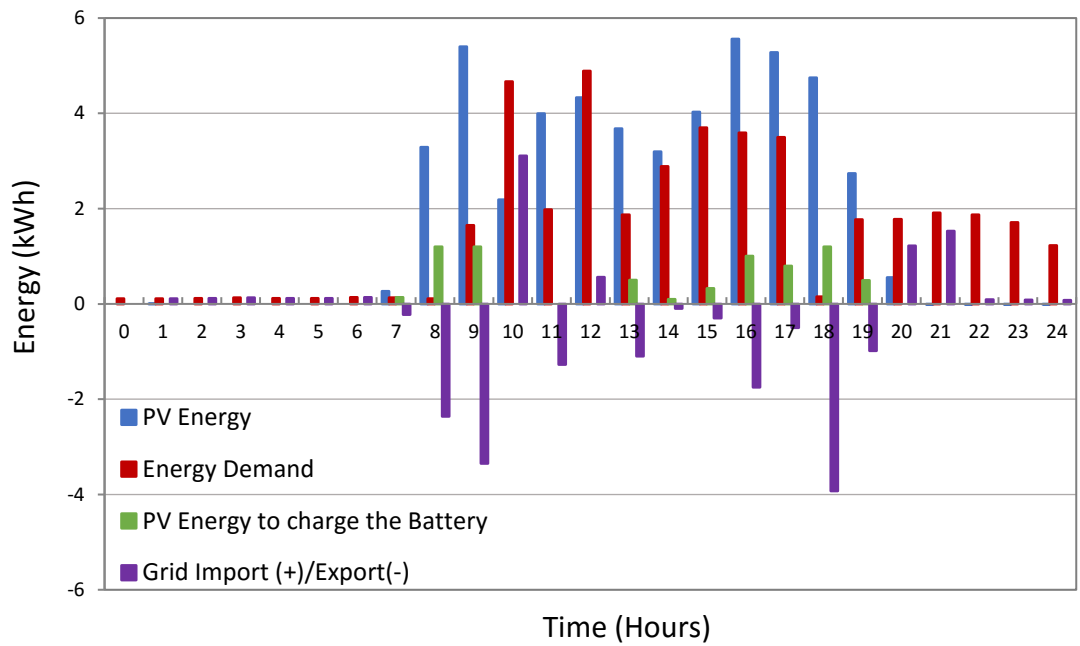


Figure 25. 24-hours energy demand, PV production and energy flow to and from the grid

Following on from this, Figure 26 shows how energy would be moved to and from the battery bank. It can be seen that excess energy is used to charge the battery bank during the day-time and energy is supplied by the battery to loads during periods when the PV array alone cannot satisfy load energy demand (where for the proposed MPC with online estimation, initial values of the estimated parameters are given by $\hat{\eta}_c(0) = 1.0$ and $\hat{\eta}_d(0) = 1.0$). It can be seen that during the last three days' energy demand is high and PV production is lower than the previous days, therefore, more PV energy is assigned to satisfy demand and less PV energy is available to charge the battery bank.

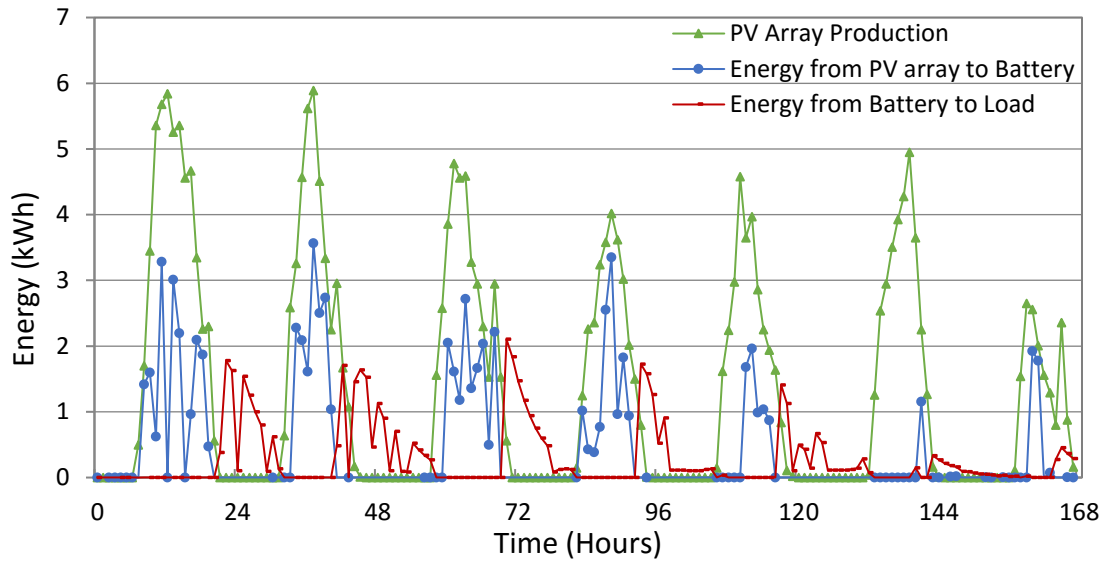


Figure 26. Energy flow from the PV array to battery and battery to satisfy load

Now in discussing the behaviour of the battery, the state of charge (SOC) of the battery bank is shown in Figure 27 for the same week shown in the previous figures. For this week, it is constrained between 15% and 85% to avoid overcharging or fully depleting the battery bank. The battery capacity for the SOC curve in Figure 27 is 60kWh, however, if the battery capacity were decreased, the SOC would reach its maximum threshold faster and vice versa.

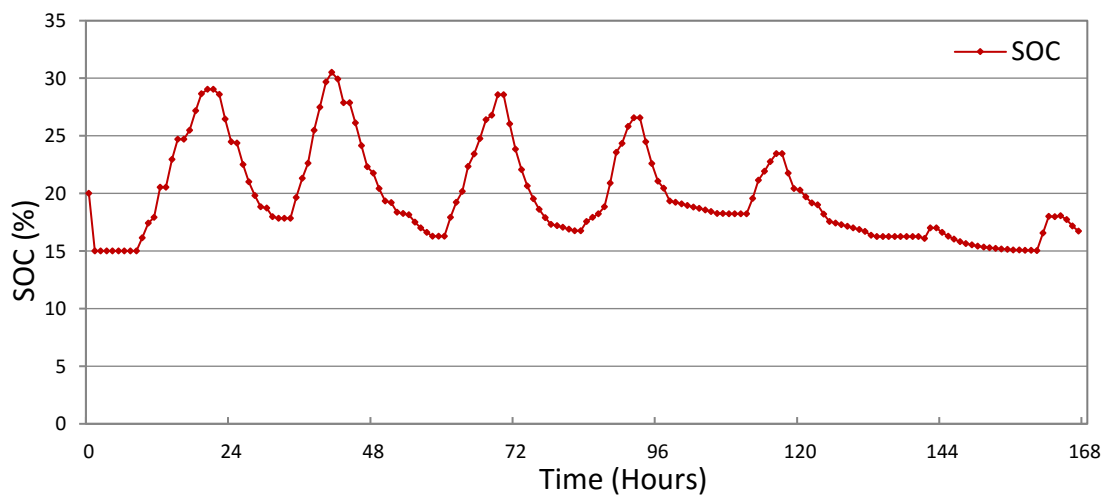


Figure 27. State-of-charge of the battery bank (Capacity=30 kWh)

Figure 28 shows the priority setup for the PV energy influences the consumption of energy. The first priority for the PV energy was to satisfy the total demand of the house (80%) and charge the battery bank (20%), the second priority was to increase the hot water cylinder temperature to its maximum threshold and the third priority was to export excess PV energy to the grid. It can be seen that whenever energy demand is satisfied, PV energy flows to the hot water cylinder and the remaining energy is exported to the grid. PV energy to the hot water cylinder (E_{PV2}) was constrained such that only 1.2 kWh was used to increase the hot water temperature within any given hour, this assumes that the household uses approximately 300 litres of hot water each day and that the water needs to be heated by 50 degrees. From this positive values of the “Grid Import/Export” in Figure 28 represent grid imports and negative values are representing grid exports.

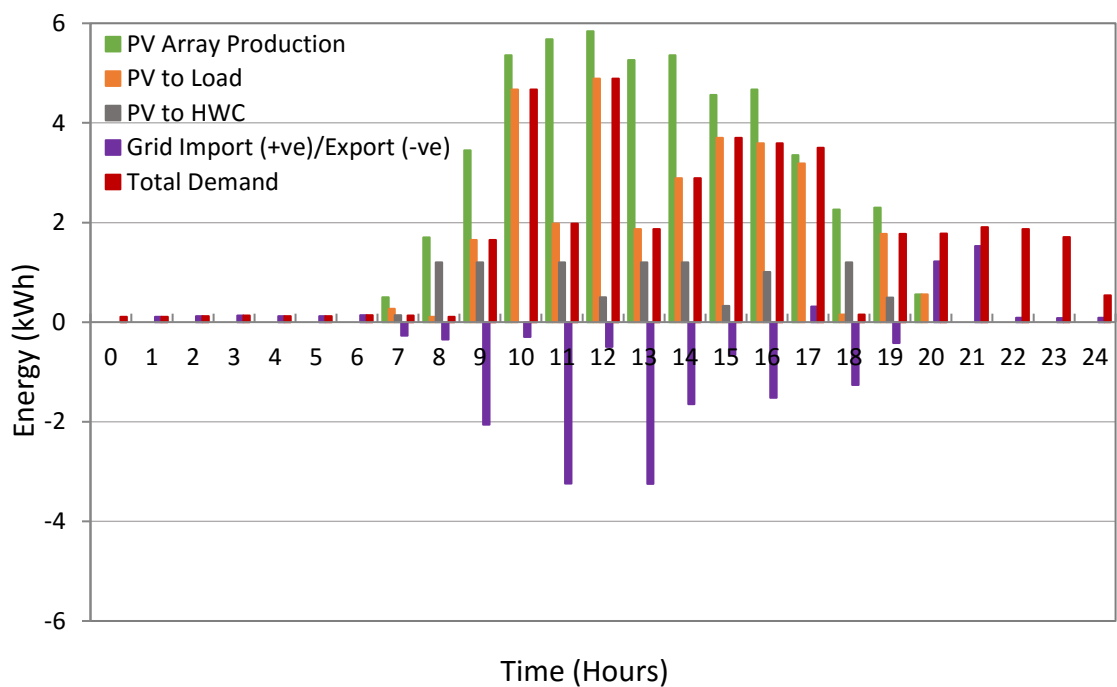


Figure 28. PV energy flow priorities according to demand

The ability of the controller to vary the load according to the solar radiation and energy demand predictions and maximizing PV energy usage with in the house, rather

than exporting available excess PV energy to the grid has the potential to minimize grid imports. The objective function in the MPC design ensure to minimize grid imports, encourage PV energy usage, charge the battery bank and store thermal energy in the hot water cylinder.

Finally, the performance of the proposed MPC was tested by analysing how closely the outputs of the controller follow the reference signals (demand and PV energy production). From Equation (19), it can be deduced that minimizing the difference between the controller output and the reference signal (demand) is equivalent to minimizing grid imports. Similarly, from Equation (21), it can be seen that minimizing the difference between the controller output and the reference signal (PV energy production) is equivalent to maximizing PV energy usage within the house. In Figure 29 it can be seen that the MPC is attempting to minimize the difference between the controller output signal and the reference signal (demand). This is equivalent to minimizing electricity imports from the grid. It can be seen in Figure 29 that the controller output follows the reference (demand) more closely on Saturday than other days of the week for this particular period. Also Figure 30 shows the MPC response in its attempt to reduce the difference between the controller output and the reference signal (PV energy production). This is equivalent to maximizing the usage of the PV array energy within the house and consequently helping reduce grid imports. It is obvious from Figure 29 and Figure 30 that the proposed control strategy is trying to minimize the difference between the reference signal and the output and is understandable that the controller cannot minimize the difference completely but attempting to minimize the gap.

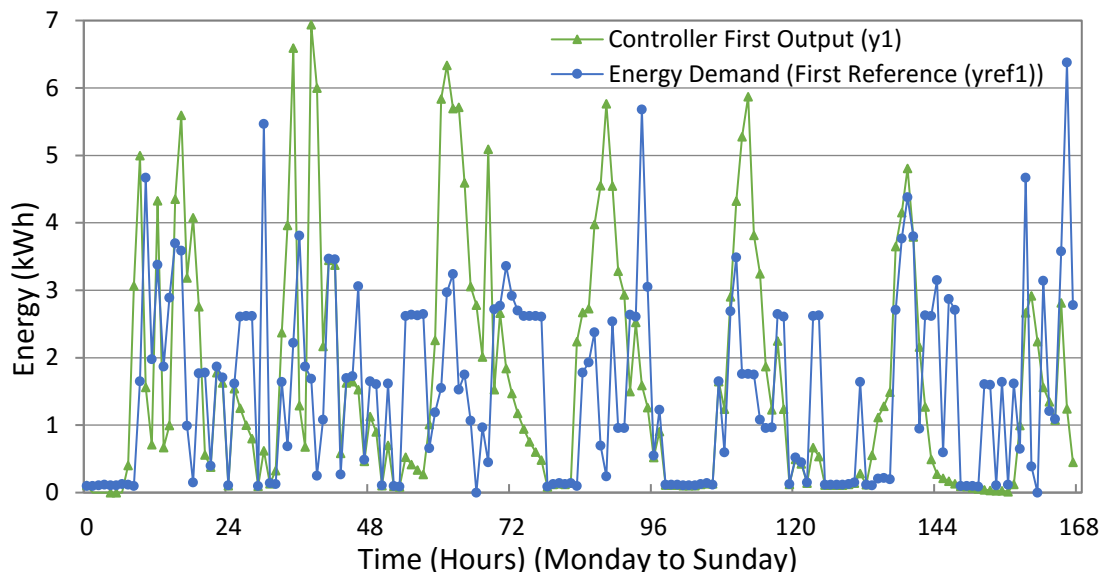


Figure 29. Controller output signal 1 vs reference signal 1

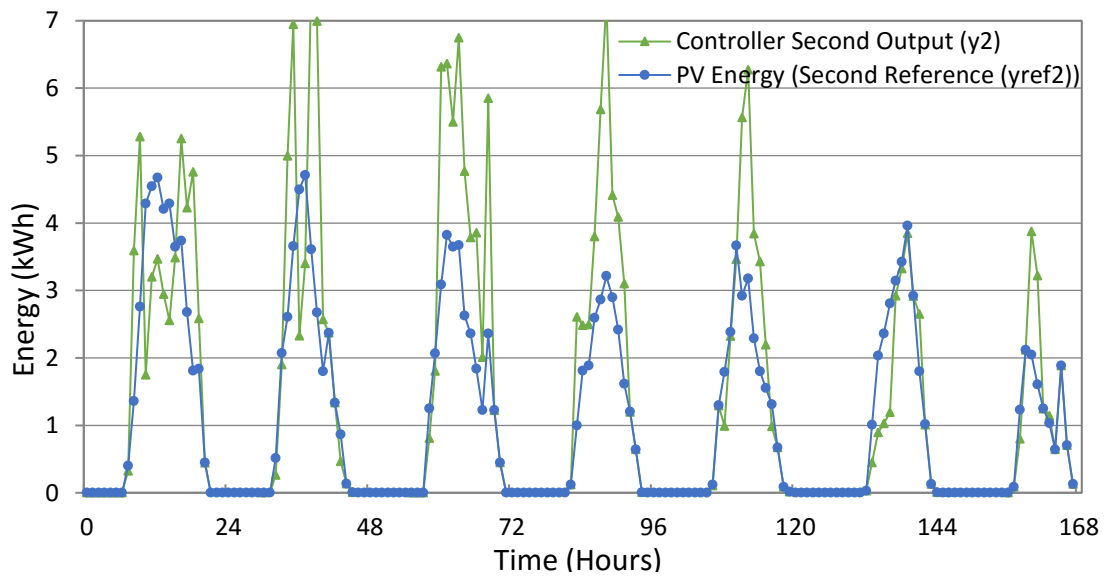


Figure 30. Controller output signal 2 vs reference signal 2

5.2. Optimal control method

To analyse the potential of the MPC approach for facilitating self-consumption, an open-loop optimal control approach was developed and results are compared with the proposed approach.

The open-loop optimal control approach was used to dispatch the hourly energy for $E_{PV1}(k)$, $E_{PV2}(k)$, $E_{PV3}(k)$, $E_{PVb}(k)$, $E_b(k)$ and $E_g(k)$ over a one week period using the same constraints and objective function used for the closed-loop MPC approach without receding horizon control, online estimation of the battery parameters and priority settings for the energy dispatch. As the objective function is quadratic, the energy flow control problem is expressed as a quadratic programming problem as given in Equation (39).

$$\min_x \frac{1}{2} x^T H x + f^T x, s. t. \begin{cases} A \cdot x \leq b, \\ A_{eq} \cdot x = b_{eq} \\ lb \leq x \leq ub. \end{cases} \quad (39)$$

where H , A and A_{eq} are matrices and f , b , b_{eq} , lb , ub and x are vectors. H and f are symmetric matrices of doubles representing the quadratic in the expression $\frac{1}{2} x^T H x + f^T x$. A_{eq} and b_{eq} are the coefficients related with the equality constraints, A and b are the coefficients related with inequality constraints, and lb and ub are the lower and upper bounds of the variables respectively. Energy dispatch variables ($E_{PV1}(k)$, $E_{PV2}(k)$, $E_{PV3}(k)$, $E_{PVb}(k)$, $E_b(k)$, $E_g(k)$), energy demand ($E_d(k)$), PV energy ($E_{PV}(k)$) and state-of-charge ($S_{oc}(k)$) are transformed into the $f(x)$ format to facilitate the experiment for the open-loop optimal control as shown in Table 15.

Table 15. Energy variables replacement for the open-loop optimal control approach

$E_{PV1}(k)$	$x_1(k)$	$E_g(k)$	$x_6(k)$
$E_{PV2}(k)$	$x_2(k)$	$E_d(k)$	$x_7(k)$
$E_{PV3}(k)$	$x_3(k)$	$E_{PV}(k)$	$x_8(k)$
$E_{PVb}(k)$	$x_4(k)$	$S_{oc}(k)$	$x_9(k)$
$E_b(k)$	$x_5(k)$		

The objective function J is transformed into the $f(x)$ form as given in Equation (40).

$$f(x) = \left\{ \begin{array}{l} [w_1x_7(k) - w_1x_1(k) - w_1x_2(k) - w_1x_3(k) - w_1x_5(k)]^2 + \\ [w_2x_8(k) - w_2x_1(k) - w_2x_2(k) - w_2x_3(k) - w_2x_4(k)]^2 + \\ [w_3x_4(k) + w_3x_5(k)]^2 \end{array} \right\} \quad (40)$$

$$f = \begin{bmatrix} -w_1 & -w_1 & -w_1 & 0 & -w_1 & 0 & w_1 & 0 & 0 \\ -w_2 & -w_2 & -w_2 & -w_2 & 0 & 0 & 0 & w_2 & 0 \\ 0 & 0 & 0 & w_3 & w_3 & 0 & 0 & 0 & 0 \end{bmatrix}$$

Constraints are given as

$$x_1(k) + x_2(k) + x_3(k) + x_4(k) \leq x_8(k)$$

$$x_1(k) + x_2(k) + x_5(k) + x_6(k) = x_7(k)$$

$$0 \leq x_1(k) \leq 7 \text{ kWh}$$

$$0 \leq x_2(k) \leq 1.2 \text{ kWh}$$

$$0 \leq x_3(k) \leq 7 \text{ kWh}$$

$$0 \leq x_4(k) \leq 7 \text{ kWh}$$

$$0 \leq x_5(k) \leq 7 \text{ kWh}$$

and

$$0.15 \leq x_9(k) \leq 0.85$$

The parameters of the PBG system for the open-loop optimal control approach are given in Table 16.

Table 16. Photovoltaic-battery-grid system Parameters

Parameters of the PBG system	Values
Nominal battery capacity	60 kWh
Battery charge efficiency	80%
Battery discharge efficiency	100%
Battery's depth of discharge	15%
Initial state of charge	15 kWh
PV array capacity	7 kW

5.2.1. Results of the optimal control

The open-loop optimal control approach was used to dispatch energy for the PBG system over a one-week period while attempting to minimize grid imports and maximize usage of the PV array. Figure 31 shows hourly energy dispatch for the closed-loop MPC and open-loop optimal control approach. It can be seen that MPC imports less energy from the grid during periods when PV production is less than the demand. MPC also exports more energy during the day due to the load management strategies and also by utilizing solar radiation and electricity demand forecasts. The MPC approach shows the potential

to reduce electricity bills by importing less energy from the grid and exporting more energy during the day by planning in advance with the help of global solar radiation and electricity consumption forecasts.

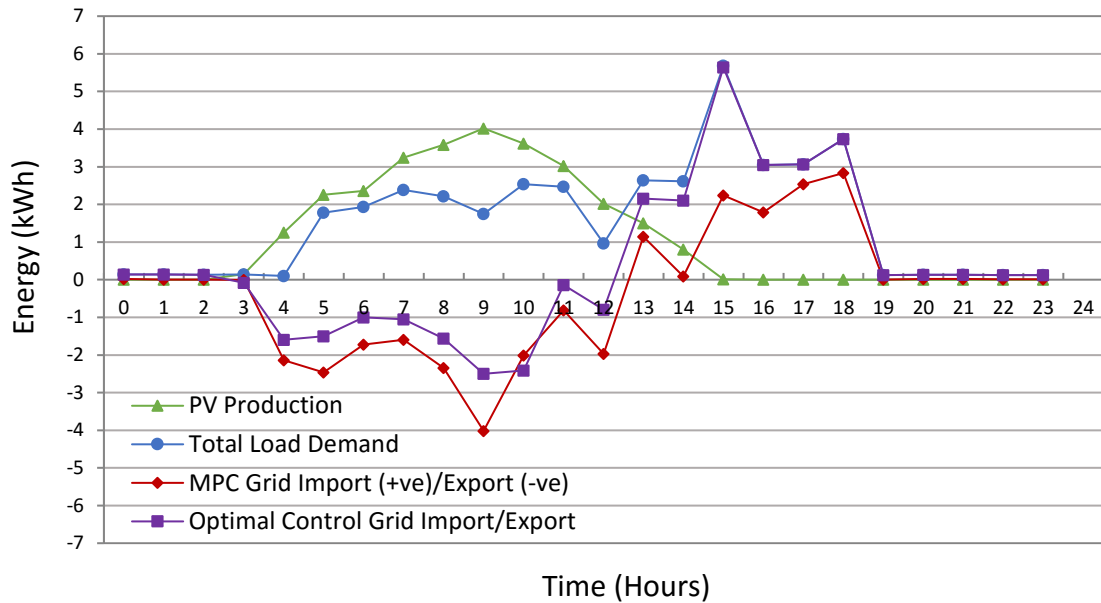


Figure 31. 24-hours analysis of grid imports/exports for the MPC and open-loop optimal control

Figure 32 elaborate this point further by showing one-week analysis of energy exported or imported to show cost saving potential for both the approaches. Overall analysis of both the approaches show that closed-loop MPC export more energy to the grid when energy demand is satisfied and excess energy is available; also import less energy from the grid than the open-loop optimal control approach.

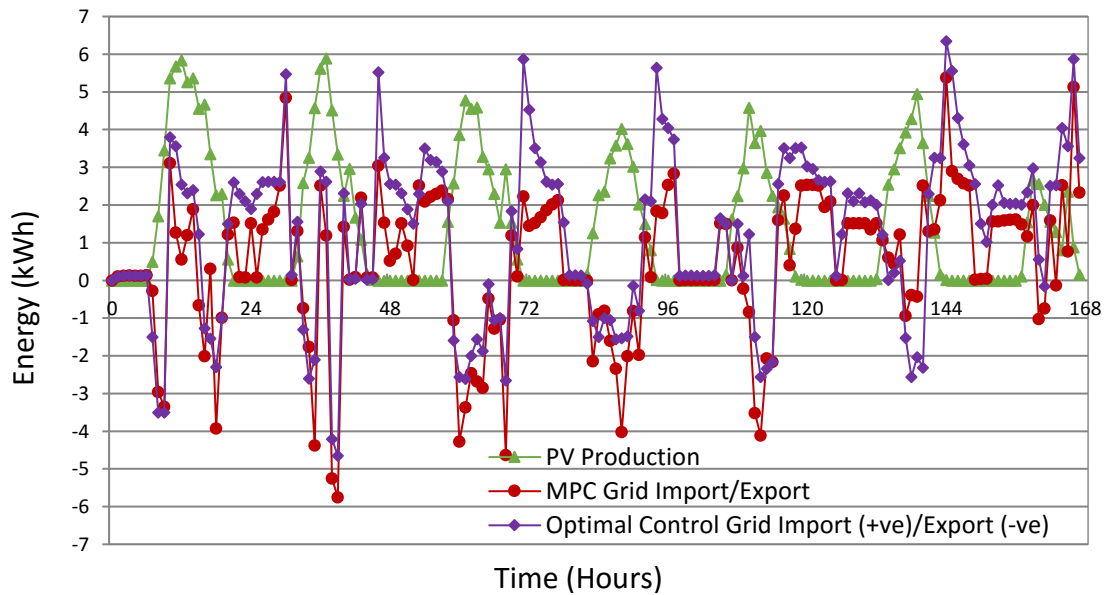


Figure 32. One-week analysis of grid imports/exports for MPC and open-loop optimal control

Table 17 show grid exports and imports for the closed-loop MPC, open-loop optimal control and a house with the PV installation without controller and battery storage. Same PV production, energy demand data, constraints and objective function were used for both the MPC and optimal control approaches.

Table 17. One-week comparison of the MPC and optimal control approaches

MPC Grid Exports (kWh)	MPC Grid Imports (kWh)	Optimal Control Grid Exports (kWh)	Optimal Control Grid Imports (kWh)	No Control Grid Exports (kWh)	No Control Grid Imports (kWh)
-89.28	165.53	-73.80	275.49	-73	198

Results in table 17 shows that 165.53 kWh energy was imported within a week period by the MPC from the grid when PV and battery storage cannot satisfy electricity demand of the house while, optimal control approach imported 275.49 kWh and the house without controller and battery storage, imported 198 kWh. In addition, MPC approach

managed to export more energy to the grid for the same hours within a week due to the utilization of the global solar radiation and electricity demand forecasts. MPC has the potential to reduce electricity imports from the grid due to intelligent battery management as well as utilization of the thermal storage capacity of the hot water cylinder.

Chapter 6. CONCLUSION AND FUTURE WORK

6.1. Conclusion

In this work artificial neural network based global solar radiation and electricity consumption forecasts were utilized for the discrete-time model predictive control system. This approach allowed the controller to plan in advance for periods of low sunshine or high energy demand for a residential house. Four forecasting approaches including non-linear auto-regressive recurrent neural network with exogenous input (NARX), Multilayer Perceptron (MLP) method, a statistical approach using auto regressive moving average (ARMA) and a reference persistence approach were experimented to find a forecasting tool which is free, simple and adaptable to any location.

Hourly time series data were used to train and test the forecasting methods for New Zealand's largest city, Auckland. Predicted values of hourly global solar radiation were compared with the measured values, and it was found that the root mean squared error was $0.243 \text{ MJ}/\text{m}^2$ for the NARX method as compared to $0.484 \text{ MJ}/\text{m}^2$, $0.315 \text{ MJ}/\text{m}^2$ and $0.514 \text{ MJ}/\text{m}^2$ for the MLP, ARMA and the benchmark persistence approaches respectively. Subsequently the NARX approach was used to forecast global solar radiation for other major cities across New Zealand. The results demonstrated the ability of the NARX approach to forecast radiation values at a later time and across a number of different locations.

Similar experiments were conducted to forecast 24 hours ahead electricity consumption for a residential house with four occupants. Regression analysis were performed to find effects of temperature, pressure, relative humidity, rain amount, wind

speed, wind direction, hour of the day and day of the week on electricity consumption. Various combinations of the eight variables were tested in order to investigate their effect on the electricity consumption prediction accuracy. It was found that NARX approach predicts 24-hour ahead electricity consumption with root mean square error of 0.252 kWh as compared to 0.486 kWh with persistence approach.

Along with the two measured disturbances, PV array energy and electricity consumption data for the same residential house have been used as reference signals for the closed-loop MPC design. Optimal dispatching problem was modelled into a control problem and solved by using MIMO state-space model. Charge and discharge modes of the battery were described by switched constraints rather than switched state-space model to simplify the predictive model.

On this basis an adaptive MPC strategy was developed for the energy dispatching of the photovoltaic-battery-grid system, to ensure that the battery bank charge and discharge processes do not occur simultaneously. Electrical appliances of the house were divided into critical loads (hot water cylinder, lighting, power sockets & cooking range) and non-critical loads (dish washer, washing machine & dryer). The MPC has shown the capability to shift non-critical loads operation to period when excess PV energy was available. Battery parameters were estimated online using an adaptive updating law. These MPC techniques were applied in the management and control of the proposed energy supply system with the aim of minimizing grid imports, minimizing use of the battery and maximizing the use of the PV array energy.

Simulation results and comparison with the open-loop optimal control approach suggested that the proposed MPC approach imported 109.96 kWh less energy from the grid within a one-week period as compared to the optimal control approach. Also MPC

approach managed to export 15.48 kWh more energy to the grid within a one-week period as compared to the optimal control approach using the same PV production and energy demand data with the same objective function and constraints. In this respect it shows that an MPC based controller for the PBG systems offers significant cost saving potential in consideration of the outcomes from this study. Future work for this area could include:

1. NARX network for global solar radiation and electricity consumption forecasts could be incorporated into the MIMO state-space model to make the framework more robust and faster.
2. More factors can be included in the objective function to improve the MPC design, for example, electricity cost signal, peak and off-peak electricity tariffs.
3. For off-grid applications battery storage is of great significance. Various types and sizes of the battery storage could be tested to analyse the efficiency of the system.
4. The proposed MPC design can be implemented on a hardware platform and can be tested in a house with a PV array installation, battery storage and grid connection to analyse the cost saving potential in real-time.
5. Further investigation is needed to develop a model that automatically relates energy (kWh) consumption to the temperature in the hot water cylinder. Energy flow to the cylinder can be stopped when a specified temperature is reached and excess PV energy should be exported to the grid. Hot water tank parameters could be included in the MIMO state space model.
6. Electricity consumption forecasts require more research to improve their accuracy.

References

- Al-Alawi, S. M. & Al-Hinai, H. A., 1998, "An ANN based approach for predicting global solar irradiation in locations with no measurements" *Renewable Energy*, vol. 14, pp. 199–204
- Arafa, M., Sallam, E. A. & Fahmy, M. M., 2014, "An enhanced differential evolution optimization algorithm", *4th International Conference on Digital Information and Communication Technology and it's Applications (DICTAP)*, pp. 216-225.
- Arun, P., Banerjee, R. & Bandyopadhyay, S., 2009, "Optimum sizing of photovoltaic battery systems incorporating uncertainty through design space approach", *Solar Energy*, vol. 83, pp. 1013–1025
- Barrero, F., Prieto, J., Levi, E., Gregor, R., Toral, S., Duran, J. M. & Jones, M., 2011, "An enhanced predictive current control method for asymmetrical six-phase motor drives", *IEEE Transactions on Industrial Electronics*, vol. 58, pp. 3242–3252
- Belfkira, R., Zhang, L. & Barakat, G., 2011, "Optimal sizing study of hybrid wind/PV/diesel power generation unit", *Solar Energy*, vol. 85, pp. 100–110
- Bourgeois, C. D. & Macdonald, I., 2006, "Adding advanced behavioural models in whole building energy simulation: a study on the total energy impact of manual and automated lighting control", *Energy and Buildings*, vol. 38, pp. 814–823
- Byrne, J. Susan., 1984, "Solution of quadratic programming problems", *NZOR*, vol. 12, pp. 73–90
- Chen, C., Wang, J., Heo, Y. & Kishore, S., 2013, "MPC-based appliance scheduling for residential building energy management controller", *IEEE Transaction on Smart Grid*, vol. 4, (3), pp. 1401–1410
- Cho, S. & Zaheer-uddin, M., 2003, "Predictive control of intermittently operated radiant floor heating systems", *Energy and Conversion Management*, vol. 44, pp. 1333–1342
- Cigler J., Tomáško, P. & Siroky, j., 2013, "BuildingLAB: A tool to analyze performance of model predictive controllers for buildings", *Energy and Buildings*, vol. 57, pp. 34–41
- Clarke, W. D., Mohtadi, C. & Tuffs, S. P., 1987, "Generalized predictive control. part 1: The basic algorithm. part 2: Extensions & interpretations", *Automatica*, vol. 23, pp. 137–160
- Cutler, R. C. & Ramaker, L. B., 1979, "Dynamic matrix control of a computer control algorithm", *Meeting of the American Institute of Chemical Engineers*, Houston, Texas
- Daniel, A. & Chen, A., 1991, "Stochastic simulation & forecasting of hourly average wind speed sequences in Jamaica", *Solar Energy*, vol. 46, pp. 1–11

- Duran, J. M., Prieto J., Barrero, F. & Toral, S., 2011, "Predictive current control of dual three-phase drives using restrained search techniques", *IEEE Transactions on Industrial Electronics*, vol. 58, pp. 3253–3263
- Erol-Kantarci, M. & Mouftah, H. T., 2010, "Using wireless sensor networks for energy-aware homes in smart grids", *IEEE Symposium on Computers and Communications (ISCC)*, p. 456-458.
- Esen H., Inalli M., Sengur A. & Esen M., 2008, "Artificial neural networks & adaptive neuro-fuzzy assessments for ground-coupled heat pump system", *Energy & Buildings*, vol. 40, pp. 1074–1083
- Fatih, O. H., Omer, N. G. & Mehmet, K., 2008, "Hourly solar irradiation forecasting using optimal coefficient 2-D linear filters and feed-forward neural network", *Solar Energy*, vol. 82, pp. 714–726
- Flax, B., 1991, "Intelligent buildings", *IEEE Communications Magazine*, Vol. 29, pp. 24–27
- Fthenakis, V. & Alsema, E., 2004, "Photovoltaics energy payback times, greenhouse gas emissions & external costs", *Progress in Photovoltaics Research & Applications*, vol. 14, pp. 275–280
- Fthenakis, V., Kim, C. H. & Alsema, E., 2008, "Emissions from photovoltaic life cycles", *Environmental Science & Technology*, vol. 42, pp. 2168–2174
- Garcia, E. C. & Morshedi, M. A., 1986, "Quadratic programming solution to Dynamic Matrix Control (QDMC)", *Chemical Engineering Communication*, vol. 46, pp. 73–87
- Giraud, F. & Salameh, Z., 2001, "Steady-state performance of a grid-connected rooftop hybrid wind-photovoltaic power system with battery storage", *IEEE Transactions on Energy Conversion*, vol. 16, pp. 1–7
- Goh, T. N. & Tan, K. J., 1977, "Stochastic modelling and forecasting of solar irradiation data", *Solar Energy*, vol. 19, pp. 755–757
- Gueymard, C. A., 2005, "Importance of atmospheric turbidity and associated uncertainties in solar irradiation & luminous efficacy modelling", *Solar Energy*, vol. 30, pp. 1603–1621
- Gueymard, C. A., 2008, "Prediction and validation of cloudless shortwave solar spectra incident on horizontal, tilted, or tracking surfaces", *Solar Energy*, vol. 82, pp. 260–271
- Hallett, S. & Wright, J., 2011, "Life without oil: why we must shift to a new energy future". Amherst, NY: Prometheus.
- Haykin, S., 1998, "Neural networks: a comprehensive foundation", (2nd edition) *Prentice Hall, Upper Saddle River*, New Jersey
- Henze, G., Kalz, D., Liu, S. & Felsmann, C., 2005, "Experimental analysis of model-based predictive optimal control for active and passive building thermal storage inventory", *International Journal of HVAC & Research*, vol. 11, pp. 189–214

- Ho, L. K., Hsu, Y. Y., Chen, F. C., Lee, E. T., Liang, C. C., Lai, S. T. & Chen, K. K., 1990, "Short term load forecasting of Taiwan power system using a knowledge-based expert system", *IEEE Transactions on Power Systems*, Vol. 5, pp. 1214–1221
- Hove, T. & Tazvinga, H., 2012, "A techno-economic model for optimising component sizing & energy dispatch strategy for PV-diesel-battery hybrid power systems", *Journal of Energy in Southern Africa*, vol. 23, pp. 18–28
- Huang, L., Walrand, J. & Ramchandran, K., 2012, "Optimal demand response with energy storage management", *2012 IEEE third international conference on smart grid communications*, pp. 61–66
- Ioannou, P. & Sun, J., 2012, "Robust adaptive control", New York, NY, USA, Dover, 2012.
- Jain, S. & Agarwal, V., 2008, "An integrated hybrid power supply for distributed generation applications fed by nonconventional energy sources", *IEEE Transactions on Energy Conversion*, vol. 23, pp. 622–631
- Jayawardena, A., Achela, D. & Fernando, K., 1998, "Use of Radial Basis Function type artificial neural networks for Runoff simulation", *Computer-Aided Civil & Infrastructure Engineering*, vol. 13, pp. 91–99
- Juan, M. L., Claudio, M., Rodolfo, D. L. & Jose, L. B., 2012, "Optimum residential load management strategy for real time pricing (RTP) demand response programs", *Energy Policy*, vol. 45, pp. 671–679
- Kalogirou S. A., 2001, "Artificial neural networks in energy systems applications: a review", *Renewable & Sustainable Energy Reviews*, vol. 5, pp. 373–401
- Kanchev, H., Lu, D., Colas, F., Lazarov, V. & Francois, B., 2011, "Energy management & operational planning of a microgrid with a PV-based active generator for smart grid applications", *IEEE Transactions on Industrial Electronics*, vol. 58, pp. 4583–4592
- Khotanzad, A., Afkhkami-Rohani, R. & Maratukulam, D., 1998, "ANNSTLF artificial neural network short-term load forecaster generation three", *IEEE Transactions on Neural Networks*, Vol. 13, pp. 1413–1422
- Kwon, W., Bruckstein, A. & Kailath, T., 1983, "Stabilizing state-feedback design via the moving horizon method", *International Journal of Control*, vol. 37, pp. 631–643
- Laustsen, J., 2008, "Energy efficiency requirements in building codes, energy efficiency policies for new buildings", *International Energy Agency. IEA Information paper*, OECD/IEA, pp. 1–85
- Levron, Y., Guerrero, J. & Beck, Y., 2013, "Optimal power flow in microgrids with energy storage", *IEEE Transactions on Power Systems*, vol. 28, pp. 3226–3234
- Liu, Y., Yuen, C., Huang, S., Ul Hassan, N., Wang, X. & Xie, S., 2014, "Peak to average ratio constrained demand side management with consumer's preference in residential smart grid", *IEEE Journal of Selected Topics on Signal Processing*, vol. 8, (6), pp. 1084–1097.

- Loutzenhier P. G., Manz H., Felsmann C., Strachan P. A., Frank T. & Maxwell G. M., 2007, "Empirical validation of models to compute solar irradiance on inclined surfaces for building energy simulation", *Solar Energy*, vol. 81, pp. 254–267
- Luenberger, G. D., 1969, "Optimization by vector space methods", *John Wiley & Sons*, New York
- Maciejowski, M. J., 2002, "Predictive control with constraints", *Pearson Education Limited*
- Maia, C. & Goncalves, M., 2009, "A methodology for short-term electric load forecasting based on specialized recursive digital filters", *Computers & Industrial Engineering*, Vol. 57, pp. 724–731
- Maitha, H. A., Ali H. A. & Hassan A. N., 2011, "Using MATLAB to develop artificial neural network Models for predicting Global Solar Irradiation in Al Ain City, UAE", Chapter 9, *Engineering Education & Research Using MATLAB*, Edited by Dr. Ali Assi, InTech, UAE
- Makarov, Y., Etingov, P., Ma, J., Huang, Z. & Subbarao, K., 2011, "Incorporating uncertainty of wind power generation forecast into power system operation, dispatch, & unit commitment procedures", *IEEE Transactions on Sustainable Energy*, vol. 2, pp. 433–442
- Martin, T. H. & Mohammad, B. M., 1994, "Training feed-forward networks with the Marquardt Algorithm", *IEEE Transactions on Neural Networks*, vol. 5, pp. 989–993
- Mellit A. & Alessandro M. P., 2010, "A 24-h forecast of solar irradiance using artificial neural network: Application for performance prediction of a grid-connected PV plant at Trieste, Italy", *Solar Energy*, vol. 84, pp. 807–821
- Mellit A., Eleuch H., Benghanem M., Elaoun C. & Massi A., 2010, "An adaptive model for predicting of global, direct & diffuse hourly solar irradiance", *Energy Conversion & Management*, vol. 51, pp. 771–782
- Mellit A. & Kalogirou S. A., 2008, "Artificial intelligence techniques for photovoltaic applications: a review", *Progress in Energy & Combustion Science*, vol. 34, pp. 574–632
- Mellit A., Kalogirou S. A., Hontoria L. & Shaari S., 2009, "Artificial intelligence techniques for sizing photovoltaic systems: a review", *Renewable & Sustainable Energy Reviews*, vol. 13, pp. 406–419
- Moghram, I. & Rahman, S., 1989, "Analysis and evaluation of five short-term load forecasting techniques", *IEEE Transactions on Power Systems*, Vol. 4, pp. 1484–1491
- Mohsenian-Rad, A. & Leon-Garcia, A., 2010, "Optimal residential load control with price prediction in real-time electricity pricing environments", *IEEE Transactions on Smart Grid*, vol. 1, pp. 120–133
- Moody, J., Utans, J., Rehfuss, S. & Siegelmann, H., 1995, "Input variable selection for Neural Networks: application to predicting the US business cycle", *Computational*

- Intelligence for Financial Engineering*, Proceedings of the IEEE/IAFE 1995, pp. 118–122
- Moura, P. S. & de-Almeida, A. T., 2010, "Multi-objective optimization of a mixed renewable system with demand-side management", *Renewable & Sustainable Energy Review*, vol. 14, pp. 1461–1468
- Moustrisa K., Paliatsos A. G., Bloutsos A., Nikolaidis K., Koronaki I. & Kavadias K., 2008, "Use of neural networks for the creation of hourly global & diffuse solar irradiance data at representative locations in Greece", *Renewable Energy*, vol. 33, pp. 928–932
- Nalbalwar, S. L., Jayesh D. R. & Sakpal, S. R., 2012, "Smart Grid: A Modernization of existing power grid", *International Journal of Advanced Engineering Research and Studies*, vol. 1, pp. 295-298.
- National Institute of Water and Atmospheric Research (<http://cliflo.niwa.co.nz/>) [cited 15/04/2014]
- Niu, D., Gu, Z. & Zhang, Y., 2009, "An AFSA-TSGM based wavelet neural network for power load forecasting", *Lecture Notes in Computer Science*, Vol. 5553, pp. 1034–1043
- Oldewurtel, F., Parisio, A., Jones, N. C., Gyalistras, D., Gwerder, M., Stauche, V., Lehmann, B. & Moraria, M., 2012, "Use of model predictive control and weather forecasts for energy efficient building climate control", *Energy and Buildings*, vol. 45, pp. 15–27
- Oldewurtel, F., Gyalistras, D., Gwerder, M., Jones, N. C., Parisio, A., Lehmann, B. & Morari, M., 2010, "Increasing energy efficiency in building climate control using weather forecasts & model predictive control", *Clima-RHEVA World Congress*, EPFL-CONF-169735
- Ordys, W. A. & Clarke, W. D., 1993, "A state-space description for GPC controllers", *International Journal of Systems Science*, vol. 24, pp. 1727–1744
- Paoli, C., Voyant, C., Muselli, M. & Nivet, L. M., 2010, "Forecasting of pre-processed daily solar radiation time series using neural networks", *Solar Energy*, vol. 84, pp. 2146–2160
- Palma, B. R., Benavides, C., Lana, F., Severino, B., Reyes, L., Llanos, J. & Saez, D., 2013, "A microgrid energy management system based on the rolling horizon strategy", *IEEE Transactions on Smart Grid*, vol. 4, pp. 996–1006
- Patel, K. & Khosla, A., 2015, "Home energy management systems in future smart grid networks: A systematic review", In *Next Generation Computing Technologies (NGCT), 2015 1st International Conference*, pp. 479-483.
- Perez, R., Moore, K., Wilcox, S., Renne, D. & Zelenka, A., 2007, "Forecasting solar irradiation: preliminary evaluation of an approach based upon the national forecast database", *Solar Energy*, vol. 81, pp. 809–812
- Peterka, V., 1984, "Predictor-based self-tuning control", *Automatica*, vol. 20, pp. 39–50

- Qi, W., Liu, J., X. Chen, X. & Christofides, D. P., 2011, "Supervisory predictive control of standalone wind/solar energy generation systems", *IEEE Transactions on Control Systems Technology*, Vol. 19, pp. 199–207
- Rahim, S., Javaid, N., Ahmad, A., Khan, S. A., Khan, Z. A., Alrajeh, N. & Qasim, U., 2016, "Exploiting heuristic algorithms to efficiently utilize energy management controllers with renewable energy sources", *Energy and Buildings*, vol. 129, pp. 452-470.
- Rahman, S. & Hazim, O., 1993, "A generalized knowledge-based short-term load-forecasting technique", *IEEE Transactions on Power Systems*, Vol. 8, pp. 508–514
- Rajagopalan, S. & Santoso, S., 2009, "Wind power forecasting and error analysis using the autoregressive moving average modelling", *Power & Energy Society General Meeting, 2009, PES '09. IEEE*, 1– 6, pp. 26–30
- Rawlings, B. J., 2000, "Tutorial overview of model predictive control", *IEEE Control Systems Magazine*, vol. 20, pp. 38–52
- Rich, H. I., Hugo T. P. & Carlos F. C., 2013, "Solar forecasting methods for renewable energy integration", *Progress in Energy & Combustion Science*, vol. 39, pp. 535–576
- Richalet, J., Rault, J. A., Testud, L. & Papon, J., 1976, "Algorithmic control of industrial process", *Proceedings: Symposium on identification and system parameter estimation. IFAC. Tbilisi, 1976*
- Richalet, J., Rault, A., Testud, J. & Papon, J., 1978, "Model predictive heuristic control: Applications to industrial processes", *Automatica*, vol. 14, pp. 413–428
- Sfetsos A. & Coonick A. H., 2000, "Univariate & multivariate forecasting of hourly solar radiation with artificial intelligence techniques", *Solar Energy*, vol. 68, pp. 169–178
- Shaahid, M. S. & Elhadidy, M. A., 2008, "Economic analysis of hybrid photovoltaic diesel battery power systems for residential loads in hot regions, A step to clean future", *Renewable and Sustainable Energy Reviews*, vol. 12, pp. 488–503
- Sossan, F., Kosek, M. A., Martinenas, S., Marinelli, M. & Bindner, H., 2013, "Scheduling of domestic water heater power demand for maximizing PV self-consumption using model predictive control", *Proceedings of ISGT, 4th European Innovative Smart Grid Technologies*
- Stryi-Hipp, G. & ESTTP Panel, 2012, "Solar heating and cooling for a sustainable energy future in Europe", *European Solar Thermal Technology Platform (ESTTP)*, <http://www.estif.org>
- Tazvinga, H., Xia, X. & Zhang, J., 2013, "Minimum cost solution to photovoltaic-diesel battery hybrid power systems for remote consumers", *Solar Energy*, vol. 96, pp. 292–299
- Teleke, S., Baran, M., Bhattacharya, S. & Huang, A., 2010, "Rule-based control of battery energy storage for dispatching intermittent renewable sources", *IEEE Transactions on Sustainable Energy*, vol.1, pp. 117–24

- Thi, H. L., Nguyen, N. T. & Do, T. V., 2015, "Advanced computational methods for knowledge engineering", *Proceedings of 3rd International Conference on Computer Sciences, Applied Mathematics & Applications*, ICCSAMA 2015.
- Thomsen, S., Hoffmann, N. & Fuchs, W. F., 2011, "PI control, PI-based state space control & model-based predictive control for drive systems with elastically coupled loads; A comparative study", *IEEE Transactions on Industrial Electronics*, vol. 58, pp. 3647–3657
- Tiwari, G. N. & Dubey, S., 2010, "Fundamentals of photovoltaic modules & their applications". *RSC Publishing*, 2010, no. 2, Cambridge
- Torres, J. L., Garcia, A., De Blas, M. & De Francisco, A., 2005, "Forecast of hourly average wind speed with ARMA models in Navarre (Spain)", *Solar Energy*, vol. 79, pp. 65–77
- Ulgen K. & Hepbasli A., 2009, "Diffuse solar irradiation estimation models for Turkey's big cities", *Energy Conversion & Management*, vol. 50, pp. 149–156
- Vahidi, A., Stefanopoulou, A. & Peng, H., 2006, "Current management in a hybrid fuel cell power system: A model predictive control approach", *IEEE Transactions on Control Systems Technology*, vol. 14, pp. 1047–1057
- Voyant, C., Randimbivololona, P., Nivet, M. L., Paoli, C. & Muselli, M., 2014, "Twenty-four hours ahead global irradiation forecasting using multi-layer perceptron", *Meteorological Applications*, vol. 21, pp. 644–655
- Vrettos, E., Witzig, A., Kurmann, R., Koch, S. & Andersson, G., 2013, "Maximizing local PV utilization using small-scale batteries and flexible thermal loads", *European PV Solar Energy Conference & Exhibition (PVSEC)*, France
- Wahab, A. H., Dukea, M., Carsona, K. J. & Anderson, T., 2011, "Studies of control strategies for building integrated solar energy system", *Proceedings of the 2011 IEEE First Conference on Clean Energy & Technology*, Malaysia
- Wang, L., 2009, "Model predictive control system design and implementation using MATLAB®", *Advances in industrial control*, ISSN 1430-9491, Springer-Verlag London
- Wang, C. & Nehrir, M., 2008, "Power management of a stand-alone wind/photovoltaic/fuel cell energy system", *IEEE Transactions on Energy Conversion*, vol. 23, pp. 957–67
- Wang, S. C., 2012. "Incentive policies and market trends of PV in China", *Solarbuzz China Conference*, 2012
- Wismer, A. D. & Chattergy, R., 1978, "Introduction to nonlinear optimization, a problem solving approach", North-Holland, New York
- Wu, Z., Tazvinga, H. & Xia, X., 2015, "Demand side management of photovoltaic-battery hybrid system", *Applied Energy*, vol. 148, pp. 294–304

Yadav, A. K. & Chandel, S. S., 2014, “Solar irradiation prediction using artificial neural network techniques: A review”, *Renewable & Sustainable Energy Reviews*, vol. 33, pp. 772–781

Xia, C., Wang, J. & McMenemy, K., 2010, “Short, medium & long-term load forecasting model & virtual load forecaster based on radial basis function neural networks”, *International Journal of Electrical Power & Energy Systems*, Vol. 32, pp. 743–750

Yousefizadeh, H. & Zilouchian, A., 2001, Neural network architectures, Chapter. 3, “Intelligent control systems using soft computing methodologies”, Edited by A. Zilouchian, M. Jamshidi, CRC Press

Zervas, P., Sarimveis, H., Palyvos, J. & Markatos, N., 2008, "Model-based optimal control of a hybrid power generation system consisting of photovoltaic arrays & fuel cells", *Journal of Power Sources*, vol. 181, pp. 327–38

Zhu, B., Tazvinga, H. & Xia, X., 2015, “Switched model predictive control for energy dispatching of a photovoltaic-diesel-battery hybrid power system”, *IEEE Transactions on Control Systems Technology*, vol. 23, pp. 1229–1236

Appendix A: MODEL PREDICTIVE CONTROL WITH CONSTRAINTS

In this section, basic ideas and terms about discrete-time model predictive control with constraints are discussed. In section A.4, multi-input-multi-output (MIMO) state-space model with an embedded integrator is discussed. Section A.3 examines the design of predictive control within one optimization window, which is expanded to demonstrate the idea of receding horizon control as well as, state feedback gains matrices and the closed loop configuration of the predictive control system. The constrained control problem in the context of quadratic programming problem is formulated and discussed.

A.1. MIMO State-space models

In the earlier formulation of model predictive control, finite impulse response (FIR) and step response models were favoured because, these models allow intrinsic dead time compensation due to the use of process model to predict future behaviour. Cutler and Ramaker, (1979) and Garcia and Morshedi, (1986) are significant works towards using FIR/step response model based design algorithms for dynamic matrix control (DMC) and quadratic DMC formulation respectively.

The FIR type of models are attractive to process engineers because the model structure gives a transparent description of process time delay, response time and gain. However, FIR model's performance deteriorates for stable plants and often require large model orders. FIR model structure typically requires 30 to 60 impulse response coefficients depending on the process dynamics and choice of sampling intervals. On the other hand, transfer function models give a more parsimonious description of process dynamics and are applicable to both stable and unstable plants. Predictive control

algorithm of Peterka, (1984) and the generalized predictive control (GPC) algorithm of Clarke et al. (1987) are significant works on transfer-function model based predictive control. Later experiments showed that state-space model-based formulation of GPC can handle multivariable plants more effectively than transfer-function model-based predictive control (Ordys and Clarke, 1993).

Recent years have seen the growing popularity of predictive control design using state-space models due to the simplicity of the design framework and its direct link with the linear quadratic regulators (Rawlings, 2000) and (Maciejowski, 2002).

Model predictive control systems are designed based on a mathematical model of the plant. By using a state-space model, the current information required for predicting ahead is represented by the state variable at the current time.

A MIMO state-space plant model is represented by Equation (a1) and (a2) which has m inputs, q outputs and n_l states with noise and disturbances.

$$x_m(k + 1) = A_m x_m(k) + B_m u(k) + B_d \omega(k) \quad (a1)$$

$$y(k) = C_m x_m(k) \quad (a2)$$

where $\omega(k)$ is the input disturbance, assumed to be a sequence of integrated white noise. This means that the input disturbance $\omega(k)$ is related to a zero-mean, white noise sequence $\epsilon(k)$ by the following difference Equation (a3).

$$\omega(k) - \omega(k - 1) = \epsilon(k) \quad (a3)$$

Note that from Equation (a1), the following difference equation is also true.

$$x_m(k) = A_m x_m(k - 1) + B_m u(k - 1) + B_d \omega(k - 1) \quad (a4)$$

By defining $\Delta x_m(k) = x_m(k) - x_m(k-1)$ and $\Delta u(k) = u(k) - u(k-1)$, then subtracting Equation (a3) from Equation (a1) leads to

$$\Delta x_m(k+1) = A_m \Delta x_m(k) + B_m \Delta u(k) + B_d \epsilon(k) \quad (a5)$$

In order to relate the output $y(k)$ to the state variable $\Delta x_m(k)$, we deduce that

$$\Delta y(k+1) = C_m \Delta x_m(k+1) = C_m A_m \Delta x_m(k) + C_m B_m \Delta u(k) + C_m B_d \epsilon(k) \quad (a6)$$

where $\Delta y(k+1) = y(k+1) - y(k)$

choosing a new state variable vector $x(k) = [\Delta x_m(k)^T \ y(k)^T]^T$, we have the following state-space matrices

$$\begin{bmatrix} \Delta x_m(k+1) \\ y(k+1) \end{bmatrix} = \begin{bmatrix} A_m & O_m^T \\ C_m A_m & I_{q \times q} \end{bmatrix} \begin{bmatrix} \Delta x_m(k) \\ y(k) \end{bmatrix} + \begin{bmatrix} B_m \\ C_m B_m \end{bmatrix} \Delta u(k) + \begin{bmatrix} B_d \\ C_m B_d \end{bmatrix} \epsilon(k)$$

$$y(k) = [O_m \quad I_{q \times q}] \begin{bmatrix} \Delta x_m(k) \\ y(k) \end{bmatrix} \quad (a7)$$

where $I_{q \times q}$ is the identity matrix with dimensions $q \times q$, which is the number of outputs, and O_m is a $q \times n_1$ zero matrix. A_m, B_m and C_m have dimension $n_1 \times n_1, n_1 \times m$ and $q \times n_1$ respectively in Equation (a7). For notation simplicity, we denote Equation (a7) by

$$x(k+1) = Ax(k) + B\Delta u(k) + B_\epsilon \epsilon(k)$$

$$y(k) = Cx(k) \quad (a8)$$

where A, B and C are matrices corresponding to the forms given in Equation (a7).

A.2 Prediction of state and output variables

Next step in the formulation of model predictive control is to calculate the predicted plant output with the future control signal as the adjustable variables. k_i is the current time and N_p is the length of the optimization window. At sampling instant k_i , $k_i > 0$, the state variable vector $x(k_i)$ is available through measurements, the state $x(k_i)$ provides the current plant information. The future control trajectory is denoted by

$$\Delta u(k_i), \Delta u(k_i + 1), \dots, \Delta u(k_i + N_c - 1) \quad (\text{a9})$$

where N_c is the control horizon dictating the number of parameters used to capture the future control trajectory. With given information $x(k_i)$, the future state variables are predicted for N_p number of samples, where N_p is called the prediction horizon which is also the length of the optimization window. The future state variables are denoted by Equation (a10) below

$$x(k_i + 1 | k_i), x(k_i + 2 | k_i), \dots, x(k_i + m | k_i), \dots, x(k_i + N_p | k_i) \quad (\text{a10})$$

where $x(k_i + m | k_i)$ is the predicted state variable at $k_i + m$ with given current plant information $x(k_i)$. The control horizon N_c is chosen to be less than (or equal to) the prediction horizon N_p .

The input ΔU and output Y are defined in Equation (a11) and (a12) respectively. The dimensions of output variables vector y , input variables vector u and state variables vector x_m are $p \times 1$, $m \times 1$ and $n_1 \times 1$ respectively.

$$\Delta U = [\Delta u(k_i)^T \Delta u(k_i + 1)^T \Delta u(k_i + 2)^T \dots \Delta u(k_i + N_c - 1)^T]^T \quad (\text{a11})$$

$$Y = [y(k_i + 1 | k_i)^T \ y(k_i + 2 | k_i)^T \ y(k_i + 3 | k_i)^T \ \dots \ y(k_i + N_p | k_i)^T]^T \quad (\text{a12})$$

$$\Delta U = N_c m \times 1, Y = N_p p \times 1$$

Now from the state-space model (A, B, C), the predicted state variables are computed sequentially using the set of future control parameters as:

$$x(k_i + 1 | k_i) = Ax(k_i) + B\Delta u(k_i) + B_d \epsilon(k_i)$$

$$\begin{aligned} x(k_i + 2 | k_i) &= Ax(k_i + 1 | k_i) + B\Delta u(k_i + 1) + B_d \epsilon(k_i + 1 | k_i) \\ &= A^2 x(k_i) + AB\Delta u(k_i) + B\Delta u(k_i + 1) + AB_d \epsilon(k_i) \\ &\quad + B_d \epsilon(k_i + 1 | k_i) \end{aligned}$$

$$\begin{aligned} x(k_i + 3 | k_i) &= Ax(k_i + 2 | k_i) + B\Delta u(k_i + 2) + B_d \epsilon(k_i + 2 | k_i) \\ &= A[A^2 x(k_i) + AB\Delta u(k_i) + B\Delta u(k_i + 1) + AB_d \epsilon(k_i) \\ &\quad + B_d \epsilon(k_i + 1 | k_i)] + B\Delta u(k_i + 2) \\ &\quad + B_d \epsilon(k_i + 2 | k_i) \end{aligned}$$

$$\begin{aligned} &= A^3 x(k_i) + A^2 B\Delta u(k_i) + AB\Delta u(k_i + 1) \\ &\quad + B\Delta u(k_i + 2) + A^2 B_d \epsilon(k_i) \\ &\quad + AB_d \epsilon(k_i + 1 | k_i) + B_d \epsilon(k_i + 2 | k_i) \end{aligned}$$

•

•

•

$$\begin{aligned} x(k_i + N_p | k_i) &= A^{N_p} x(k_i) + A^{N_p-1} B\Delta u(k_i) + A^{N_p-2} B\Delta u(k_i + 1) \\ &\quad + A^{N_p-N_c} B\Delta u(k_i + N_c - 1) \\ &\quad + A^{N_p-1} B_d \epsilon(k_i) \\ &\quad + A^{N_p-2} B_d \epsilon(k_i + 1 | k_i) + \dots + B_d \epsilon(k_i \\ &\quad + N_p - 1 | k_i) \end{aligned} \quad (\text{a13})$$

With the assumption that $\epsilon(k)$ is a zero-mean white noise sequence, the predicted value of $\epsilon(k_i + i | k_i)$ at future samples i assumed to be zero. The prediction of state

variable and output variable is calculated as the expected values of the respective variables, hence, the noise effect to the predicted values being zero.

For $N_p = 4$ and $N_c = 2$

$$\begin{aligned} x(k_i + 4 | k_i) &= A^4 x(k_i) + A^3 B \Delta u(k_i) + A^2 B \Delta u(k_i + 1) \\ &\quad + A^3 B_\epsilon \epsilon(k_i) + A^2 B_\epsilon \epsilon(k_i + 1 | k_i) \\ &\quad + B_\epsilon \epsilon(k_i + 2 | k_i) \end{aligned}$$

For $N_p = 4$ and $N_c = 4$

$$\begin{aligned} x(k_i + 4 | k_i) &= A^4 x(k_i) + A^3 B \Delta u(k_i) + A^2 B \Delta u(k_i + 1) \\ &\quad + AB \Delta u(k_i + 2) + B \Delta u(k_i + 3) \end{aligned}$$

Now the predicted output variables are computed from predicted state variables as:

$$y(k_i + 1 | k_i) = CAx(k_i) + CB\Delta u(k_i)$$

$$\begin{aligned} y(k_i + 1 | k_i) &= Cx(k_i + 1 | k_i) \\ &= CA^2 x(k_i) + CAB\Delta u(k_i) + CB\Delta u(k_i + 1) \end{aligned}$$

$$\begin{aligned} y(k_i + 3 | k_i) &= Cx(k_i + 2 | k_i) \\ &= CA^3 x(k_i) + CA^2 B \Delta u(k_i) + CAB \Delta u(k_i + 1) \\ &\quad + CB \Delta u(k_i + 2) \end{aligned}$$

•
•
•

$$\begin{aligned} y(k_i + N_p | k_i) &= Cx(k_i + N_p - 1 | k_i) \\ &= CA^{N_p} x(k_i) + CA^{N_p-1} B \Delta u(k_i) \\ &\quad + CA^{N_p-2} B \Delta u(k_i + 1) + \dots \\ &\quad + CA^{N_p-N_c} B \Delta u(k_i + N_c - 1) \end{aligned} \tag{a14}$$

For $N_p = 4$ and $N_c = 2$

$$y(k_i + 4 | k_i) = CA^4x(k_i) + CA^3B\Delta u(k_i) + CA^2B\Delta u(k_i + 1)$$

For $N_p = 4$ and $N_c = 4$

$$\begin{aligned} y(k_i + 4 | k_i) \quad y(k_i + 4 | k_i) &= CA^4x(k_i) + CA^3B\Delta u(k_i) \\ &+ CA^2B\Delta u(k_i + 1) + CAB\Delta u(k_i + 2) \\ &+ CB\Delta u(k_i + 3) \end{aligned}$$

Equation (a13) and (a14) can be collected together in a compact matrix form as

$$Y = Fx(k_i) + \Phi\Delta U \quad (a15)$$

Where

$$F = \begin{bmatrix} CA \\ CA^2 \\ CA^3 \\ \vdots \\ CA^{N_p} \end{bmatrix}; \quad \Phi = \begin{bmatrix} CB & 0 & 0 & \cdots & 0 \\ CAB & CB & 0 & \cdots & 0 \\ CA^2B & CAB & CB & \cdots & 0 \\ \vdots & \vdots & \vdots & \cdots & \vdots \\ CA^{N_p-1}B & CA^{N_p-2}B & CA^{N_p-3}B & \cdots & CA^{N_p-N_c}B \end{bmatrix}$$

where dimensions of Y is $N_p p \times 1$, x is $n \times 1$, F is $N_p p \times n$, Φ is $N_p p \times N_c m$ and ΔU is $N_c m \times 1$. The control calculations are based on minimizing the predicted deviations between the predicted output and the reference trajectory. The predicted error vector is defined as

$$\hat{E}(k_i + 1) = Y_r(k_i + 1) - Y(k_i + 1) \quad (a16)$$

This is $N_p p \times 1$ vector. The objective of the control calculations is to determine the control moves $\Delta U(k_i)$ for the next N_c time intervals. The $N_c m$ -dimensional vector $\Delta U(k_i)$ is calculated such that an objective function is minimized. Also the predicted

error over the prediction horizon N_p and the size of the control move over the control horizon N_c is minimized.

A.3 Optimization

The objective of the predictive control system for a given reference signal $r(k_i)$ at sample time k_i , within a prediction horizon N_p to bring the predicted output as close as possible to the reference signal. To find the optimum control parameter vector ΔU , the objective is translated into a design such that the error function between the reference signal and the predicted output is minimized as shown in Equation (a16). The cost function J which reflects the control objective is defined as

$$J = (R_s - Y)^T(R_s - Y) + \Delta U^T \bar{R} \Delta U \quad (a17)$$

where the first term is linked to the objective of minimizing the errors between the predicted output and the reference signal while the second term reflects the consideration given to the size of ΔU when the objective function J is made to be as small as possible. \bar{R} is the diagonal matrix in the form that $\bar{R} = r_w I_{N_c \times N_c}$ ($r_w \geq 0$) where r_w is used as a tuning parameter for the desired closed-loop performance. For the case when $r_w = 0$, the cost function in Equation (a17) is interpreted as the situation where we would not want to pay any attention to how large the ΔU might be and our goal would be solely to make the error $(R_s - Y)^T(R_s - Y)$ as small as possible. For the case when $r_w > 0$, the cost function in Equation (a17) is interpreted as the situation where we would carefully consider how large the ΔU might be and cautiously reduce the error $(R_s - Y)^T(R_s - Y)$.

The optimal ΔU which will minimize J , by using Equation (a15), J can be expressed as

$$J = (R_s - Fx(k_i))^T (R_s - Fx(k_i)) - 2\Delta U^T \Phi^T (R_s - Fx(k_i)) + \Delta U^T (\Phi^T \Phi + \bar{R}) \Delta U \quad (a18)$$

First derivative of the cost function J is given by

$$\frac{\partial J}{\partial \Delta U} = -2\Phi^T (R_s - Fx(k_i)) + 2(\Phi^T \Phi + \bar{R}) \Delta U \quad (a19)$$

The necessary condition of the minimum J is given by

$$\frac{\partial J}{\partial \Delta U} = 0 \quad (a20)$$

By using these condition, the optimal solution for the control signal can be expressed as

$$\Delta U = (\Phi^T \Phi + \bar{R})^{-1} \Phi^T (R_s - Fx(k_i)) \quad (a21)$$

with the assumption that $(\Phi^T \Phi + \bar{R})^{-1}$ exists. The matrix $(\Phi^T \Phi + \bar{R})^{-1}$ is called the Hessian matrix in the optimization literature. The optimal solution of the control signal is linked to the reference signal $r(k_i)$ and the state variable $x(k_i)$ via Equation (a22)

$$\Delta U = (\Phi^T \Phi + \bar{R})^{-1} \Phi^T (\bar{R}_s r(k_i) - Fx(k_i)) \quad (a22)$$

A.4 Constraints for the MIMO state-space model

Constraints are specified for each input independently for the MIMO state-space model. Constraints for the upper limits are given by Equation (a23)

$$[\Delta u_1^{max} \ \Delta u_2^{max} \ \dots \ \Delta u_m^{max}] \quad (a23)$$

And constraints for the lower limits are given by Equation (a24)

$$[\Delta u_1^{min} \Delta u_2^{min} \dots \Delta u_m^{min}] \quad (a24)$$

Variable with rate of change is specified as

$$\Delta u_1^{min} \leq \Delta u_1(k) \leq \Delta u_1^{max}$$

$$\Delta u_2^{min} \leq \Delta u_2(k) \leq \Delta u_2^{max}$$

.

.

.

$$\Delta u_m^{min} \leq \Delta u_m(k) \leq \Delta u_m^{max} \quad (a25)$$

Similarly, constraints for the upper limit of the control signal are given by

$$u_1^{max} \ u_2^{max} \ \dots \ u_m^{max}$$

And for lower limit as

$$u_1^{min} \ u_2^{min} \ \dots \ u_m^{min}$$

Also the amplitude of each control signal is required to satisfy the constraints as specified in Equation (a26)

$$u_1^{min} \leq u_1(k) \leq u_1^{max}$$

$$u_2^{min} \leq u_2(k) \leq u_2^{max}$$

.

.

.

$$u_m^{min} \leq u_m(k) \leq u_m^{max} \quad (a26)$$

Constraints for each output and state variables are specified similarly if required. It should be noted that constraints for each input and output in a MIMO system are specified independently.

A.5 Constraints as part of the optimal solution

Constrained variables are parametrized using the same parameter vector ΔU and since the predictive control problem is solved using the receding horizon control framework, the constraints are taken into consideration for each moving horizon window. This firstly allows us to vary the constraints at the beginning of each optimization window and secondly to provide the means to tackle the constrained controlled problem numerically. If the constraints on the rate of change of the control signal $\Delta u(k)$ at time k_i , then the constraints at sample time k_i are defined as

$$\Delta u^{min} \leq \Delta u(k_i) \leq \Delta u^{max} \quad (a27)$$

The predictive control scheme calculates future instances $(k + 1, K + 2 \dots K + N_p)$ from the time instance k_i . The constraints at future samples, $\Delta u(k_i), \Delta u(k_i + 1), \Delta u(k_i + 2), \Delta u(k_i + 3) \dots \Delta u(k_i + N_p - 1)$ are given as

$$\Delta u^{min} \leq \Delta u(k_i) \leq \Delta u^{max}$$

$$\Delta u^{min} \leq \Delta u(k_i + 1) \leq \Delta u^{max}$$

$$\Delta u^{min} \leq \Delta u(k_i + 2) \leq \Delta u^{max}$$

.

.

.

$$\Delta u^{min} \leq \Delta u(k_i + N_p - 1) \leq \Delta u^{max}$$

In principle, all the constraints are defined within the prediction horizon but in some cases smaller set of sampling instants are chosen to impose the constraints, instead of all the future samples to reduce computational load. The requirement to obtain optimal solutions using quadratic programming is to decompose the constraints into two parts to reflect the lower limit, and the upper limit with opposite sign is define as

$$\Delta U^{min} \leq \Delta U \leq \Delta U^{max}$$

Can be expressed by two inequalities as follow

$$-\Delta U \leq -\Delta U^{min} \quad (a28)$$

$$\Delta U \leq \Delta U^{max} \quad (a29)$$

Equation (a28) and (a29) can be written in matrix from as

$$\begin{bmatrix} -I \\ I \end{bmatrix} \Delta U \leq \begin{bmatrix} -\Delta U^{min} \\ \Delta U^{max} \end{bmatrix} \quad (a30)$$

where ΔU^{min} and ΔU^{max} are column vectors with N_c elements of ΔU^{min} and ΔU^{max} , respectively. The output constraints are expressed in terms of ΔU as follow

$$Y^{min} \leq Fx(k_i) + \Phi \Delta U \leq Y^{max} \quad (a31)$$

Further, the model predictive control with the hard constraints is proposed which has the objective of finding the parameter vector ΔU which is minimizing the cost function J as given in Equation (a32) below.

$$J = (R_s - Fx(k_i))^T (R_s - Fx(k_i)) - 2\Delta U^T \Phi^T (R_s - Fx(k_i)) + \Delta U^T (\Phi^T \Phi + \bar{R}) \Delta U \quad (a32)$$

Subject to the inequality constraints

$$\begin{bmatrix} M_1 \\ M_2 \\ M_3 \end{bmatrix} \Delta U \leq \begin{bmatrix} N_1 \\ N_2 \\ N_3 \end{bmatrix} \quad (a33)$$

where $\Phi^T \Phi + \bar{R}$ is a Hessian matrix and is assumed to be positive definite. As the cost function J is quadratic and constraints are linear inequalities, the solution for the optimal predictive control is similar to finding an optimal solution for a standard quadratic programming problem. For compactness of expression, Equation (a33) can be expressed as

$$M \Delta U \leq \gamma \quad (a34)$$

Where M is a matrix representing constraints. The number of rows and columns in the matrix M is equal to the number of constraints and the dimension of ΔU respectively. When the constraints are fully imposed, the number of constraints is equal to $4 \times m \times N_c + 2 \times q \times N_p$, where m is the number of inputs and q is the number of outputs.

A.6 Numeric solution of MPC using quadratic programming

Quadratic programming (QP) is the problem of minimizing a quadratic objective function of many variables subject to a set of linear equality or inequality constraints and possibly constraints on variable values. QP attracts more attention than linear programming (LP) approach because it allows the modelling and investigation of interactions between variables, such as a demand change resulting from a price change, both of which would obviously affect total profits. In LP, the assumption that price is independent of demand should be made to achieve the objective (Byrne, 1984). Using QP is also useful because it provides the ease of accessing the code if anything goes wrong or to write safety ‘jacket’ software for real-time applications. To be consistent with the

literature of quadratic programming, the decision variable is denoted by x . The constraints and objective function J are expressed as given in Equation (a35) below.

$$J = \frac{1}{2} x^T E x + x^T F \quad (a35)$$

$$Mx \leq \gamma \quad (a36)$$

where E, F, M and γ are compatible matrices and vectors in the quadratic programming problem. E is assumed to be symmetric and positive definite.

A.7 Quadratic programming for equality and inequality constraints

To find the constrained minimum of a positive definite quadratic function with linear equality constraints $Mx = \gamma$ is the simplest problem of QP. Each linear equality constraint defines a hyperplane. Positive definite quadratic functions have their level surfaces as hyperellipsoids. Intuitively, the constrained minimum is located at the point of tangency between the boundary of the feasible set and the minimizing hyperellipsoid. On the other hand, the number of constraints could be larger than the number of decision variables in the minimization with inequality constraints. The inequality constraints $Mx \leq \gamma$ may contain active and inactive constraints. An inequality $M_i x \leq \gamma_i$ is considered to be active if $M_i x = \gamma_i$ and inactive if $M_i x < \gamma_i$, where M_i together with γ_i form the i th inequality constraints and are the i th row of M matrix and the i th element of γ vector, respectively.

A.8 Hildreth's quadratic programming procedure

(Luenberger, 1969) and (Wismer and Chattergy, 1978) have proposed a simple algorithm called the Hildreth's quadratic programming procedure to solve the dual

functional problem. In this algorithm, a decent procedure is employed with direction vectors equal to the usual basis vectors $e_i = (0, 0, \dots, 1, 0, \dots, 0)$. Specifically, the infinite sequence of direction vectors be $\{e_1, e_2, \dots, e_n, e_1, e_2, \dots, e_n, \dots\}$. thus the vector λ can be varied by one component at a time. At a given step in the process, having obtained a vector $\lambda \geq \theta$, priority is given to the solution of single component λ_i . The objective function may be regarded as a quadratic function of this single component. λ_i is adjusted to minimize the function, or if that would require $\lambda_i < 0$, $\lambda_i = 0$ can be adjusted. In any case, however the objective function is minimized. Then the next component λ_{i+1} is considered. If one complete cycle through the components to be one iteration is considered and taking the vector λ^m to λ^{m+1} , the method can be expressed explicitly as

$$\lambda_i^{m+1} = \max(0, \omega_i^{m+1}) \quad (a37)$$

with

$$\omega_i^{m+1} = -\frac{1}{h_{ii}} \left[k_i + \sum_{j=1}^{i-1} h_{ij} \lambda_j^{m+1} + \sum_{j=i+1}^n h_{ij} \lambda_j^m \right] \quad (a38)$$

where the scalar h_{ij} is the ij th element in the matrix $H = ME^{-1}M^T$, and k_i is the i th element in the vector $K = \gamma + ME^{-1}F$. Also it can be noted that in Equation (a38), there are two sets of λ values in the computation, one involves λ^m and the other involves the updated λ^{m+1} .

The converged λ^* vector contains either zeros or positive values of the Lagrange multipliers, x can be written as

$$x = -E^{-1}(F + M^T \lambda^*) \quad (a39)$$

It can be noted that Hildreth's quadratic programming algorithm is based on an element-by-element search, consequently it does not require any matrix inversion. As a result, if the active constraints are linearly independent and their number is less than or equal to the number of decision variables, then the dual variables will converge. However, if one or both of these requirements are violated, then the dual variables will not converge to a set of fixed values. The iteration will terminate when the iterative counter reaches its maximum value. As there is no matrix inversion, the computation will continue without interruption and give near-optimal solution with constraints if the situation of conflict constraints arise which is one of the key strength of using this approach in real-time applications. Further this approach has the ability to automatically recover from an ill-conditioned constrained problem for the safety of plant operation.

The one-dimensional search technique in Hildreth's quadratic programming procedure has been shown to converge to the set of λ^* , When the conditions are satisfied. λ^* contains zeros for inactive constraints and the positive components corresponding to the active constraints. The positive component collected as a vector is called λ_{act}^* with its value defined by

$$\lambda_{act}^* = -(M_{act}E^{-1}M_{act}^T)^{-1}(\gamma_{act} + M_{act}E^{-1}F) \quad (a40)$$

where M_{act} and γ_{act} are the constraints data matrix and vector with deletion of the row elements that corresponding to the zero elements in λ^* . The proof of the convergence relies on the existence of a set of bounded λ_{act}^* . This is virtually determined by the existence of the $M_{act}E^{-1}M_{act}^T$ (Wang, 2009).

A.9 Summary

Discrete-time MPC with constraints was discussed. The current plant information was represented by the state variable vector $x(k_i)$, the prediction of the future behaviour of the plant output relies on the state-space model where the optimal control trajectory was captured by the set of parameters that define the incremental control movements. The objective of the control system was expressed in terms of the error function between the reference and the predicted output signal within the optimization window. Although the optimal control trajectory was calculated for N_c future samples, the implementation of the predictive control used only the first sample, $\Delta u(k_i)$ while ignoring the rest of the trajectory. The optimization procedure repeated itself when the next sample period arrived, based on the receding horizon control principle, where feedback was naturally incorporated in the control system design.

Plant operational limits, including limits on the input variables, the incremental change of the input variables, state variables and plant output variables were defined. Also the steps involved in solving the constrained optimization problem using a quadratic programming procedure at every sampling instance to obtain the optimal solution of the decision variables have been presented.

MPC with disturbances was discussed and disturbance matrix was incorporated in the state-space model equations. Global solar radiation prediction and energy demand prediction as discussed in chapter 2 and 3 respectively were used as measured disturbances in the MPC development in to plan for periods of low sunshine or high energy demand.

Appendix B: HOURLY LOAD ENERGY DEMAND AND PV ARRAY

PRODUCTION DATA

B.1 Hourly load energy demand data

Table 18. Load energy demand ($E_d(k)$) profiles in kWh for a residential house

Date and Time	Load Energy Demand (kWh)	Date and Time	Load Energy Demand (kWh)
1/08/2015 0:00	0.11	4/08/2015 11:59	1.78
1/08/2015 1:00	0.11	4/08/2015 12:59	1.93
1/08/2015 2:00	0.12	4/08/2015 13:59	2.38
1/08/2015 3:00	0.13	4/08/2015 14:59	2.21
1/08/2015 4:00	0.12	4/08/2015 15:59	1.75
1/08/2015 5:00	0.12	4/08/2015 16:59	2.54
1/08/2015 6:00	0.14	4/08/2015 17:59	2.47
1/08/2015 7:00	0.13	4/08/2015 18:59	0.96
1/08/2015 8:00	0.11	4/08/2015 19:59	2.64
1/08/2015 9:00	1.65	4/08/2015 20:59	2.61
1/08/2015 10:00	4.67	4/08/2015 21:59	5.68
1/08/2015 11:00	1.98	4/08/2015 22:59	3.05
1/08/2015 12:00	4.89	4/08/2015 23:59	3.06
1/08/2015 13:00	1.87	5/08/2015 0:00	3.74
1/08/2015 14:00	2.89	5/08/2015 1:00	0.12
1/08/2015 15:00	3.7	5/08/2015 2:00	0.13
1/08/2015 16:00	3.59	5/08/2015 3:00	0.13
1/08/2015 17:00	3.5	5/08/2015 4:00	0.12
1/08/2015 18:00	0.15	5/08/2015 5:00	0.12
1/08/2015 19:00	1.77	5/08/2015 6:00	0.12
1/08/2015 19:59	1.78	5/08/2015 7:00	0.14
1/08/2015 20:59	1.91	5/08/2015 8:00	1.65
1/08/2015 21:59	1.87	5/08/2015 9:00	1.63
1/08/2015 22:59	1.71	5/08/2015 10:59	1.65
1/08/2015 23:59	1.62	5/08/2015 11:00	2.11
2/08/2015 0:00	1.62	5/08/2015 12:00	2.69
2/08/2015 1:00	2.61	5/08/2015 13:00	3.49
2/08/2015 2:59	2.62	5/08/2015 14:00	1.76
2/08/2015 3:00	2.62	5/08/2015 15:00	1.76
2/08/2015 4:00	2.61	5/08/2015 16:00	1.75
2/08/2015 5:00	5.47	5/08/2015 17:00	1.09
2/08/2015 6:00	0.15	5/08/2015 18:00	3.47
2/08/2015 7:00	1.64	5/08/2015 19:00	3.48

2/08/2015 8:00	1.64	5/08/2015 20:00	2.65
2/08/2015 9:00	2.2	5/08/2015 21:00	2.61
2/08/2015 10:00	2.22	5/08/2015 22:00	2.64
2/08/2015 11:00	3.81	5/08/2015 23:00	3.03
2/08/2015 12:00	1.87	6/08/2015 0:00	2.96
2/08/2015 13:00	1.69	6/08/2015 2:59	2.66
2/08/2015 14:00	0.25	6/08/2015 3:00	2.62
2/08/2015 15:00	3.59	6/08/2015 4:00	2.63
2/08/2015 16:00	3.47	6/08/2015 5:00	0.12
2/08/2015 17:00	3.46	6/08/2015 6:00	0.13
2/08/2015 18:00	2.78	6/08/2015 7:00	1.63
2/08/2015 19:00	1.7	6/08/2015 8:00	1.63
2/08/2015 20:00	1.73	6/08/2015 9:00	1.64
2/08/2015 21:00	4.57	6/08/2015 10:00	1.66
2/08/2015 22:00	2	6/08/2015 11:00	1.64
2/08/2015 23:00	1.65	6/08/2015 12:00	1.63
3/08/2015 0:00	1.61	6/08/2015 13:00	1.62
3/08/2015 1:00	1.62	6/08/2015 14:00	1.72
3/08/2015 2:00	1.62	6/08/2015 15:00	1.73
3/08/2015 3:00	0.11	6/08/2015 16:00	2.71
3/08/2015 4:00	2.6	6/08/2015 17:00	2.71
3/08/2015 5:00	2.62	6/08/2015 18:00	3.77
3/08/2015 6:00	2.64	6/08/2015 19:00	4.38
3/08/2015 7:00	2.63	6/08/2015 20:00	6.31
3/08/2015 8:00	2.65	6/08/2015 21:00	3.46
3/08/2015 9:00	3.17	6/08/2015 22:00	2.63
3/08/2015 10:00	1.2	6/08/2015 23:00	2.62
3/08/2015 11:00	1.56	7/08/2015 0:00	5.66
3/08/2015 12:00	2.97	7/08/2015 1:00	3.11
3/08/2015 13:00	3.24	7/08/2015 2:00	2.87
3/08/2015 14:00	3.04	7/08/2015 3:00	2.71
3/08/2015 15:00	1.75	7/08/2015 4:00	2.61
3/08/2015 16:00	2.58	7/08/2015 5:00	0.11
3/08/2015 17:00	1.5	7/08/2015 6:00	0.11
3/08/2015 18:00	0.97	7/08/2015 7:00	0.1
3/08/2015 19:00	0.46	7/08/2015 8:00	1.61
3/08/2015 20:00	2.72	7/08/2015 9:00	1.6
3/08/2015 21:00	2.77	7/08/2015 9:59	1.62
3/08/2015 22:00	5.87	7/08/2015 10:59	1.64
4/08/2015 0:00	2.92	7/08/2015 11:59	1.63
4/08/2015 1:00	2.7	7/08/2015 12:59	1.62
4/08/2015 2:00	2.62	7/08/2015 13:59	2.16
4/08/2015 3:00	2.62	7/08/2015 14:59	4.67
4/08/2015 4:00	2.62	7/08/2015 15:59	1.9
4/08/2015 5:00	2.61	7/08/2015 16:59	1.5

4/08/2015 6:00	0.1	7/08/2015 17:59	3.15
4/08/2015 7:00	0.14	7/08/2015 18:59	1.22
4/08/2015 8:00	0.14	7/08/2015 19:59	3.6
4/08/2015 9:00	0.13	7/08/2015 20:59	3.58
4/08/2015 9:59	0.14	7/08/2015 21:59	6.38
4/08/2015 10:59	0.1	7/08/2015 22:59	2.78

B.2 Hourly PV array production data

Table 19. PV Array production ($E_{PV}(k)$, kWh)

Date and Time	PV Array Output (kWh)	Date and Time	PV Array Output (kWh)
1/08/2015 0:00	0	4/08/2015 11:59	2.26
1/08/2015 1:00	0	4/08/2015 12:59	2.36
1/08/2015 2:00	0	4/08/2015 13:59	3.24
1/08/2015 3:00	0	4/08/2015 14:59	3.58
1/08/2015 4:00	0	4/08/2015 15:59	4.02
1/08/2015 5:00	0	4/08/2015 16:59	3.62
1/08/2015 6:00	0	4/08/2015 17:59	3.02
1/08/2015 7:00	0.5	4/08/2015 18:59	2.02
1/08/2015 8:00	1.7	4/08/2015 19:59	1.5
1/08/2015 9:00	3.45	4/08/2015 20:59	0.8
1/08/2015 10:00	5.36	4/08/2015 21:59	0.01
1/08/2015 11:00	5.68	4/08/2015 22:59	0
1/08/2015 12:00	5.84	4/08/2015 23:59	0
1/08/2015 13:00	5.26	5/08/2015 0:00	0
1/08/2015 14:00	5.36	5/08/2015 1:00	0
1/08/2015 15:00	4.56	5/08/2015 2:00	0
1/08/2015 16:00	4.67	5/08/2015 3:00	0
1/08/2015 17:00	3.35	5/08/2015 4:00	0
1/08/2015 18:00	2.26	5/08/2015 5:00	0
1/08/2015 19:00	2.3	5/08/2015 6:00	0
1/08/2015 19:59	0.56	5/08/2015 7:00	0
1/08/2015 20:59	0	5/08/2015 8:00	0
1/08/2015 21:59	0	5/08/2015 9:00	0.15
1/08/2015 22:59	0	5/08/2015 10:59	1.62
1/08/2015 23:59	0	5/08/2015 11:00	2.24
2/08/2015 0:00	0	5/08/2015 12:00	2.98
2/08/2015 1:00	0	5/08/2015 13:00	4.58
2/08/2015 2:59	0	5/08/2015 14:00	3.65
2/08/2015 3:00	0	5/08/2015 15:00	3.97

2/08/2015 4:00	0	5/08/2015 16:00	2.86
2/08/2015 5:00	0	5/08/2015 17:00	2.25
2/08/2015 6:00	0	5/08/2015 18:00	1.94
2/08/2015 7:00	0.64	5/08/2015 19:00	1.64
2/08/2015 8:00	2.59	5/08/2015 20:00	0.84
2/08/2015 9:00	3.26	5/08/2015 21:00	0.11
2/08/2015 10:00	4.57	5/08/2015 22:00	0.02
2/08/2015 11:00	5.62	5/08/2015 23:00	0
2/08/2015 12:00	5.89	6/08/2015 0:00	0
2/08/2015 13:00	4.51	6/08/2015 2:59	0
2/08/2015 14:00	3.34	6/08/2015 3:00	0
2/08/2015 15:00	2.25	6/08/2015 4:00	0
2/08/2015 16:00	2.96	6/08/2015 5:00	0
2/08/2015 17:00	1.67	6/08/2015 6:00	0
2/08/2015 18:00	1.08	6/08/2015 7:00	0
2/08/2015 19:00	0.17	6/08/2015 8:00	0
2/08/2015 20:00	0.01	6/08/2015 9:00	0
2/08/2015 21:00	0	6/08/2015 10:00	0
2/08/2015 22:00	0	6/08/2015 11:00	0
2/08/2015 23:00	0	6/08/2015 12:00	0.04
3/08/2015 0:00	0	6/08/2015 13:00	1.26
3/08/2015 1:00	0	6/08/2015 14:00	2.54
3/08/2015 2:00	0	6/08/2015 15:00	2.95
3/08/2015 3:00	0	6/08/2015 16:00	3.51
3/08/2015 4:00	0	6/08/2015 17:00	3.93
3/08/2015 5:00	0	6/08/2015 18:00	4.28
3/08/2015 6:00	0	6/08/2015 19:00	4.95
3/08/2015 7:00	0	6/08/2015 20:00	3.65
3/08/2015 8:00	0	6/08/2015 21:00	2.25
3/08/2015 9:00	1.56	6/08/2015 22:00	1.27
3/08/2015 10:00	2.58	6/08/2015 23:00	0.16
3/08/2015 11:00	3.86	7/08/2015 0:00	0.01
3/08/2015 12:00	4.78	7/08/2015 1:00	0
3/08/2015 13:00	4.56	7/08/2015 2:00	0
3/08/2015 14:00	4.59	7/08/2015 3:00	0
3/08/2015 15:00	3.28	7/08/2015 4:00	0
3/08/2015 16:00	2.95	7/08/2015 5:00	0
3/08/2015 17:00	2.3	7/08/2015 6:00	0
3/08/2015 18:00	1.53	7/08/2015 7:00	0
3/08/2015 19:00	2.95	7/08/2015 8:00	0
3/08/2015 20:00	1.53	7/08/2015 9:00	0
3/08/2015 21:00	0.56	7/08/2015 9:59	0
3/08/2015 22:00	0	7/08/2015 10:59	0
4/08/2015 0:00	0	7/08/2015 11:59	0
4/08/2015 1:00	0	7/08/2015 12:59	0.11

4/08/2015 2:00	0	7/08/2015 13:59	1.54
4/08/2015 3:00	0	7/08/2015 14:59	2.65
4/08/2015 4:00	0	7/08/2015 15:59	2.56
4/08/2015 5:00	0	7/08/2015 16:59	2.01
4/08/2015 6:00	0	7/08/2015 17:59	1.56
4/08/2015 7:00	0	7/08/2015 18:59	1.29
4/08/2015 8:00	0	7/08/2015 19:59	0.8
4/08/2015 9:00	0	7/08/2015 20:59	2.36
4/08/2015 9:59	0.15	7/08/2015 21:59	0.88
4/08/2015 10:59	1.25	7/08/2015 22:59	0.16